UCL Université catholique de Louvain

École polytechnique de Louvain (EPL)

Study of selective protein adsorption on stimuli-responsive polymer brushes

Dissertation presented by
Amanda BRZESKA

for obtaining the Master's degree in
Chemical and Materials Engineering

Supervisor(s)
Christine DUPONT, Sophie DEMOUSTIER

Reader(s)
Anna BRATEK-SKICKI, Delphine MAGNIN

Academic year 2016-2017

Abstract

Protein adsorption is the first step when a solid surface gets in contact with a biological fluid, and its effect can be either beneficial or detrimental. The control of this phenomenon has important implications in biomaterials science, biofouling, food industry or biosensors. Surface modification with stimuli-responsive polymer brushes offers promising perspectives to control protein adsorption. Thin coatings of these «smart materials» can indeed be chemically modified in a certain biological aim, such as to stimulate the adsorption or the desorption of proteins. This study aims at developing mixed polymer brushes sensitive to the ionic strength and the pH of the surrounding medium, in order to tune their properties toward selective protein adsorption from a mixture, such as human blood plasma containing serum albumin, globulins and fibrinogen.

In this study, complex stimuli-responsive polymer brushes were developed, composed of poly(2-(dimethylamine)ethyl methacrylate) (PDMAEMA) and poly(ethylene oxide) (PEO), according to the «grafting to» approach on a gold substrate. PDMAEMA is a weak positively-charged polyelectrolyte at pH 7.4 and PEO is a neutral protein-repellent polymer.

First, the coated polymer brushes were characterized using X-ray photoelectron spectroscopy (XPS), time-of-flight secondary ion mass spectrometry (ToF-SIMS), atomic force microscopy (AFM), water contact angle and streaming potential measurements, and revealed the presence of both polymers on the surface.

Protein adsorption was then studied at biological pH 7.4 and ionic strength 10^{-3}M, using quartz crystal microbalance (QCM). Desorption was carried out by rinsing with a sodium chloride solution at pH 9.0 and ionic strength 0.15M. The switchable behavior of the polymer brushes depending on the conditions allowed to demonstrate partial reversibility of protein adsorption.

Adsorption of mixed protein solutions was then studied by ToF-SIMS using principal component analysis (PCA), in order to identify the adsorbed proteins and to investigate the selectivity of polymer brushes. Adsorption from solutions of human serum albumin (HSA), fibrinogen (Fb), lysozyme (Lys) and/or avidin (Avi) was studied and discussed. PCA revealed selective adsorption of HSA from an HSA/Avi solution.

The obtained results showed that polymer brushes exhibit promising properties towards the control of protein adsorption, and offer many perspectives in biomaterials science and bioengineering.

Acknowledgements

First, I would like to thank Anna Bratek-Skicki for allowing me to join her project, for her guidance, support and precious advices throughout the semester. Thank you also for inviting me to the Institute of Catalysis and Surface Chemistry in Cracow, to perform additional experiments for my master thesis.

I would also like to thank my supervisor Christine Dupont for her guidance and professional comments on my work, her patience, and encouragements that allowed me to stay optimistic.

I also want to express gratitude to the research team of the Institute of Condensed Matter and Nanosciences, Claude Poleunis, Pierre Eloy, Aurélien Vander Straeten, for helping me to perform and/or understand the experiments made on ToF-SIMS, XPS and AFM.

I am very grateful to my supervisor Sophie Demoustier, and Delphine Magnin, to have accepted being part of my final jury.

I also want to thank the research team of the Institute in Cracow to have allowed me to perform experiments on their instruments, particularly Maja Morga.

Finally, thank you to my parents for their support in all situations, throughout the five years of my studies at EPL.

List of Figures

List of Symbols

$\%_{desorption}$	Desorption percentage
Δf	Frequency variation in QCM-D
Δf_a	Frequency variation upon protein adsorption
Δf_d	Frequency variation after rinsing
Δf_d	Frequency variation after the desorption steps
Δf_P	Frequency variation upon polymer grafting
Δm	Variation of mass
$\Delta m_{adsorption}$	Adsorbed mass per unit area
$\Delta m_{desorption}$	Mass per unit area after desorption
ΔP	Hydrostatic pressure
$\Delta_{ads}G$	Gibbs free energy variation during adsorption
$\Delta_{ads}H$	Enthalpy variation during adsorption
$\Delta_{ads}S$	Entropy variation during adsorption
ϵ	Dielectric constant
η	Dynamic viscosity (streaming potential measurements)
η	Viscosity
$\mathcal{A}$	Hamaker constant for the interaction between a protein and a planar surface
μ_q	Shear Modulus of a quartz crystal
ν	Frequency of the associated electromagnetic wave
ρ	Bulk density of brush composition
ρ_q	Density of a quartz crystal
Σ	Reduced tethered density

σ	Grafting density
θ_C	Static water contact angle
ε	Extinction coefficient
ζ	Zeta potential
A	Absorbance
a	Radius of a sphere (representing the protein)
c	Concentration in solution
C_f	Calibration constant
D	Dissipation
d	Distance between grafting points of a polymer brush, or crystal spacing in monochromator (XPS)
E_b	Binding energy
E_k	Kinetic energy
E_S	Streaming potential
E_{lost}	Lost energy
E_{stored}	Stored energy
f_0	Resonance frequency of a quartz crystal
h	Distance between the protein and the planar surface
h	Height of a polymer brush, or Planck constant
I	Intensity of transmitted light
I_0	Intensity of incident light
K_e	Overall electric conductivity
l	Path length
n	Overtone number, or diffraction order
N_A	Avogadro's number
r	End-to-end average distance of a polymer
R_e	Electric resistance
R_g	Radius of gyration
t_q	Thickness of a quartz crystal

Part I

Introduction

1 | State of the art

1.1 Context of the study

Proteins play a key role in biomaterials science. When biomedical devices are immersed into biological fluids, proteins immediately and uncontrollably adsorb onto the device surface. It is important for the integration of prostheses by the body, immunological tests, and drug delivery devices. However, in the case of bioimplants, it may also lead to their failure. Protein adsorption also occurs in biotechnological, agricultural and various industrial applications, where it leads to degradation and failure of devices. There is a high demand for a simple, inexpensive approach of modifying surfaces for controllable performances toward protein adsorption, and many scientists rose to this challenge.

Polymers at interfaces have fascinated physicists and chemists for more than half a century. Highly flexible hydrophilic polymers were investigated, as well as hydrophobic surfaces on the contrary, to control protein adsorption on surfaces through their wetting properties. Hydrogels releasing biocidal agents were also used to prevent fouling by proteins, until several associated environmental issues were pointed out. Novel approaches focused on molecular interactions between proteins and surfaces, and their nanoscopic properties. Polymer brushes have gained much attention for the past decades due to their unique structure, and the simple and controllable polymerization techniques to generate them. Theoretical and experimental research on polymer brushes has been conducted for a better understanding of their outstanding properties and, currently, the focus has shifted to various applications in the domains of materials science and engineering [1]. In order to improve the efficiency of biomaterials, polymer brushes are one of the most promising methods to control protein adsorption.

1.2 Protein adsorption

1.2.1 Protein properties

Proteins are the most abundant biological macromolecules occurring in all cells of living organisms. They are formed by one or more polypeptide chains folded into a structure that bestows them their biological function. Polypeptides are linear polymers of amino acid sequences covalently linked together through peptide bonds. Each amino acid contains an amine ($-NH_2$) and a carboxyl ($-COOH$) group, as well as a side chain which defines its diverse properties : they can be nonpolar or polar, carrying no charge or exhibit an acidic or basic character at neutral pH. Nonpolar amino acids are hydrophobic, as they form no hydrogen bonds with water molecules. 20 different amino acids are commonly found in humans and, with the varying proportions of each of them, they form proteins with very diverse properties, such as charge, size or solubility.

Moreover, physico-chemical properties of proteins are also a consequence of their structure, dictated by their conformation at four different organization levels. The primary structure is defined as the covalent bonds between the amino acids. The secondary structure is formed by chain arrangements often stabilized by hydrogen bonding between NH and CO groups, as well as hydrophobic and Van der Waals interactions. The most common secondary structures are α helices and β sheets. The ternary structure refers to the three-dimensional folding of these structures together with unordered parts, held by electrostatic and hydrophobic forces. This metastable shape is often spherical or globular, whereas human fibrinogen, for example, is an elongated fibrous molecule. In some proteins, several polypeptide subunits interact, giving rise to a quaternary structure. These levels are represented in Fig. 1 [2].

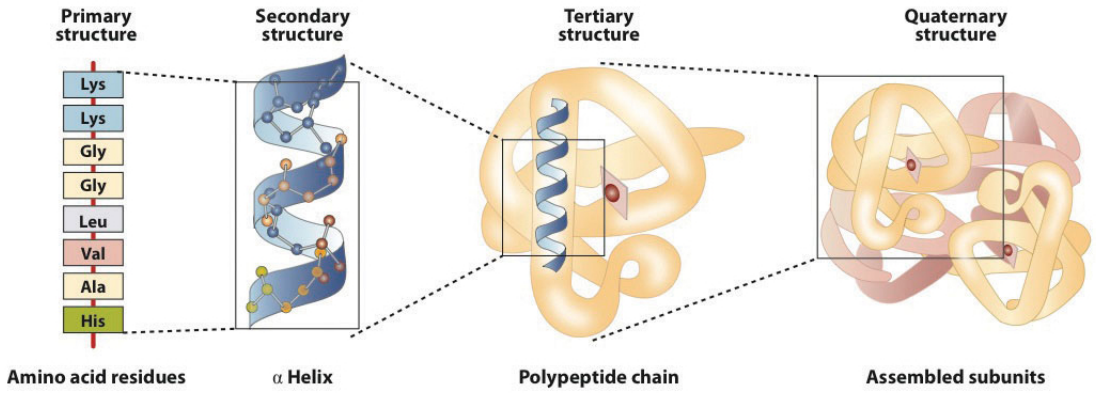

Fig. 1. Levels of structure in proteins [3].

The spatial arrangement of proteins enables the formation of active sites able to perform a biological function and plays a crucial role in their interactions with surfaces. Hydrophobic residues are usually located inside the molecule, hidden from water, while polar parts are usually exposed to the aqueous phase and can interact with surfaces [4]. For the interior parts to interact, the protein has to unfold.

Furthermore, proteins have a large amount of charges distributed along their molecules and their net charge and isoelectric point (iep) depend on the content of these ionized groups and their pKa values. The isoelectric point is the pH at which a molecule is neutral, *i.e.* the zwitterion form is dominant. An amino acid possessing neutral side chains has two pK_a values, pK_{a1} and pK_{a2}, for the carboxylic acid and the amine groups respectively. The isoelectric point is halfway between them and can be calculated as the average of them in the following equation :

$$\text{iep} = \frac{pK_{a1} + pK_{a2}}{2}$$

A third acid dissociation constant can be introduced for amino acids containing other ionisable groups in the side chains, acidic or basic. The isoelectric point is then the mean of the pK_a values relevant to the protonation/deprotonation of the form with no net charge. An example of an acid-base equilibria is given for tyrosine in Fig. 2.

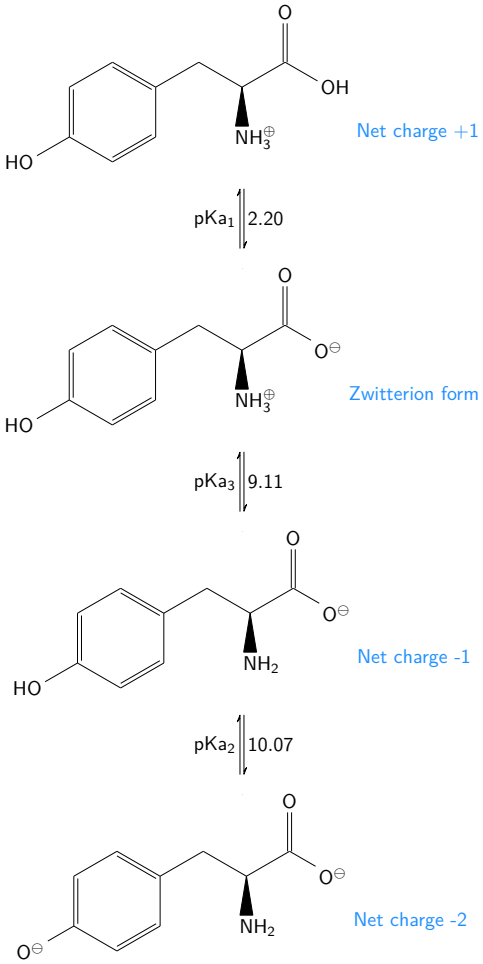

Fig. 2. Acid-base equilibria for tyrosine.

The neutral form of tyrosine is between pK_{a1} and pK_{a3}, so that calculation of its isoelectric point is

then $\text{iep}_{Tyr} = \frac{2.20+9.11}{2} = 5.66$.

Inappropriate protein conformation can result in various neurodegenerative diseases such as Alzheimer, Huntington and Parkinson diseases [5]. Native proteins can lose the preferential location of polar and nonpolar residues triggered, for example, by heating, application of external stresses, a change of pH or ionic strength. This transition is called *denaturation*. Denatured proteins lose their properties, become less dense, and are not able to perform their biological function anymore.

1.2.2 Problem statement

Protein interactions with surfaces are a major concern in many applications, mainly due to their role played in biocompatibility of materials. Protein adsorption is always the first step when a solid surface gets in contact with a biological fluid and its effect can be either beneficial or detrimental. This is why, in some cases, the immobilization of proteins can be desired while, in other cases, protein accumulation has to be prevented, making the control of protein adsorption a major issue.

Biomedical devices

First, when a medical device or a biomaterial is introduced into the body, protein adsorption almost immediately occurs at its surface. In the case of orthopedic prostheses for instance, this is beneficial because proteins allow the further attachment of cells and the integration of the material to the bone tissue. On the other hand, the efficiency of other biological implants can be reduced and result in harmful side-effects. For example, plasma proteins adsorb on stents a few seconds or minutes after their contact with blood, allowing platelet adhesion, which can lead to thrombus formation [6]. Moreover, adsorbed proteins provide a conditioning layer for microbial colonization and bacterial biofilm formation, causing chronic infections [7]. Fig. 3 shows SEM images of biofilms formed on different medical devices that lead to infections and required removal from patient.

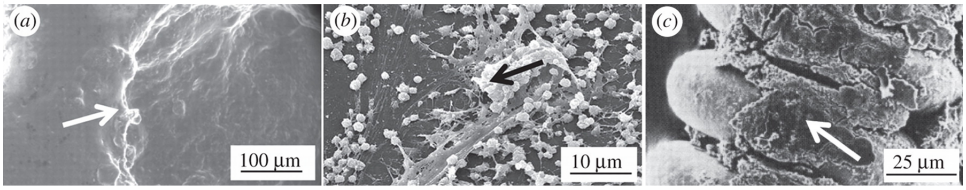

Fig. 3. SEM images of biofilms on various medical devices : (a) a ventilation tube ; (b) a connector ; (c) a pacemaker wire. Adapted from [8].

Biosensors

Electrochemical biosensors are of particular interest in the diagnosis of many diseases [9]. However, the accumulation of biomolecules on their electrode and the sensor surface is an important concern, reducing the efficiency of sensing devices. On the other hand, high densities of immobilized bioactive molecules are needed on the sensor surface, that can be achieved through efficient protein adsorption [10].

Marine biofouling

Marine biofouling is the contamination by undesired biological material, such as bacteria and algae, of ship hulls, buoys, sonar devices, offshore structures, underwater cables, and other marine components, as shown in Fig. 4. It is the result of complex interactions between proteins and surfaces, that lead to further adhesion and anchoring of living organisms. Materials with anti-fouling properties are therefore of particular interest in marine applications, where fouling issues lead to device deterioration and failure, and to energy dissipation, increased corrosion, fuel consumption and environmental costs.

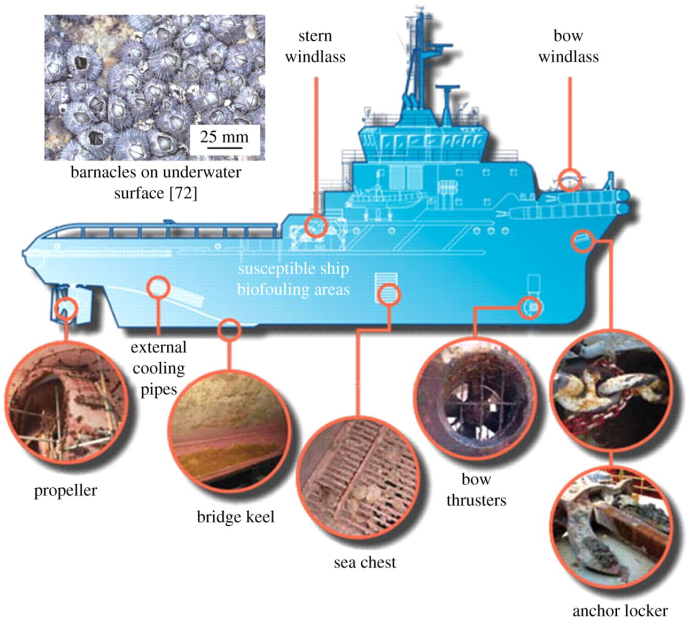

Fig. 4. Fouling of different parts of a ship by bacteria and algae [8].

Food industry

A major concern is also the formation of biofilms in the food processing industry, leading to health and sanitary issues. Biofilm formation begins with the adhesion of organic (protein) or inorganic matter on clean products and the layer grows until subsequent accumulation of other hazardous organisms. Fungi may for example grow on biofilms and cause poor taste and odour problems [8]. They are difficult to remove and often resistant to common sanitation procedures [11].

Biotechnology

In the process industry, fouling by protein adsorption strongly affects the bioreactor performances and also has to be minimized [12]. For instance, in heat exchangers, ultrafiltration membranes or even nuclear power plants, biofilms increase friction, energy needs and pipe pressure drops, as well as decrease heat-transfer efficiency. Dangerous pathogenic micro-organisms are also found in biofilms in potable water supplies [8].

In conclusion, it is essential to predict and control protein adsorption, in order to prevent it in certain areas, while to increase it where desirable, and this can be achieved by functionalization of the surfaces.

1.2.3 Protein behavior at solid interfaces

When a solid surface comes into contact with a biological fluid, proteins almost instantaneously adsorb on it, and are no longer free to diffuse away. Later, it is more difficult for proteins to reach an empty spot and the process becomes slower [4]. Some conformation changes of the protein molecules occur immediately in order to adapt to the new environment and others may continue for days, but adsorption does usually not result in fully denatured proteins. The created film acts then as a substrate for further adhesion of cells or microorganisms. The orientation of adsorbed proteins on the surface also changes the properties of the adsorbed phase because proteins are not uniform across their surface. If a fixed portion of the protein is exposed to the bulk phase, it influences the surface bioactivity [4]. For instance, the exposure of the variable part of an antibody allows for antigen recognition. Protein adsorption is generally not reversible, but changing the pH or the salt concentration can increase the desorption process. The protein molecules leaving the surface may then be conformationally altered compared to the native protein.

Thermodynamic approach

The thermodynamic principles governing protein adsorption are described by the formula :

$$\Delta_{ads}G = \Delta_{ads}H - T\Delta_{ads}S$$

Negative as well as positive changes in enthalpy have been observed upon spontaneous adsorption. They are caused by intermolecular forces - Van der Waals, Coulomb, Lewis acid-base forces. The Gibbs free energy variation $\Delta_{ads}G$ is negative for the spontaneous adsorption process. This means that the entropic term $T\Delta_{ads}S$ is greater than the positive enthalpic term $\Delta_{ads}H$. Indeed, protein adsorption is generally strongly driven by entropic changes, arising from changes in water binding to the surface and the protein, and unfolding of the protein on the surface [4, 5].

Driving forces

The mechanism of protein adsorption is not fully understood, but there are a few parameters that influence the phenomenon and act synergistically, or antagonistically : the surface properties (wettability, polarity, charge, topography features), the protein nature (size, stability, bulk concentration, functionality, affinity for surface) and the solution conditions (pH, salt, temperature) [12, 5]. In this section, the main contributions from electrostatic, dispersion and hydrophobic forces will be discussed.

Electrostatic interactions First of all, in an aqueous environment, both proteins and the support are generally electrically charged and surrounded by counter-ions. Amino-acids that make up proteins contain both acidic and basic functional groups, which can be associated or dissociated. Proteins adsorb best on surfaces with opposite charge and a maximum is reached when the charge density of the protein matches the one of the surface, resulting in a zero net charge at the interface [5]. Proteins

may also adsorb on surfaces with the same charge by binding through localized opposite charges in their structure or exposed interior groups after conformational changes. Electrostatic interactions are strongly affected by the ionic strength of the solution. At low salt concentration, cationic proteins bind to anionic surfaces reversibly [5]. At high ionic strength, ions from the salt screen electrostatic interactions, and therefore decreasing the adsorption. Moreover, increasing the ionic strength is used for protein desorption. Adsorption processes controlled by other types of interactions, such as wettability, may however be enhanced [12]. At pH far from the isoelectric point of the protein, the charged proteins then exhibit repulsive forces between each other, which prevent them from aggregating. On the other hand, at the isoelectric point, there are as many positive as negative charges so that the net charge is zero, although highly charged patches still remain on the protein surface. Repulsive electrostatic forces are then reduced and attraction forces are predominant, causing aggregation of proteins at the neutral surface. For this reason, the maximum protein adsorption often occurs at the isoelectric point [5].

Van der Waals forces Van der Waals forces also play a role in the adsorption process. For a sphere (the protein) of radius a and a distance h of closest approach between the sphere and the planar surface, for $h << a$, the Gibbs free energy change attributed to Van der Waals forces $\Delta_{ads}G_{VdW}$ is simplified into :

$$\Delta_{ads}G_{VdW} = -\frac{\mathcal{A}a}{6h} \tag{1.1}$$

where $\mathcal{A}$ is the Hamaker constant for this specific interaction. Dispersion forces between proteins and sorbents are usually attractive but small, because of the small dimensions of protein molecules and the low value of the Hamaker constant related to such systems [13].

Surface wettability It has been frequently reported that proteins adsorb in larger quantities on hydrophobic surfaces than hydrophilic ones. On a hydrophobic surface, the protein unfolds and adsorbs through its hydrophobic patches. Then it spreads along the surface in order to minimize the hydrophobic area in contact with the solvent. Water molecules are released from the interface, as shown in Fig. 5, leading to an entropy gain of the system. This driving force originating from dehydration when at least one of the contacting surfaces is hydrophobic largely outweighs electrostatic repulsion or dispersion interactions [14].

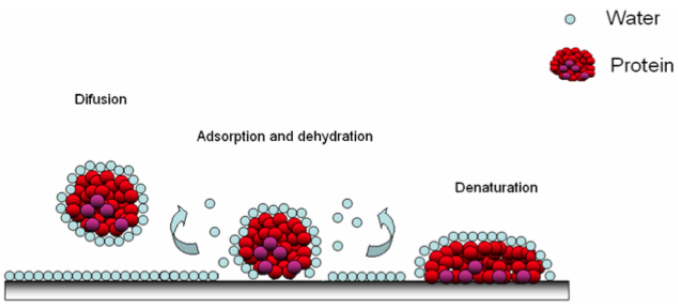

Fig. 5. Process of hydrated protein adsorption along with dehydration [5].

On the other hand, with hydrophilic surfaces, there is no such dehydration force. The hydration of the support and the protein is favorable, so water molecules at the interface impede adsorption. The interaction is then governed by polar and charged functional groups of the protein.

A distinction has to be made between structurally stable proteins that have a strong internal cohesion ("hard" proteins) and structurally labile proteins with a weak internal cohesion ("soft" proteins). Hard proteins adsorb mostly by electrostatic attraction and undergo limited structural changes upon adsorption, while soft proteins can even overcome electrostatic repulsion by going through severe conformational changes leading to higher entropy [5, 14]. Protein adsorption is therefore electrostatically controlled on hydrophilic surfaces for hard proteins, while soft proteins can adsorb at all kinds of surfaces (Fig. 6).

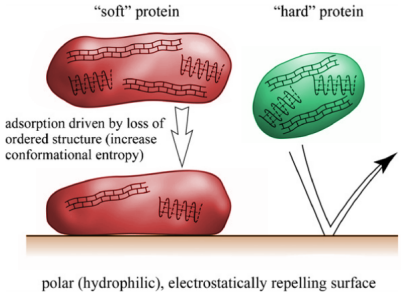

Fig. 6. Soft protein : adsorption onto a hydrophilic and electrostatically repelling surface by loss of ordered structure. Hard protein : no adsorption on electrostatically repelling surface. Adapted from [14].

In conclusion, table 1.1 outlines the theoretical predictions of protein adsorption at different surfaces.

Table 1.1. Scheme to predict whether ("yes") proteins adsorb or not ("no") at surfaces. The "+" and "-" signs refer to the net electric charge of the protein and the surface [14].

	Surface			
	Hydrophobic		*Hydrophilic*	
Protein	+	−	+	−
Stable structure				
+	Yes	Yes	No	Yes
−	Yes	Yes	Yes	No
Labile structure				
+	Yes	Yes	Yes	Yes
−	Yes	Yes	Yes	Yes

Multiprotein systems

At most surfaces in contact with complex protein solutions, adsorption depends on time and concentration. An example of this behavior which is expected to occur is the *Vroman effect*. With time, adsorbed proteins with lower affinity may be replaced by more surface-active ones, but that are present in lower concentrations [4]. However, when adsorbed proteins relax to irreversibly adsorbed states in a time-dependent manner, the replacement of one protein by another also depends on relaxation effects

[15].

1.2.4 Control of protein adsorption

Scientists aim at controlling and predicting protein adsorption. Their ideas follow two different directions. One is interested in designing materials with appropriate macroscopic surface properties, such as water wettability. The other approach focuses on molecular interactions between the proteins and the surface. For reducing protein adsorption, the aim is always to minimize the interfacial free energy between the surface and the solution.

Pre-adsorbing one protein to prevent further adsorption may be a simple way of protection, but there is always the risk of an exchange with time [12]. Various coatings were investigated in order to resist the adhesion of proteins, most of them are based on the use of polymers. They can be highly flexible hydrophilic polymers or hydrogels. Controlling surface wettability is considerably used in biotechnological applications, industrial processes and in agricultural applications. For instance, new contact lens materials are based on polymers incorporating crosslinked hyaluronic acid as a wetting agent and show a considerable reduction of protein adsorption [16]. Other techniques based on biomimetic non-fouling were also developed. Nevertheless, they make use of the Lotus effect of hydrophobic surfaces [7]. Hydrophobic materials have also been used in the field of blood compatibility, where a layer of adsorbed proteins reduces the reactivity of the surface [12].

Polymer layers are of particular interest in resisting protein deposition. The interaction between a particle (e.g. a protein) and a polymer-coated surface is described by the model in Fig. 7. The net interaction energy (bold line) is a superposition of three contributions : (a) short-range interaction, such as electrostatic attraction, hydrogen bonding and hydrophobic interaction, (b) long-range Van der Waals attraction and (c) repulsive, steric interaction between the particle and the brush [17].

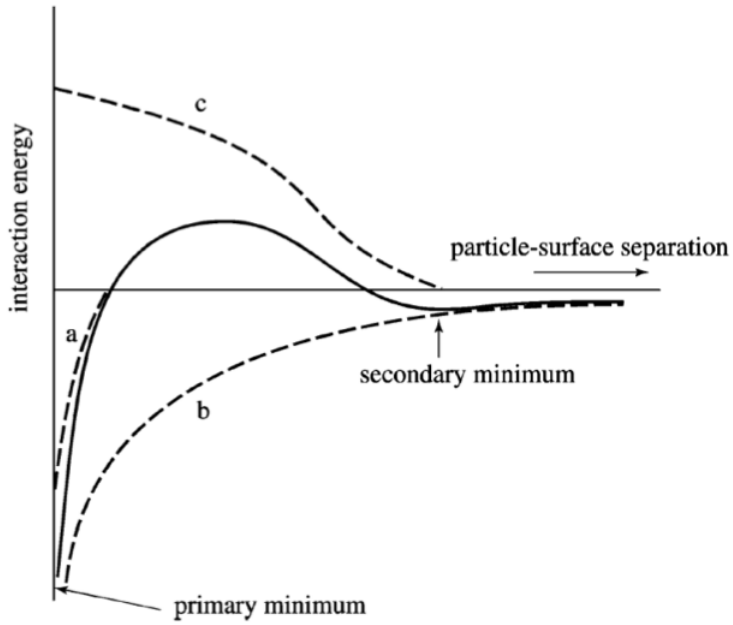

Fig. 7. Interactions between a particle and a polymer-coated surface : (a) short-range particle-surface contact ; (b) long-range Van der Waals attraction and (c) repulsive osmotic interaction. The solid line represents the overall interaction [13].

Resistance to protein adsorption can be attributed to those factors depending on the way the protein adsorbs on the polymer brushes. Three modes of adsorption can be distinguished and are represented in Fig. 8. In the case of low brush density or small enough proteins, these latter can be intercalated between polymer chains and adsorb at the solid surface. This insertion mechanism is called *primary adsorption*. However, if the brush density (or the protein) is large enough, proteins are simply deposited onto the brush-solvent interface and can approach the surface by compressing the brush - it is *secondary adsorption*. Large rodlike proteins are likely to adsorb in this way. *Ternary adsorption* occurs within the grafted layer [17].

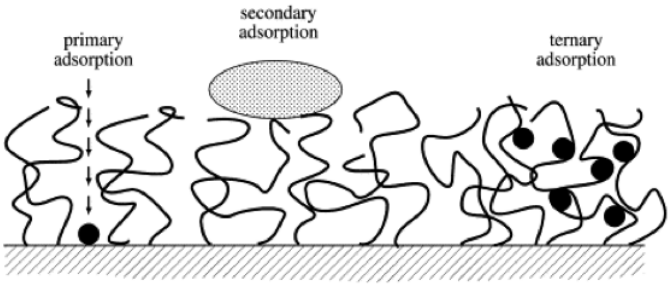

Fig. 8. Modes of protein adsorption on a polymer brush : (left) primary ; (centre) secondary and (right) ternary [13].

The resultant can be tuned by choosing the adequate polymer brush parameters. In primary adsorption, short range particle-surface attraction is dominant and may be repressed by increasing the

grafting density. Secondary adsorption is due to Van der Waals forces and could be reduced by increasing the brush thickness.

Zwitterionic polymer brushes make an important class of nonfouling polymers. Increasing the thickness of grafted sulfoxybetaine- and carboxybetaine-bearing polymer chains seemed to decrease protein adsorption. It was also highly suppressed from thick polymer brush layers bearing phosphorylcholine groups [18]. Modified dextrans also showed to be effective in reducing protein adsorption [19]. Ikada and co-workers reported that polyacrymide-grafted polyurethane surfaces reduced bovine serum albumin and immunoglobulin adsorption [1]. The highly hydrated glycocalyx is also known to prevent the undesirable nonspecific adhesion of proteins and cells [1].

However, poly(ethylene glycol) (PEG or PEO) is the most well-known protein-repellent and widely used polymer for preventing protein adsorption. It is a neutral, highly hydrophilic and flexible polymer. A densely grafted hydrophilic polymer brush acts as an inert shielding layer that reduces interactions between the surface and the solution. The dependence of protein adsorption to the grafting density is believed to be due to steric repulsion caused by the compression of stretched chains. The entropic contribution to the total free energy of the system is indeed unfavorable and the system tends therefore to minimize the adsorption [1]. Furthermore, in an aqueous solution, its chains are highly mobile and associate with water through hydrogen bonds, leading to high exclusion volumes. Its protein-repellent properties are then attributed to steric repulsion [13].

Self-assembled monolayers or layer-by-layer assembly techniques are used to modify surfaces with polymers [7]. Moreover, various lithography methods, such as electron-beam lithography or scanning probe lithography, and surface-initiated polymerizations are also used to fabricate complex surfaces displaying *patterned* domains. For instance, patterned poly(2-(dimethylamino)ethyl methacrylate) (PDMAEMA) brushes were produced by a combination of block copolymer micelle lithography to prepare a patterned gold substrate, and surface-initiated atom transfer radical polymerization of PDMAEMA on the gold nanoparticles. To avoid protein adsorption on the substrate between the polymer nanopattern, the surface was then passivated by addition of a protein resistant PEO layer. The resulting patterns allowed to directly visualize and spatially control protein adsorption on the nanoscale. AFM results before and after protein adsorption and desorption are shown in Fig. 9. After the brushes were exposed to proteins, the pattern became blurry, the average height of the nanostructures decreased and big aggregates appeared on the surface, meaning that some proteins on the outer edge of the brushes formed aggregates and merged initially separated nanostructures, as seen in the model in Fig. 10. After protein desorption, an ordered pattern appeared again, but the average height of the nanostructures increased. Residual proteins were actually located inside the brushes, causing volume expansion of the nanostructures, as illustrated in the schematic model [20].

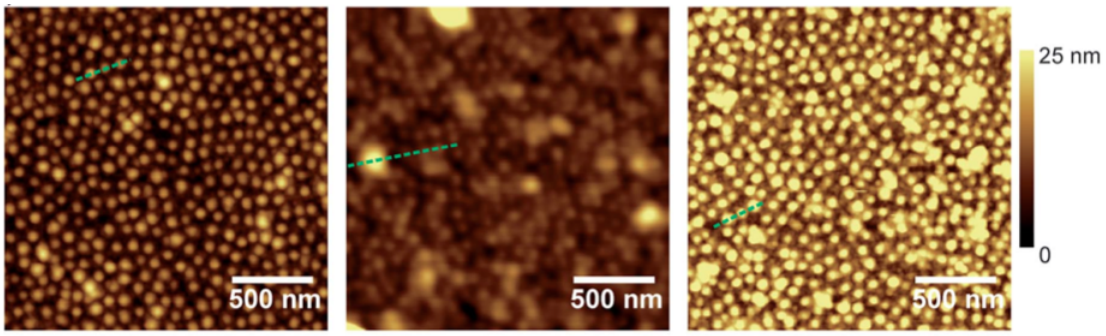

Fig. 9. AFM topography of patterned PDMAEMA brushes : (left) before protein adsorption ; (middle) after protein adsorption and (right) after protein desorption [20].

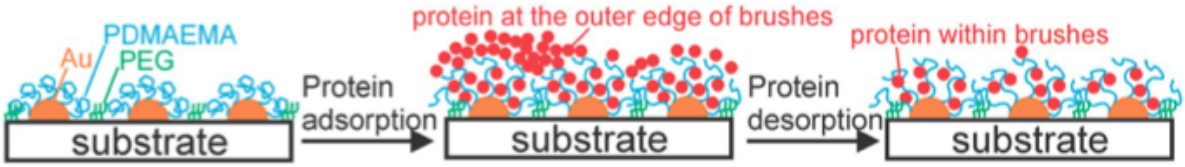

Fig. 10. Schematic model of patterned PDMAEMA brushes : (left) before protein adsorption ; (middle) after protein adsorption and (right) after protein desorption [20].

1.3 Polymer brushes

1.3.1 Definition and properties

In order to enhance the performance of a material in the biological environment, while maintaining its favorable bulk properties, the surface of the material has to be modified, to acquire new properties, such as biocompatibility, corrosion resistance or wettability. This research is interested in coating surfaces with polymer brushes. They present the advantage of being adaptable to various substrates, they exhibit excellent long-term mechanical stability, their chemical composition and the morphology can be precisely controlled and their properties are tunable. One of the main features of polymer brushes is their responsiveness to different external stimuli, such as a variation in temperature, pH or ionic strength. Van der Waarden was the first to take interest in polymer brushes in the 1950s, when he showed that grafting polymer chains to colloidal particles prevented flocculation. They have been considered in many applications more recently, such as dielectric materials, bioselective surfaces, nanofluidic devices, microreaction vessels, biomimetic material fabrication and cell growth control [21].

A *polymer brush* consists of macromolecular chains end-tethered by one extremity to a supporting surface - the *substrate* - under two specific conditions. First, the brush height h in a given solvent has to be larger than the end-to-end average distance $< r^2 >^{1/2}$ of the non-grafted chains dissolved in the same solvent. Second, the distance d between grafting points has to be smaller than the chain end-to-end average distance [22].

A commonly used parameter to describe the structure of immobilized polymer chains is called the *reduced tethered density*. It is defined as the number of chains in an area that a free non-overlapping polymer chain would normally fill in the same conditions. It is noted Σ and given in equation 1.2, where R_g is the radius of gyration of a tethered chain at specific conditions of solvent and temperature.

$$\Sigma = \sigma \pi R_g^2 \tag{1.2}$$

σ is the grafting density defined by $\sigma = \frac{h \rho N_A}{M_n}$, with ρ the bulk density of the brush composition, M_n the molecular weight of the brush, and N_A, Avogadro's number. Three different regimes can be distinguished, evaluated by the distance d between their grafting points : the chains interactions are stronger when d is smaller. They are illustrated in Fig. 11 :

- When the size of grafted polymers h approaches the distance d between grafting points, meaning at low grafting density, the chains do not interact with each other and collapse. It is the *mushroom regime* (when $\Sigma < 1$);
- In the *crossover* or *transition regime*, at intermediate density, the chains interact and start to overlap ($1 < \Sigma < 5$);
- At high density, the repulsive interactions between the chains make them stretch away perpendicularly to the surface. It is the *brush regime* ($\Sigma > 5$) [22].

When the polymer chains stretch away from the surface, the number of possible conformations decreases, leading to a loss of entropy. This induces a retracting force to maintain the chains in coiled conformation.

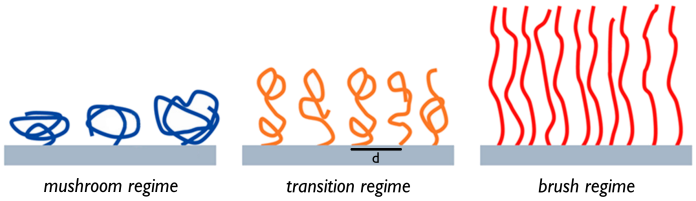

Fig. 11. Various regimes of grafted polymer chains, depending on the distance d between grafting points.

Polymer chains can be grafted on substrates with different shapes (planar, spherical), and different architectures can be created. Block copolymer brushes, gradient polymers and Y-shaped polymers, can for example be immobilized at interfaces in the brush regime.

1.3.2 Synthesis

Polymer brushes on solid surfaces can be formed by several methods, depicted in Fig. 12. Polymers can be deposited on the surface, via a process called *physisorption*, where one block of a block copolymer is selectively adsorbed, while the other one interacts with the solvent. It is a reversible technique, but the adsorption is made through a weak physical bond (hydrogen bonds, Van der Waals interactions), making it thermally unstable and the blocks can be displaced by other molecules with a strong affinity for the surface.

To overcome these drawbacks, polymer chains can also be attached through strong covalent bonds via *chemisorption* by either the "grafting-to" or "grafting-from" methods.

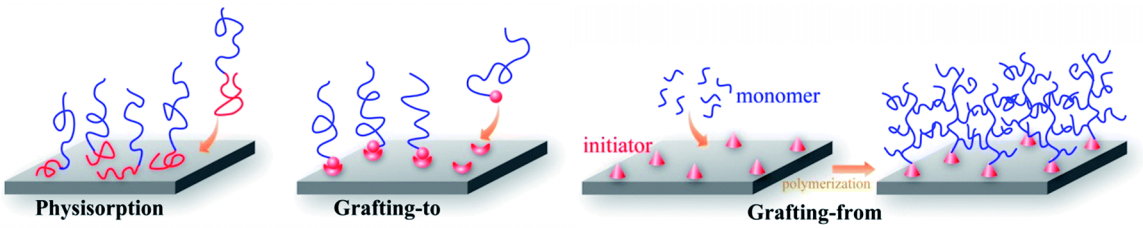

Fig. 12. Different methods to synthesize polymer brushes : physisorption, "grafting-to" and "grafting-from" methods.

The *"grafting-to"* approach consists of a tethering process performed via end-functionalized polymer chains which interact with the surface. It is a rather simple method, but attached chains form a repulsive barrier, through which new polymer chains have to diffuse to reach the active sites. For this reason, only low grafting thicknesses and densities can be generated. Increasing the polymer concentration in the solution and the grafting time can improve the density of the brushes. In the case of

mixed polymer brushes, two different "grafting-to" methods can be distinguished. It can be sequential, with a rinsing step between the grafting of each polymer, or simultaneous, when two polymers are simultaneously introduced to the surface.

The grafting can also be performed by direct polymerization form a solution of monomers on the surface, where initiators were previously immobilized. It is the *"grafting-from"* method. Higher grafting densities are achieved because chains grow simultaneously and do not impede each other. However, it is more complex to perform, due to limitations of the initiator surface coverage and its efficiency, the rate of diffusion of monomer to the active sites and the occurrence of side reactions. Hence, the distribution of the molecular weight is harder to control. This is why controlled and/or living polymerization techniques are usually applied [22].

1.3.3 Stimuli-responsiveness

Surface modification with functional polymer brushes may lead to the design of "smart" systems in which the polymer chain conformation can be manipulated by environmental conditions like temperature, ionic strength (I), light or pH. That kind of materials provide an "ON/OFF" control of their properties, attractive in many practical applications.

Thermoresponsive poly(2-(N-morpholino)ethyl methacrylate) brushes grafted on silica particles were synthesized using aqueous ATRP. At 34 °C, the particles began to aggregate, which is close to the cloud point of these polymers, where a phase-separation occurs, giving a cloudy appearance [23].

Huck *et al.* described Pickering emulsions using ion-specific responsive colloids based on poly(2-(methacryloyloxy)-ethyl-trimethyl-ammonium chloride) (PMETAC) brushes grafted on silica nanoparticles. The addition of ClO_4^- ions changed the surface hydrophilicity of the particles, leading to their aggregation and the generation of Pickering emulsions [24].

Wu and coworkers fabricated light-responsive colloids by grafting optically responsive polyspiropyran brushes onto silica colloids. These brushes undergo a reversible change from a hydrophobic to a hydrophilic state upon irradiation with UV light. The "hairy" colloids are then able to switch between oil and water phases upon shining UV or visible light on the colloidal dispersion [25].

The properties of surface-tethered polyelectrolytes can be tuned by changes in ions (nature, concentration) to which they are exposed - the ionic strength - and by the pH. The conformation of the polymer chains is governed by electrostatic interactions, solvation and excluded volume effects. Conformational changes of poly(acrylic acid) (PAA) upon changes of pH and ionic strength of the surrounding medium were studied by Delcroix and presented in Fig. 13. PAA is a weak polyelectrolyte undergoing pH-dependent deprotonation of its carboxylic functions. At low I and low pH, no effect of the saline solution compared to pure water on PAA chains was observed. When the pH was increased, PAA brushes became progressively negatively charged and swollen, so that they protruded in solution. At low pH and high I, however, PAA chains were not charged, and shrank, leading to a brush thickness decrease. When both pH and I were high, negative charges increased along PAA chains and the high

amount of salt led to a strong shrinking of chains, which expelled water but entrapped counterions [26].

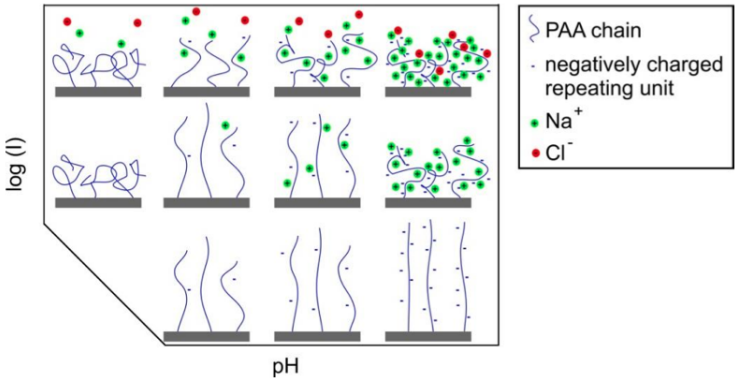

Fig. 13. Scheme of PAA conformation in function of pH and I of the surrounding medium [26].

Designing and understanding the behavior of *mixed* polymer brushes is more complex, but they offer promising tunable properties due to the combination of different stimuli-responsive functionalities. Two water-soluble polymers, that do not segregate individually, are mixed and tethered to the surface via their reactive groups, often thiols, silanes, amine or carboxylic groups, by a chemisorptive approach (see section 1.3.2) [27]. For instance, mixed pH-responsive brushes of poly(dimethylsiloxane) (PDMS$-NH_2$) and carboxy-terminated poly(2-vinylpyridine) (P2VP-COOH) were fabricated on epoxy-functionalized electrode surfaces by Motornov *et al.* [28]. The control of ion transport through nanoscopic channels was allowed to create a gating mechanism, owing to the switchable properties of these brushes. Delcroix *et al.* designed mixed brushes of poly(acrylic acid) (PAA) and poly(ethylene oxide) (PEO) via the "grafting-to" approach for tuning protein adsorption onto smart materials. Proteins were shown to adsorb effectively into pure PAA brushes, but only partially desorbed from the brushes by changes in pH and ionic strength. The properties of the mixed polymer brushes were however adjusted by different ratios of PEO and PAA, allowing to achieve a highly switchable behavior toward protein adsorption. High amounts of albumin were indeed adsorbed on PEO/PAA brushes and 86% of these could then be desorbed upon pH and I change. Further cycles of adsorption/desorption could be achieved [29].

2 | Objective and methodology

2.1 Objective and strategy

The goal of this study is to develop mixed stimuli-responsive polymer brushes sensitive to the ionic strength and the pH of the surrounding medium, with a view to tune their properties toward selective protein adsorption from a mixture of proteins, such as human blood plasma containing serum albumin, globulins and fibrinogen.

The results obtained in this work will be significant for material science, namely in the biotechnology and biomedical domains, where uncontrolled protein adsorption is a major issue.

To achieve this objective, the study is done in two major steps. First, mixed polymer brushes will be fabricated and characterized with X-ray photoelectron spectroscopy (XPS) and atomic force microscopy (AFM) among others. To achieve selectivity of protein adsorption, they will be composed of protein adsorbing and protein-repellent polymers.

Then, their potential to selectively adsorb one protein from a mixture will be investigated through quartz crystal microbalance with dissipation monitoring (QCM-D). A strategy to distinguish adsorbed proteins on the coatings will be implemented, based on a highly sensitive technique : time-of-flight secondary ion mass spectrometry (ToF-SIMS).

2.2 Methodology

The first part of this thesis aimed at a deep understanding of the principles behind protein adsorption and at presenting current methods to control it. A review of the work already accomplished in the field of stimuli-responsive polymer brushes was also presented.

The second part will describe the materials and the methods used in this research to characterize the designed polymer brushes and to monitor protein adsorption.

In the third part, the results of the study will be presented and discussed. After the characterization of the coatings, extensive QCM experiments on single protein adsorption and desorption will first be

analyzed, then the selectivity of some protein mixtures will be investigated using ToF-SIMS results, and principal component analysis of the ToF-SIMS data.

Finally, conclusions will be drawn regarding the objective of this work, and further perspectives in that area will be highlighted.

Part II

Materials and methods

3 | Materials

3.1 Gold substrate

The surfaces used in QCM are circular quartz sensors coated with a 100 nm gold layer. The surfaces used in XPS, AFM and water contact angle measurements are gold substrates of approximately 1 cm^2 or larger rectangles for streaming potential measurements. They were prepared by thermal evaporation of gold above a titanium interlayer onto silicon wafers and shaped with a diamond tip (UCL, Belgium).

3.2 Polymers

Mixed polymer brushes were prepared from two different polymers : poly(2-(dimethylamine)ethyl methacrylate) (PDMAEMA) and poly(ethylene oxide) (PEO). Thiol-terminated polymers were purchased from Polymer Source Inc. (Dorval, Canada) for grafting on gold substrates. All polymer solutions were prepared using ultra-pure water (Purelab Ultra Elga instrument).

3.2.1 Poly(2-(dimethylamine)ethyl methacrylate) (PDMAEMA)

Poly(2-(dimethylamine)ethyl methacrylate) (PDMAEMA) is a weak cationic polyelectrolyte. It is widely studied owing to its swelling behavior and switchable charge density depending on the pH and ionic strength. This pH-responsiveness is due to the protonation or deprotonation of the dimethylamino groups [20]. PDMAEMA brushes have an isoelectric point at pH 9.0, so that they are positively charged and swollen due to hydration at pH 7.4. A schematic structure of protonated and deprotonated PDMAEMA is shown in Fig. 14, as well as an illustration of the corresponding swelling and deswelling behaviors of PDMAEMA chains in Fig. 15.

PDMAEMA used in this study had a molar mass of $M_n = 8500\,\mathrm{g\,mol^{-1}}$ and a polydispersity index of 1.3. Stock solutions were prepared at a concentration of $3\,\mathrm{mg\,ml^{-1}}$ in ultra-pure water and were diluted prior to each experiment ($0.5\,\mathrm{mg\,ml^{-1}}$). The PDMAEMA structure with reactive disulfide bonds as purchased by the manufacturer is shown in Fig. 16.

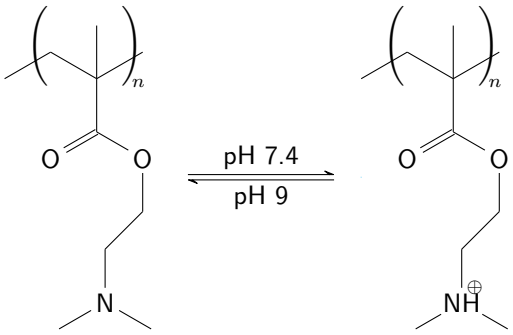

Fig. 14. Skeletal formulas of protonated and deprotonated PDMAEMA.

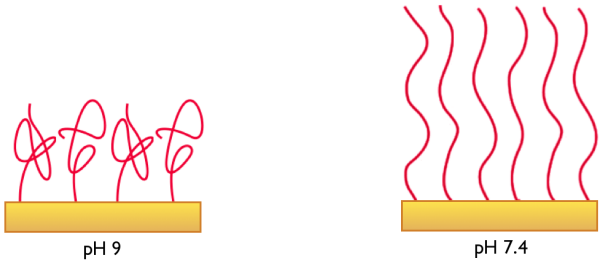

Fig. 15. Swelling and deswelling of PDMAEMA chains on a substrate in low ionic strength medium, due to changes in hydration at different pH.

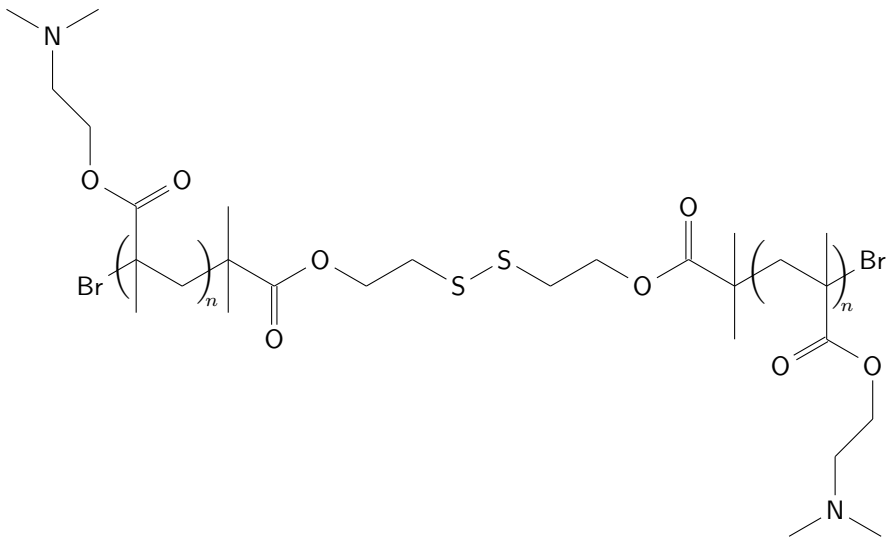

Fig. 16. Skeletal formula of PDMAEMA-2S.

3.2.2 Poly(ethylene oxide) (PEO)

Poly(ethylene oxide) (PEO), also commonly known as poly(ethylene glycol) (PEG), is a linear polymer with a polyether structure, as represented in Fig. 17 [1]. The nonfouling nature of PEG is explained by the large amount of water binding to its chains, forming a barrier that prevents protein adsorption. It

was reported that the grafting density of 0.5 chains/nm^2 is optimal for its protein-repellent properties [30].

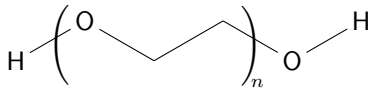

Fig. 17. Skeletal formula of PEO.

PEO used in this study had a molar mass of $M_n = 1100\,\mathrm{g\,mol^{-1}}$, which is approximately 23 units, and its polydispersity index was 1.08. Stock solutions of PEO were prepared at a concentration of $5\,\mathrm{mg\,ml^{-1}}$ in ultra-pure water and were diluted prior to each experiment ($\approx 1\,\mathrm{mg\,ml^{-1}}$ for a mixed polymer brush prepared from a solution containing 70% PEO in volume).

3.3 Proteins

All proteins, except avidin, were purchased from Sigma-Aldrich. Avidin was purchased from Thermo Fischer Inc. Stock solutions, at concentrations $3\,\mathrm{mg\,ml^{-1}}$ and $0.1\,\mathrm{mg\,ml^{-1}}$ for avidin, were prepared at pH 7.4 and NaCl concentration 10^{-3}M at room temperature. The solutions were filtered using a 0.45 µm filter to eliminate any aggregates. The effective protein concentration was then measured with a spectrophotometer, as explained in section 3.3.5. They were diluted before each experiment to concentrations of $0.2\,\mathrm{mg\,ml^{-1}}$, or $0.1\,\mathrm{mg\,ml^{-1}}$ if the mixture contained avidin. The pH of all solutions was adjusted to 7.4 before each experiment by adding solutions of NaOH or HCl, purchased from Sigma Aldrich.

3.3.1 Human serum albumin

Human serum albumin (HSA) is the most abundant protein in human blood. It is a heart-shaped globular protein (Fig. 18) with an 8 nm length and 3 nm thickness. It has a molecular mass of 66 kDa and an isoelectric point around pH 4.8. HSA is a "soft" protein, which means it can undergo conformation changes upon adsorption [13].

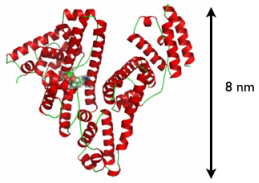

Fig. 18. Heart shape of human serum albumin [31].

3.3.2 Fibrinogen

The fibrinogen molecule (Fb) is linear with a total length of 47.5 nm (Fig. 19). It consists of three nodules held together by a cylindrical rod of about 8 to 15 Å. The end nodules are spherical in shape

and have a diameter of 6.5 nm, while the middle one is slightly smaller [32]. Fibrinogen is the largest protein used in this study and its molecular mass is 340 kDa. Its isoelectric point is around pH 5.8.

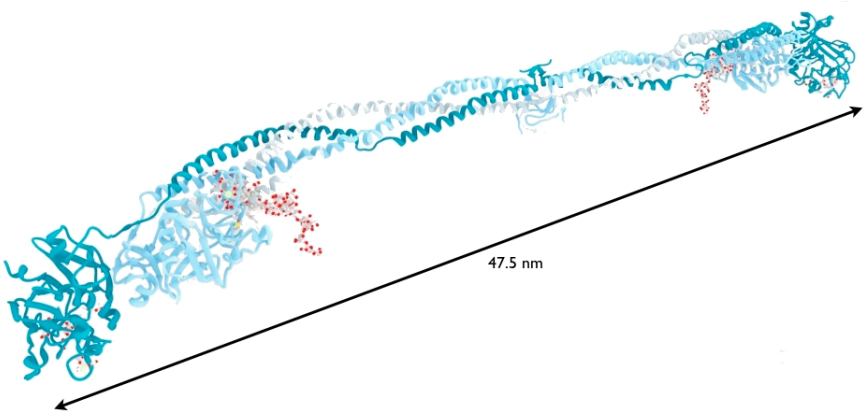

Fig. 19. Linear trinodular shape of fibrinogen [33].

3.3.3 Lysozyme

Lysozyme (Lym) is smaller than HSA and fibrinogen (about 14.3 kDa and 3 to 5 nm of diameter) and it is a hard protein, meaning it does not undergo many conformational changes upon adsorption. Moreover, its high isoelectric point is situated around pH 11, which means it is positively charged at pH 7.4 and should not adsorb on positively charged polymer brushes **??**.

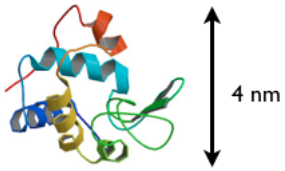

Fig. 20. Shape of lysozyme molecule [34].

3.3.4 Avidin

Avidin (Avi) is a glycoprotein containing 4 subunits with a total molecular weight of about 67 kDa. It is rather small, having a diameter of 4 nm, and its isoelectric point is at pH 10.5 [35].

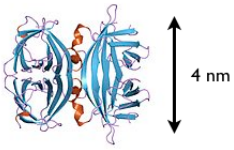

Fig. 21. Tetrameric shape of avidin [35].

3.3.5 Spectrophotometry for protein concentration measurement

To measure protein concentration in an aqueous solution, its light absorption is measured with a spectrophotometer (UV-1700 Spectrophotometer Shimadzu Inc., Japan). Most proteins absorb light at characteristic wavelengths, for instance tryptophan absorbs light at 280 nm. Lambert-Beer law given below relates the fraction of the incident light absorbed by a solution to the path length l corresponding to the thickness of the absorbing layer and the concentration c of proteins.

$$A = \log \frac{I_0}{I} = \varepsilon c l \qquad \text{(Lambert-Beer law)}$$

where I_0 is the intensity of the incident light (parallel and monochromatic), I is the intensity of the transmitted light, and ε is the extinction coefficient. The fraction $\log \frac{I_0}{I}$, noted A, measures the ability of the solution to absorb light at a given wavelength and is called the *absorbance*.

The principle of a spectrophotometer is illustrated in Fig. 22. The incident light wavelength at 280 nm is selected in the monochromator and transmitted to the cuvette containing the protein solution. A portion of light is absorbed by the sample and the transmitted light travels to a detector, allowing to measure the absorbance [36].

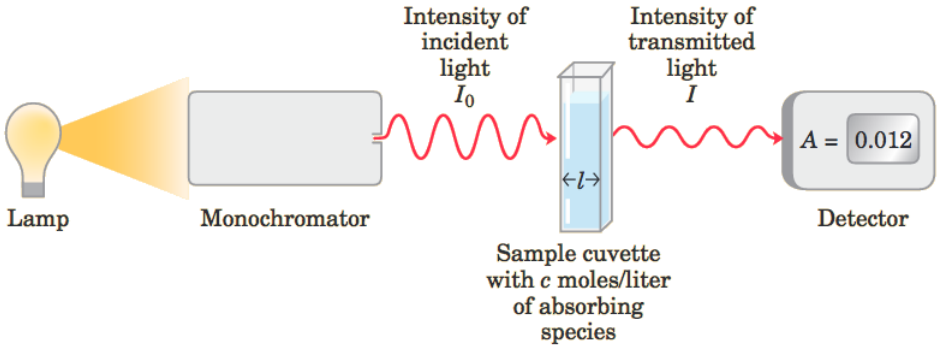

Fig. 22. The principal components of a spectrophotometer [36].

3.4 Cleaning solutions

All gold surfaces were cleaned in a "piranha" solution for 2 min, prepared with 95% sulfuric acid and 30% hydrogen peroxide (both purchased from VWR Prolabo Chemicals, Leuven, Belgium), in a volume ratio of 2:1. They were rinsed 10 times with deionized water, whereupon they were dried out with a nitrogen gas stream and cleaned in a UV/ozone environment for 15 min. Finally, they were flushed with absolute ethanol and dried again under nitrogen. The gold substrates prepared on silicon wafers were additionally treated with acetone and methanol before the piranha and UV/ozone treatments. Absolute ethanol, acetone and methanol were also purchased from VWR Prolabo Chemicals, Leuven.

Joints and metal components of the QCM-D were washed in a 2% Hellmanex II solution (Helmma,

France) in an ultrasound incubator. After each experiment, QCM tubes were also rinsed with the same solution.

4 | Methods

4.1 Preparation of polymer brushes

The homopolymer brushes, as well as mixed PDMAEMA/PEO brushes, were prepared following the simultaneous "grafting-to" approach, as outlined in Fig. 23. First, solutions of single polymers or randomly mixed chains were prepared. For a ratio of PDMAEMA/PEO equal to 30/70 in volume in the grafting solution, the concentration of PDMAEMA was of 0.5 mg ml^{-1} and 450 µl of PEO highly concentrated at 5 mg ml^{-1} was added to 2 ml of PDMAEMA solution. A gold substrate was then immersed in the solution for 15 to 20 min. The polymer chains move through diffusion and randomly attach to the wafer via the reactive thiol groups.

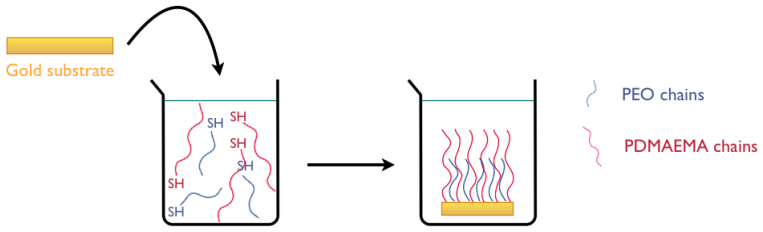

Fig. 23. "Grafting-to" method used to fabricate mixed PEO/PDMAEMA brushes.

The convention PDMAEMA/PEO X/Y will be used throughout this work to describe the ratio in volume of PDMAEMA (X) and PEO (Y) in the grafting solution.

4.2 Surface characterization

4.2.1 X-ray photoelectron spectroscopy

First of all, the surface chemistry of the gold substrates coated with polymer brushes needs to be determined, using X-ray photoelectron spectroscopy (XPS). XPS, also known as electron spectroscopy for chemical analysis (ESCA), is a surface analysis technique that can be applied to a broad range of materials. It allows both qualitative and quantitative knowledge of the chemical composition, and the chemical and electronic states of elements present at the studied surface to be determined. Electrons

from a large area (some mm^2) and from the top 2 to 10 nm of the material are analyzed. The spatial resolution can be as small as 7.5 µm and the depth resolution approaches 1 nm [37] [38].

Working principle

When X-ray photons (typically Al Kα or Mg Kα) carrying energy $h\nu$ are hitting on the sample surface, photoelectrons from the core levels are ejected with a kinetic energy E_k. This phenomenon is called the *photoelectric* or *photoemission effect* and is represented schematically in Fig. 24. The kinetic energy can then be related to the binding energy E_b of the electron, that is the energy required to overcome the Coulomb attraction of the electron to the nucleus.

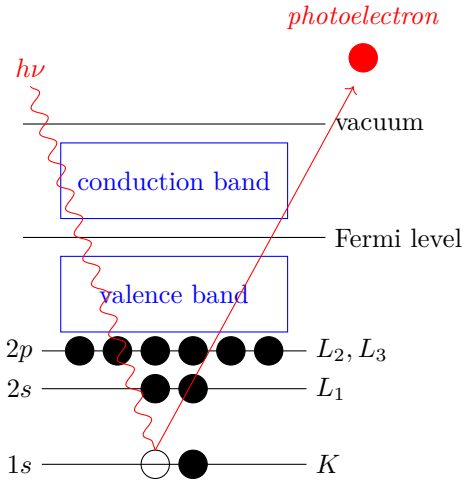

Fig. 24. Photoelectric effect occuring in XPS [39].

Instrumentation

The XPS instrument consists in three main parts illustrated in Fig. 25 : an X-ray source, an electron analyzer and a detector, all enclosed in ultra-high vacuum (less than 10^{-7} Pa) for electron detection and avoiding surface reactions and contaminations.

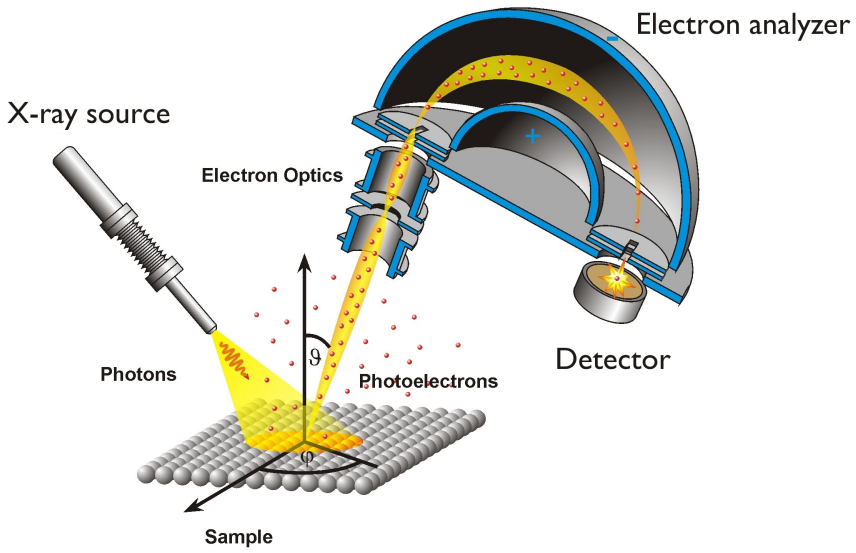

Fig. 25. Main components of an XPS instrument. Adapted from [40].

An X-ray source (commonly Al or Mg X-rays) provides photons that excite photoelectrons from dore levels and from all elements of the periodic table (except hydrogen). A *quartz crystal monochromator* is added to generate a well-defined source of photons. An electrostatic transfer lens system transports and the photoelectrons and refocuses the electrons to increase the throughput. At the entrance of the electron analyzer, the electrons energy has to match its pass energy [38]. Electrons are finally detected by the detector, and a kinetic energy spectrum is recorded.

Data treatment

Ejected electrons are counted over a range of kinetic energies and a photoelectron spectrum is recorded. A wide energy scan immediately gives the chemical composition of the sample ("survey" spectrum), and high resolution spectra allow to determine the atomic levels, the chemical shifts and bonds of the element from which the electrons were emitted. The spectra are given as functions of the binding energy E_b. Moreover, XPS is a quantitative technique, meaning that the recorded intensities of the peaks are proportional to the number of emitting atoms at the analyzed surface [41].

The first step of the analysis is the identification of electrons associated to each binding energy. After the accurate calibration for the energy scale is accomplished by adjusting the $\underline{\mathbf{C}}-$(C,H) component of the C1s peak to 284.8 eV, the peak positions provide this information with the help of reference binding energy values found in tables.

One photoelectric line is often the result of multiple overlapping peaks in a range of energies, representing different chemical states of an element. The second important step is thus to make a peak model that fits the spectral data and has a chemical meaning, so the fit should be guided by the known chemistry of the sample.

Experimental set-up

Five different gold samples were analyzed by XPS : pure gold, PEO, PDMAEMA, and PDMAEMA/PEO 90/10 grafted on gold and dried, as well as a PDMAEMA powder.

XPS measurements were conducted with a Kratos Axis Ultra spectrometer (Kratos Analytical, Manchester, UK) using a monochromatized Al X-ray source. The pressure in the chamber was 10^{-6} Pa. Before the experiment, the samples were dried. They were fixed on the holder with a piece of double-sided insulating tape. The direction of photoelectrons was perpendicular to the sample surface. The pass energy was set to 160 eV for the survey scans and 40 eV for narrow scans. The obtained spectra for each sample were as follows : survey spectrum, C1s, O1s, S2p, Au4f and C1s again to check the charge stability and the absence of degradation with time.

The data treatment in this research was performed with the CasaXPS program (Casa Software Ltd., UK). The spectra were decomposed using linear background lines. Atomic fractions were calculated using the peak areas normalized on the basis of acquisition parameters and sensitivity factors provided by the manufacturer.

4.2.2 Atomic force microscopy

Atomic force microscopy (AFM) is a type of scanning probe microscopies (SPM) providing the topographic map of a surface. Its lateral resolution is quite low (~30 nm), but the vertical resolution can be up to 0.1 nm. AFM requires minimal sample preparation and is a very versatile technique : it detects single molecular recognition events and can be used to measure several physical properties (elasticity, adhesion) [13].

Working principle

A probe with a very sharp pyramidal tip mounted on a cantilever scans over the sampled surface, and attractive or repulsive interactions between the tip and the sample cause the lever to be deflected. Both vertical and lateral deflections are measured. This is measured by reflection of a laser beam from the back of the lever's surface : any change in deflection causes a change in the direction of the reflected beam. The latter then strikes a detector sensitive to its position, which generates an image of the topography of the sample. The principle of AFM is represented schematically in Fig. 26.

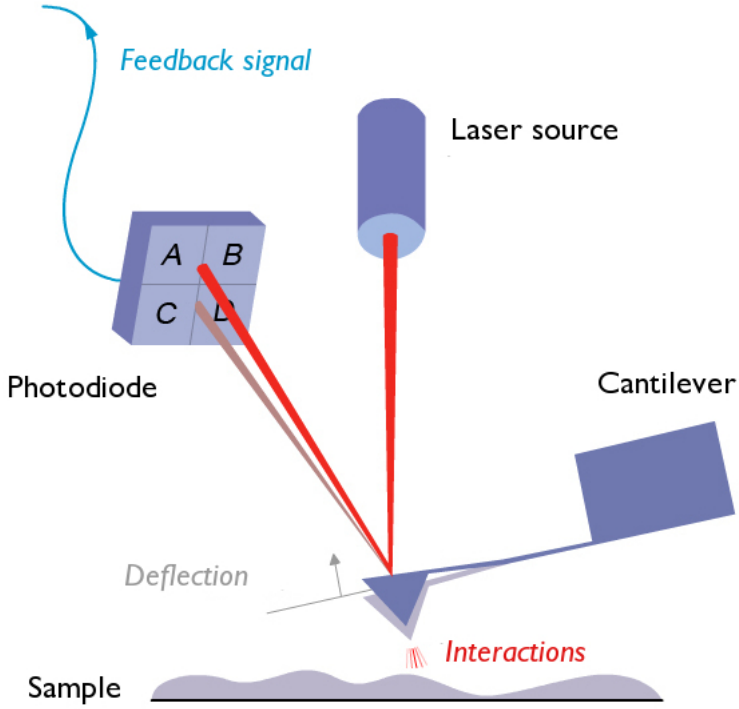

Fig. 26. Main components of an AFM device and working principle.

The system can be operated in three different modes. In *contact mode*, the device uses a feedback loop to adjust the force and the tip height for keeping the deflection constant and the tip moves over the surface. The distance between the tip and the sample is around 1 or 2 Å, which is close to the length of a chemical bond, leading to strong repulsive forces. In *non-contact mode*, the cantilever oscillates, but makes no contact with the surface. As the interatomic separation is higher, attractive forces appear. This mode causes the least disruption, but is not widely used due to the possibility of the tip jumping into contact with the surface because of the attractive forces. In *tapping mode*, the cantilever oscillates and the tip makes intermittent contact with the sample. The feedback loop keeps the oscillation of the tip constant in frequency and in amplitude. Interacting forces in all modes as a function of the distance between the tip and the sample are represented graphically in Fig. 27 [42].

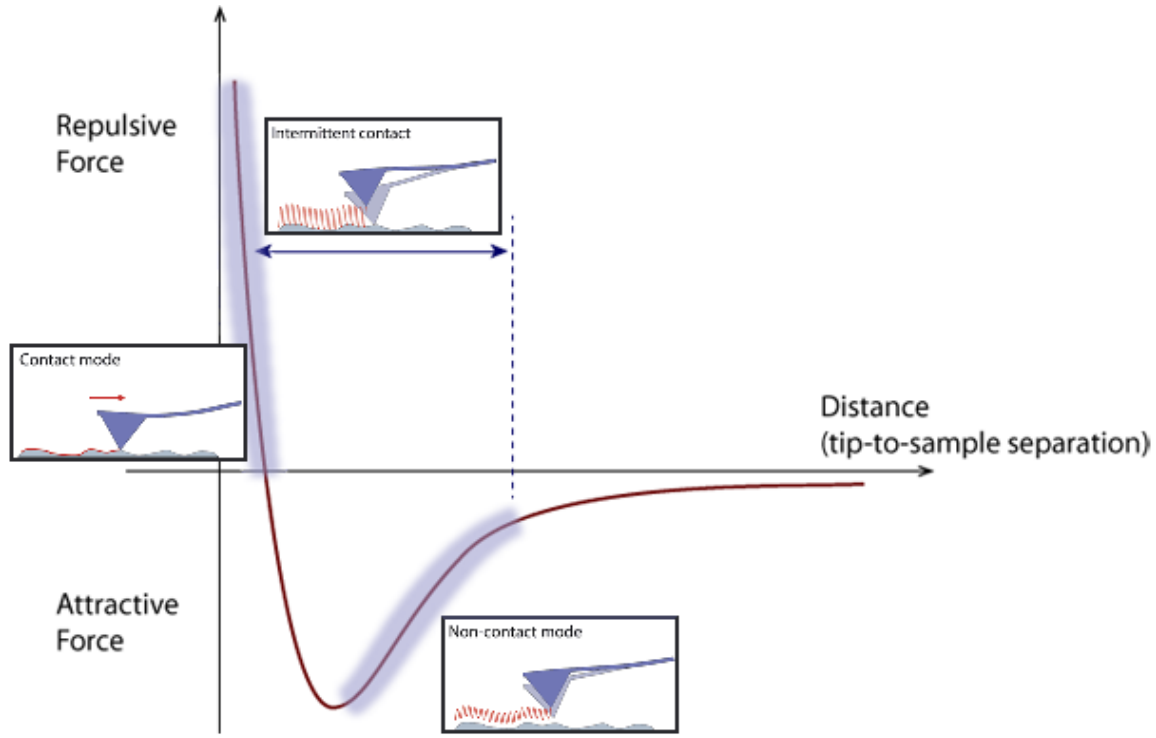

Fig. 27. Interacting force between the tip and the sample as a function of the distance between them. Adapted from [42].

Experimental set-up

AFM measurements were performed in light tapping mode using a Nanoscope IIIa Multimode apparatus (Bruker Nano Inc., Santa Barbara, USA). The samples were attached to the holder with a small piece of double-sided adhesive tape and the experiments were performed at room temperature, in air on dry samples. The obtained images were flattened and processed using the image analysis software Gwyddion (open-source software for SPM data analysis, David Nečas, Petr Klapetek).

4.2.3 Static water contact angle measurements

The wettability of polymer brushes refers to the ability of a liquid to spread out or to adhere to their surface. It is important to assess the hydrophobic or hydrophilic character of the polymer brushes to explain their adsorption and desorption abilities. The wetting can be characterized by measuring the contact angle (θ_C) between the solid surface and the profile of a deposited liquid drop.

The contact angle depends on the balance between cohesion and adhesion forces between the liquid and the solid surface. A contact angle larger than 90° indicates the wetting is unfavorable and the liquid minimizes contact with the surface : it is hydrophobic. On the other hand, a contact angle smaller than 90° means the wetting is favorable and the liquid spreads out on the hydrophilic surface. This is illustrated in Fig. 28) [43].

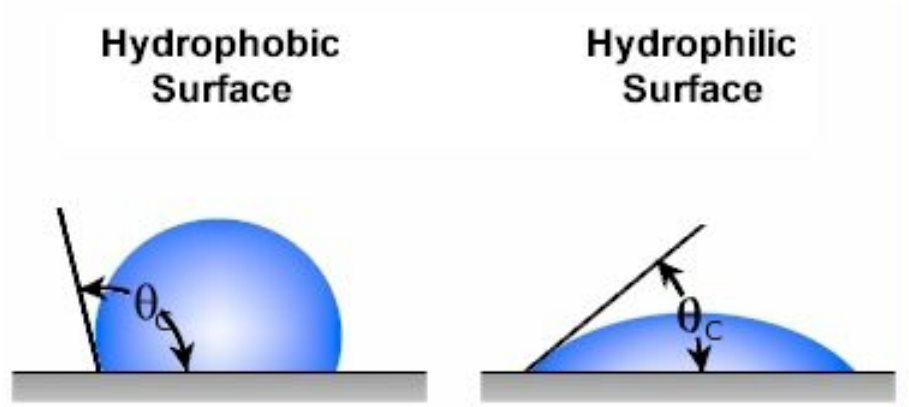

Fig. 28. Contact angle θ_C for hydrophobic and hydrophilic surfaces. Adapted from [43].

Thermodynamic background

Young's equation 4.1 describes the relationship between the contact angle θ_C and three surface tensions keeping the liquid drop in equilibrium, where γ_{lv} is the interfacial tension between the liquid and the vapor phases, γ_{sl} is the interfacial tension between the liquid and γ_{sv} is the solid phases and the interfacial tension between the solid and the vapor phases, also called the surface free energy of the solid phase. They are represented in Fig. 29.

$$\gamma_{sv} - \gamma_{sl} = \gamma_{lv} \cos\theta_C \tag{4.1}$$

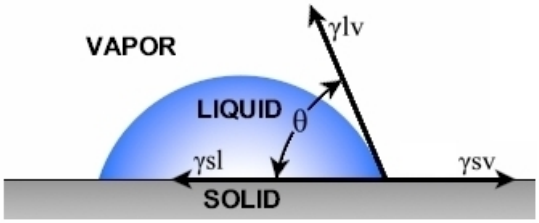

Fig. 29. Interfacial tensions keeping the equilibrium of the liquid drop on the solid surface. Adapted from [44].

Experimental set-up

The static measurements were done using the *surface tension sessile drop method*. It consists in depositing an ultrapure water drop on the sample surface with a syringe and analyzing its profile with a goniometer. The measurements were conducted at ambient temperature. The instrument was purchased from Electronisch Ontwerpbureau De Boer (The Netherlands). The droplet volume was 0.3 µl and the contact angle was measured at 15 s after the deposition. The measurement was repeated on two different samples of each case, at least three times, and the average value of the contact angle was calculated.

4.2.4 Streaming potential measurements

Zeta potential

The distribution of ions in an aqueous solution is affected by the presence of a solid surface or particle. Indeed, free ions in solution rearrange at the surface, where counter ions accumulate and form an *electrical double layer* (EDL) of non-zero net charge : in the inner region of the EDL, called the Stern or compact layer, the ions are immobile, due to the strong electrostatic interaction ; the outer region - the diffuse layer - consists of less firmly attached and mobile ions. Within the diffuse layer, a boundary exists between ions that travel with the particle and those that do not, called the *slipping plane*. The potential at this boundary is known as the *zeta potential* or ζ potential (cf. Fig. 30) [45].

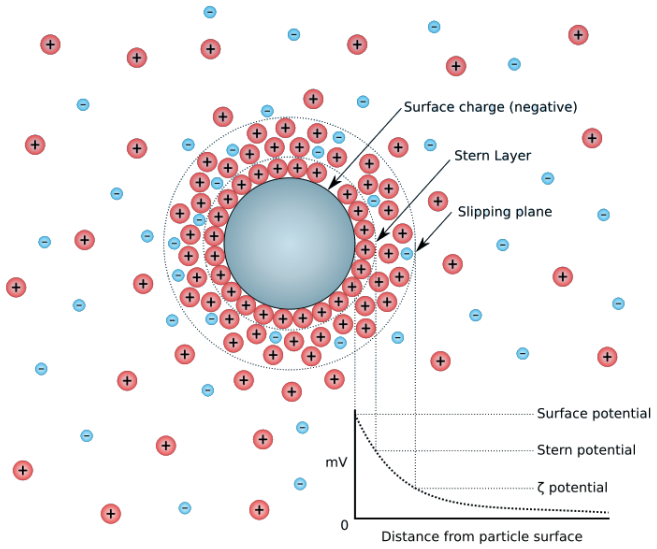

Fig. 30. Graphical representation of the electrical double layer and the zeta potential on a colloidal particle [45].

The ζ potential gives an indication on the stability of the colloidal system. If all particles have a large zeta potential, they tend to repel each other and not to flocculate. However, when the zeta potential is low, there is no force preventing the particles to come together and aggregate.

The zeta potential is dependent on the pH, so that any zeta potential value should be assigned to a given pH.

Measurement technique

The zeta potential of planar surfaces (polymers, glass) is usually measured through the *streaming potential*. When a liquid is forced through a charged microchannel, the ions in the diffuse layer move and the EDL is subjected to shear, creating a *streaming potential* (cf. Fig. 31).

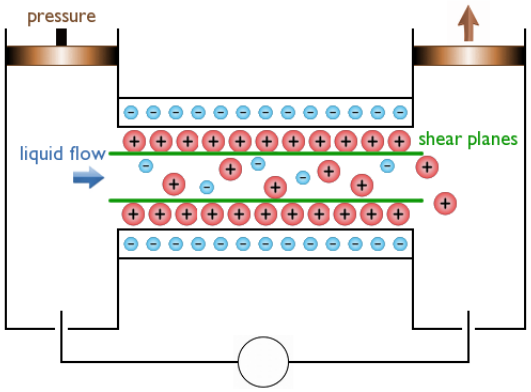

Fig. 31. Principle of streaming potential measurement.

Experimental set-up

Streaming potential measurements were conducted in the J. Haber Institute of Catalysis and Surface Chemistry, Polish Academy of Sciences, in Cracow, Poland. The streaming potential was determined using the set-up shown in Fig. 32 and 33. The whole set-up was placed inside an earthened Faraday cage to avoid disturbances stemming from external electric fields. The cell consisted of two Teflon blocks with two inlet and outlet compartments. The main part of the cell was a parallel plate channel with dimensions $2b_c \times 2c_c \times L = 0.027 \times 0.29 \times 6.2$ cm^3, formed by gold substrates separated by a perfluoroethylene spacer, where b_c and c_c are the defined as half of the cross-section side dimensions of the plate, and L is its length. The electrolyte flows through the cell owing to the regulated hydrostatic pressure difference by changing the height of the conductivity cell and the occurring streaming potential is measured using two Ag/AgCl electrodes, placed in glass tubes connected to the openings of the cell. The overall cell electric conductivity K_e was determined using a pair of Pt electrodes. Keithley 6512 Electrometer with a high input resistance was used, allowing the measurements to be carried out at practically zero current conditions. The other pair of electrodes was used to determine the cell resistance. A series of streaming potential measurements was conducted for four different pressures forcing the flow [46].

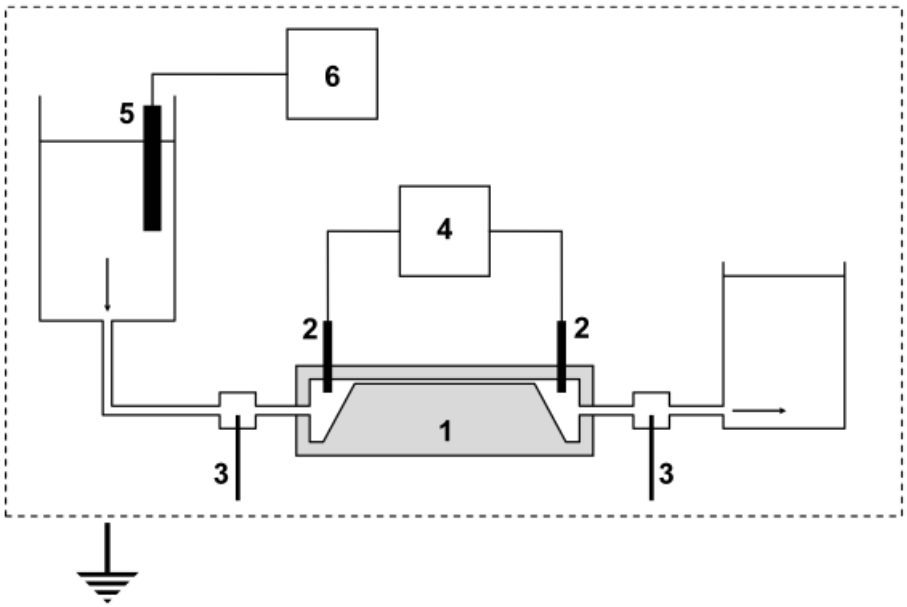

Fig. 32. Schematic view of the experimental set-up used for the streaming potential measurement : (1) the cell; (2) electrodes for streaming potential measurements; (3) electrodes for cell resistance measurements; (4) electrometer; (5) conductivity cell; (6) conductometer [46].

First, the streaming potential of the gold substrate was measured at I= 10^{-3}M and pH 7.4 to observe further changes with the coatings. Next, the channel was filled with a PDMAEMA solution having a concentration of 0.5 mg ml^{-1} and a natural pH, covering the gold surface in the cell. The deposition time was 20 min, keeping the flow rate low in order to create diffusion-controlled transport conditions. Then NaCl at I= 10^{-3}M was forced through the channel from different heights (different pressures) and the streaming potential measurements were performed.

The same experiment was then performed with a solution of PDMAEMA/PEO 30/70 in order to observe the effect of PEO on the surface charge. Finally, the HSA solution (0.2 mg ml^{-1}) was flushed to observe a ζ potential variation upon protein adsorption on the mixed brushes [46].

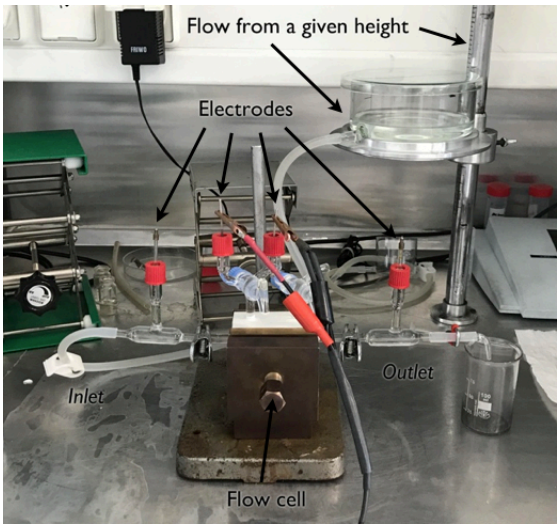

Fig. 33. Photography of the experimental set-up used for the streaming potential measurement. Courtesy of the *J. Haber Institute of Catalysis and Surface Chemistry, Polish Academy of Sciences* in Cracow, Poland.

Data treatment

The streaming potential E_S was measured as a function of the hydrostatic pressure ΔP of driving electrolyte flows through the channel and the slope of this dependence was measured. Knowing K_e, the apparent ζ potential of a substrate surface was calculated from the Smoluchowski relationship, where η is the dynamic viscosity of the solution, ε is the dielectric permittivity, and R_e is the net electric resistance of the cell.

$$\zeta = \frac{\eta L}{4\epsilon b_c c_c R_e}\left(\frac{\Delta E_S}{\Delta P}\right) = \frac{\eta K_e}{\epsilon}\left(\frac{\Delta E_S}{\Delta P}\right) \qquad \text{(Smoluchowski equation)}$$

4.3 Protein adsorption and desorption monitoring

4.3.1 Quartz crystal microbalance with dissipation monitoring

Quartz crystal microbalance (QCM) enables to monitor in situ and in real time the formation of polymer brushes and the adsorption of proteins on a quartz crystal with gold electrodes. The experimental set-up and the QCM instrument are shown in Fig. 34.

Fig. 34. Quartz crystal microbalance instrument, with four operating cells containing quartz crystals [47].

Frequency measurement

Quartz possesses a combination of properties making it the most suitable material for QCM. It can be grown at low cost with relatively high purity and perfection, it is easy to process and is Earth's second most abundant mineral. Concerning mechanical properties, quartz is hard, but not brittle [48].

However, it is mostly chosen as a material in instruments containing oscillators because it exhibits the *piezoelectric effect*. Piezoelectricity is the ability of a material to generate a mechanical strain upon the application of an electrical potential. Indeed, each quartz crystal has a different vibrational mode which causes shear deformation under an applied voltage, as shown in Fig. 35.

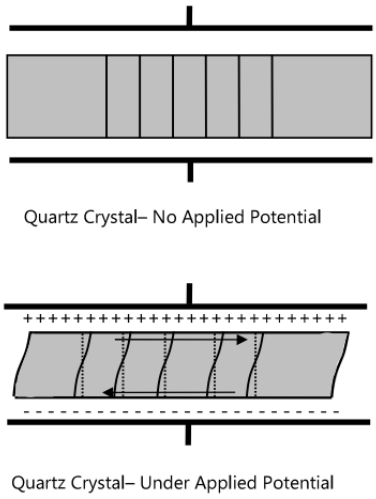

Fig. 35. Graphical representation of thickness shear deformation of a quartz crystal [49].

An alternating potential induces the oscillation of the crystal at its resonance frequency f_0, given in equation 4.2, where μ_q is the shear modulus, ρ_q is the density and t_q is the thickness of the crystal [49].

$$f_0 = \frac{1}{2t_q}\sqrt{\frac{\mu_q}{\rho_q}} \tag{4.2}$$

The frequency decreases or increases if any small amount of matter is adsorbed or removed from the surface. It is then possible to correlate those changes in frequency with changes in mass, using a linear relationship between them, brought out by Sauerbrey in 1959 [50].

$$\Delta m = -C_f \frac{\Delta f_n}{n} \qquad \text{(Sauerbrey relation)}$$

where Δm and Δf_n are the changes in mass and normalized frequency respectively, and C_f is a calibration constant depending on the overtone number n, usually close to $17.7\,\mathrm{ng\,cm^{-2}\,s^{-1}}$.
This equation is valid under three assumptions : the adsorbed layer is sufficiently thin compared to the quartz crystal, it is rigidly adsorbed and evenly distributed over the active area of the crystal [50].

Dissipation monitoring

Quartz crystal microbalance with dissipation monitoring (QCM-D) also provides information about the viscoelastic properties of the adsorbed layers, by measuring the dissipation of the quartz crystal. Dissipation occurs when the driving potential is shut off and the oscillating crystal dissipates energy, and is defined as D according to Eq. 4.3.

$$D = \frac{E_{lost}}{2\pi E_{stored}} \tag{4.3}$$

where E_{lost} is the energy lost during one oscillation cycle, and E_{stored} is the total energy stored in the oscillator. Figure 36 shows the dissipation when the voltage is turned off. This procedure is repeated

hundreds of times per second. If the adsorbed layer is rigid, the damping is slower and the dissipation is lower, while a soft film presents a faster damping and a higher D [50].

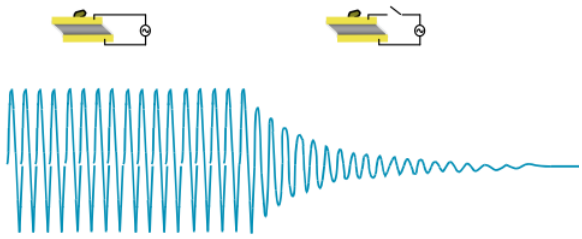

Fig. 36. Dissipation signal generated by turning off the driving potential across the crystal [50].

Experimental set-up

The Q-Sense E4 System instrument was purchased from Gothenburg, Sweden. All experiments were conducted at 20 °C. First, a stable baseline for ultra-pure water was obtained, before introducing the polymer solution to form a brush. Loosely bound polymer molecules were then removed by ultra-pure water. Before each protein introduction at I= 10^{-3}M and pH 7.4, a saline solution of NaCl at the same pH and ionic strength as the protein solution was flushed. Protein adsorption was maintained until stable signals - a plateau - were obtained. The desorption process consisted of four stages : rinsing with an NaCl solution at the same pH and ionic strength as for the protein adsorption, rinsing with ultra-pure water, desorption with a saline solution of 0.15 M NaCl at pH 9.0, and a final rinsing step with ultra-pure water.

Water and salt solutions were always flowed into the measurement cells with a flow rate at 50 µl min^{-1}, while polymers and proteins were flowed at 25 µl min^{-1}.

Fig. 37 shows the frequency graph of a typical experiment. To estimate the mass of polymer, the frequency change Δf_P was measured by comparing the ultra-pure water baseline to the water introduction step after polymer attachment. The mass of adsorbed proteins was calculated from the variation of frequency Δf_a by comparing frequencies at NaCl steps before and after protein introduction. Finally, the desorption percentage ($\%_{desorption}$) was calculated as :

$$\%_{desorption} = \left(1 - \frac{\Delta m_{desorption}}{\Delta m_{adsorption}}\right) \times 100 \tag{4.4}$$

where $\Delta m_{desorption}$ is the remaining mass of proteins after the desorption steps, calculated from the frequency shift Δf_d.

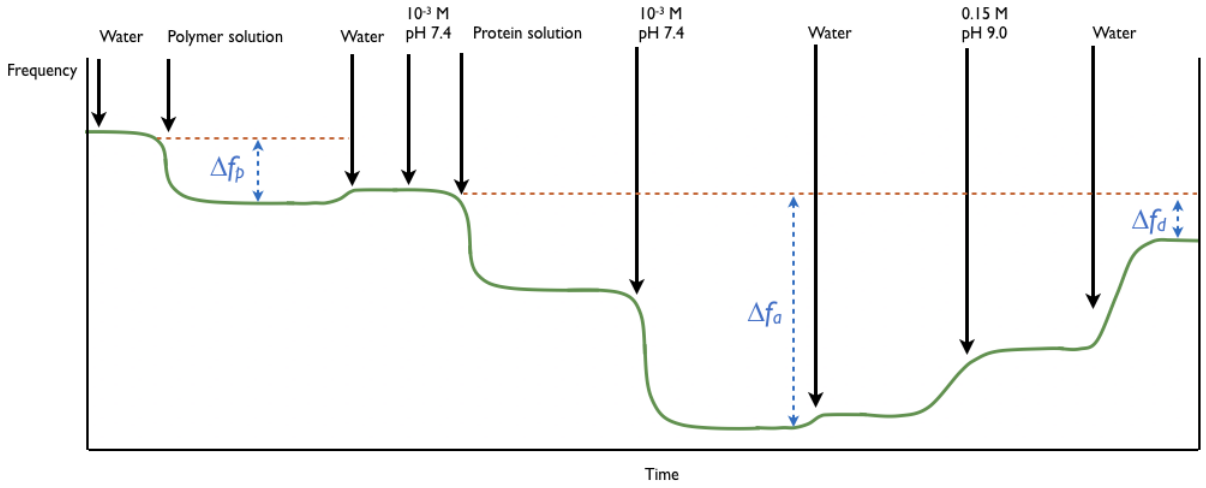

Fig. 37. Typical QCM graph of a protein adsorption/desorption onto polymer brushes.

The masses per unit area at different stages of the experiment were computed using the Sauerbrey equation via the QStomize software. All QCM-D monitoring graphs presented show the 7th overtone.

4.3.2 Time-of-flight secondary ion mass spectrometry

Time-of-flight secondary ion mass spectrometry (ToF-SIMS) provides information about elemental and molecular surface composition. A three-dimensional analysis of a surface may also be obtained, as well as chemical imaging. This technique analyzes the uppermost 1 or 2 nm and is best suited for ultra-thin layers and nanoscale sample features. The spatial resolution is less than 0.1 µm. The results are considered semi-quantitative, but the sensitivity is very high, allowing to detect trace elements on the order of ppm to ppb. The purpose of using ToF-SIMS in this research is to identify the proteins adsorbed on polymer brushes from mixtures [51].

Working principle

The ToF-SIMS instrument is composed of three main components in an ultra-high vacuum to allow a good transportation of ions : a particle gun, the flight path and the mass detector. They are shown in Fig. 38.

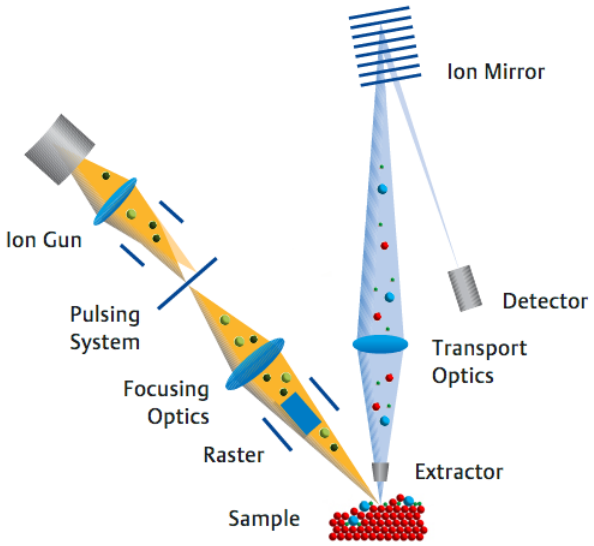

Fig. 38. ToF-SIMS main components and trajectory of primary and secondary ions. Adapted from [52].

A fine pulsed ion beam (typically Cs, Ga, Bi or C_{60}) strikes the surface of the material and leads to a cascade of collisions. Chemical species from the outermost surface are dislodged. Particles removed from the closest sites from the highly energetic collisions are mainly dissociated ions, while particles generated from farther sites tend to be larger molecular fragments. Particles from the 2-3 outermost monolayers have sufficient energy to overcome the surface binding energy and leave the sample [52]. They are positively or negatively ionized and are called secondary ions. They are then accelerated by an electrostatic field into a flight path up until the detector.

ToF-SIMS is based on the fact that ions with same energies but different masses travel with different velocities : lighter ions fly with a higher velocity than heavier ions. It is then possible to measure their mass on a scale of nanoseconds from the exact time ("time-of-flight") at which they reach the detector and to yield positive and negative secondary ion mass spectra. This cycle is repeated at a rate of 50 kHz [51].

Experimental set-up and data processing

An IonTof V (IONTOF GmbH, Münster, Germany) instrument was used in this study. Bi_3^{++} liquid metal ions were used to produce the primary beam with an energy up to 60 keV. The experiment was operated in ultra-high vacuum in the chamber, around 10^{-7} Pa, to avoid undesired collisions and allow a good transportation of particles through the path. Data and spectra processings were carried out using the SurfaceLab 6.1 software supplied with the instrument.

Principal component analysis

The data obtained with ToF-SIMS consists in n samples with m peaks on their spectrum, which can rise up to hundreds of ion peaks. In this study, a main list of 55 peaks corresponding to positive ions was selected and used in the analysis. Interpreting these spectra to obtain some chemical information can be a great challenge. Multivariate statistical methods are a valuable tool to make the analysis easier. *Principal component analysis* (PCA) is the most widely used because of its established history and wide availability [53]. This technique is used to reduce the dimensionality of data with a minimal loss of information. In other words, it reduces the hundreds of individual ion peaks that the analyst must interpret to only a few components. To achieve this, the data is represented in a new set of variables, called *principal components* (PC), which aid in identifying how the original variables are correlated. PCs are linear combinations of the peaks intensities.

The $n \times m$ data is arranged into a centered data matrix $\mathbf{X}$, where each row contains the spectrum of a sample and each column contains the intensity of an individual peak.

$$\mathbf{X} = \begin{bmatrix} x_{11} & \dots & x_{1m} \\ \vdots & \ddots & \vdots \\ x_{n1} & \dots & x_{nm} \end{bmatrix} \tag{4.5}$$

Prior to PCA, various pre-processing techniques are applied to the data. First, the data were normalized, in this study by dividing the spectra by the total intensity of all peaks. Second, the data is centered around the origin by subtracting the mean of the data for each variable, a process called *mean centering* and illustrated in Fig. 39. After pre-processing of data, the principal components are to be determined.

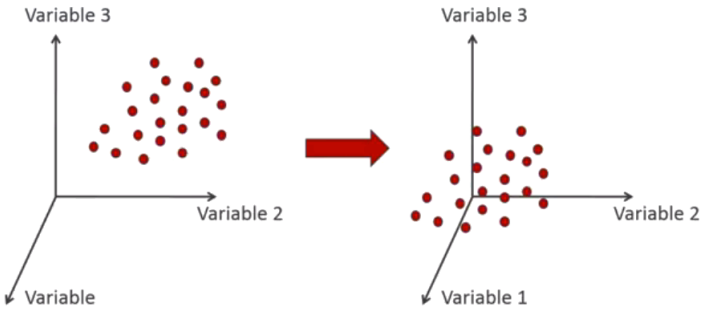

Fig. 39. Mean centering pre-processing method in PCA.

The first principal component, PC1, is chosen as the direction of greatest variance in the data, that is where the data is the most spread out. The second PC is chosen the same way, while being orthogonal to PC1. To represent the data as a function of PC1 and PC2, a hyperplane is formed from the principal components and the data is projected onto it. Fig. 40 illustrates how the principal components are defined.

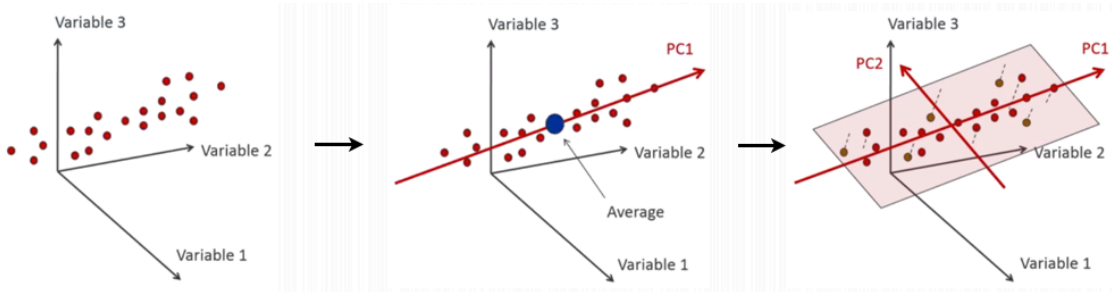

Fig. 40. Principal components determination.

The distance from the mean along the PC is called a *score* (see Fig. 41) of a data point and the weight of a variable in the linear combination is its *loading*. In other words, the loading shows to how much a variable contributes to a principal component.

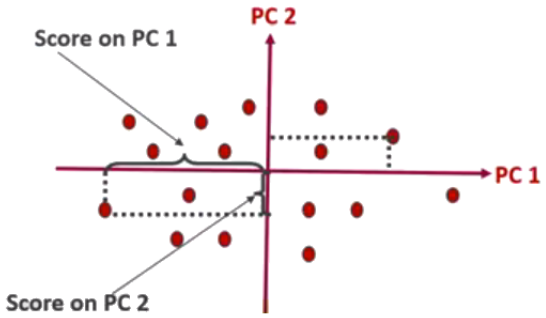

Fig. 41. Illustration of scores of a data point in PCA.

All PCA computations were performed on MATLAB (The MathWorks Inc. 2013, Natick, USA) using the NESAC/BIO Toolbox (Daniel J. Graham, Washington University). The confidence intervals on all scores plots are equal to 95%.

Part III

Results and discussions

5 | Polymer brush characterization

The first step of the study was to design stimuli-responsive mixed polymer brushes. This chapter reports on the use of different methods to monitor their formation on the gold substrate, and to characterize the properties related to their ability to adsorb proteins. First, the atomic and functional composition of the brushes was analyzed by XPS, while the topography of the surfaces was observed by AFM. Then, the hydrophilic/hydrophobic properties, and the surface charge of the coatings was examined by static water contact angle and streaming potential measurements respectively. Finally, the polymer brushes were characterized by ToF-SIMS measurements with principal component analysis in order to determine characteristic peaks of the polymers for further analysis of proteins adsorbed on the brushes.

5.1 Atomic and functional composition

The five different samples analyzed by XPS were the following :

- Pure gold ;
- PEO homobrushes grafted on gold and dried ;
- PDMAEMA powder ;
- PDMAEMA homobrushes grafted on gold and dried ;
- PDMAEMA/PEO 90/10 grafted on gold and dried.

The powder of PDMAEMA was analyzed to observe the differences between the polymer composition before and after grafting on gold.

5.1.1 Atomic composition

The atomic composition of the different brushes is given in Fig. 42.

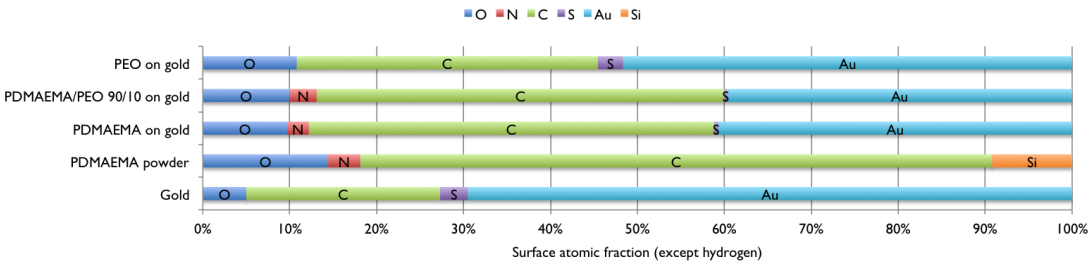

Fig. 42. Atomic composition of homo- and mixed polymer brushes measured by XPS.

First, the successful grafting of the PEO homobrush on gold can be evidenced by the higher O and C amount and the lower Au fraction compared to the pure gold substrate.

It can also be noticed that the compositions of PDMAEMA and PDMAEMA/PEO are very similar. This suggests that the mixed polymer brush created from a ratio of PDMAEMA/PEO equal to 90/10 in the grafting solution contains mostly PDMAEMA. Nitrogen is present on these samples, which confirms the presence of PDMAEMA brushes on the gold substrate.

Additionnally, the presence of sulfur is detected on grafted polymers. However, no sulfur was detected in the powder of PDMAEMA. The survey spectrum of the powder can be found in Appendice A.2.

Table 5.1 presents theoretical and experimental ratios of elemental surface atomic fractions C/O, C/N and O/N, for PDMAEMA powder and PDMAEMA grafted on the gold substrate. It can be observed that the experimental results do not change significantly between both samples, but they do not always correlate with theoretical values computed from the polymer stoeciometry. While the C/O ratios are fairly close, C/N and O/N are approximately twice higher than the predicted values. Indeed, gold surfaces get easily contaminated, or oxidized, as indicated by the high surface atomic fractions in O and C on the pure gold sample.

Table 5.1. Theoretical ratios of different elements in the PDMAEMA molecule, and the experimental XPS results, for PDMAEMA coated on gold and PDMAEMA powder.

	C/O	**C/N**	**O/N**
Theoretical fraction	4	8	2
PDMAEMA powder	5.0	19.6	3.9
PDMAEMA grafted on gold	4.8	18.6	3.9

A contamination by silicon can also be noticed in the polymer powder, which may originate from the adhesive substance found in the tape used to attach the powder sample to the metallic holder of the XPS instrument.

5.1.2 Peak decomposition

To have a better understanding, it is necessary to analyze the functional composition of the coatings, by decomposing each XPS peak into the chemical states of an element. The complete results from these decompositions are shown in Appendix A.2.

The N 1*s* peak shows that PDMAEMA is well present in the created homo- and mixed brushes. The C−**N** function is expected in the polymer either as such, or in its protonated forms C−$\mathbf{N}^{+}$H. Additionnally, the samples can get contaminated. The decomposition into the different forms of nitrogen was only possible for PDMAEMA powder, while the nitrogen peaks on surfaces coated with PDMAEMA were not easily sufficiently resolved to allow for decomposition. Those peaks are shown in Appendix A.3.

The O 1*s* peak of PDMAEMA was less easy to decompose due to the small shift between its two components (533.4 eV for the simple bond and 531.9 eV for the double bond with C). The **O**=C peak is slightly more intense than the **O**−C one due to oxidation of the molecules. In the powder, this peak also includes oxygen bonds to the silicon contaminants. However, only the **O**−C component was found in PEO, as expected.

The S 2*p* peak was well detected only on the PDMAEMA/PEO sample, and can be decomposed into two doublets assigned to bound thiolate (S 2*p* 3/2 at E_b =162 eV) and unbound thiol (S 2*p* 1/2 at E_b =163 eV) in a ratio of 2:1. The decomposition of the peak shows that PDMAEMA and PEO were well grafted on the gold substrate, even though some physisorbed species may also be present on the substrate [13].

Table 5.2. Binding energies of different carbon chemical states [54].

Carbon attribution	**Binding energy [eV]**
C-(C,H)	284.8
C-**C**OO	285.4
C-N	286.1
C-O	286.3
O-**C**=O	289.0

Finally, the carbon 1*s* peak was decomposed into 5 different components, grouped in 3 states of similar binding energies, as shown in Table 5.2. Pure PEO brushes are characterized by a larger **C**−O peak due to their high amount of oxygen in an ether function, compared to PDMAEMA and mixed brushes where PDMAEMA is predominant. This peak in PEO is clearly seen on the high resolution spectrum in Fig. 43. In PDMAEMA and mixed brushes, the carbons singly bound to carbon or hydrogen (**C**−(C,H)) are predominant, as seen in Fig. 44a and 44b. However, when obtained proportions between different states are compared to the theoretical ones, a lack of the **C**−(N,O) function, or an excess of O−**C**=O and **C**−(C,H) functions can be concluded. This can be explained by a degradation of PDMAEMA during the measurements (e.g. manipulation, drying), or a contamination of the samples during the synthesis of polymers and the experiment.

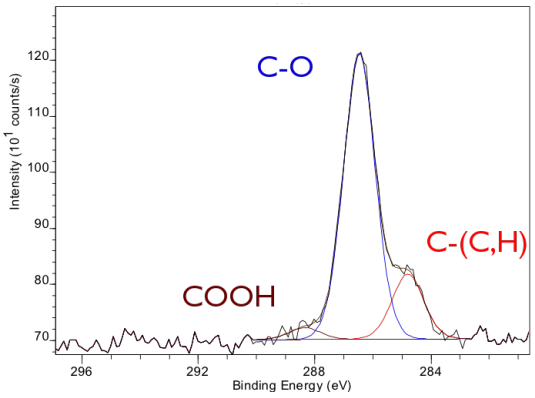

Fig. 43. PEO brush on gold : XPS decomposition of the carbon peak C 1*s*.

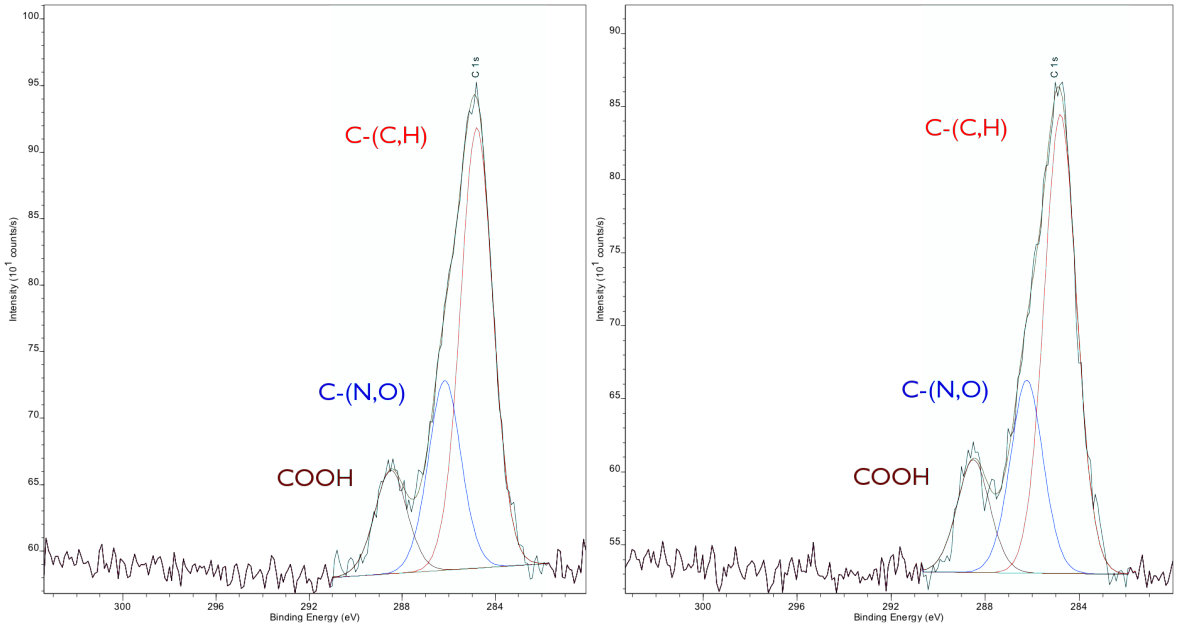

(a) PDMAEMA brush on gold. **(b)** PDMAEMA/PEO 90/10 mixed brush on gold.

Fig. 44. XPS decomposition of the carbon peak C 1*s*.

5.2 Topography

The topography of the homopolymer brushes of PDMAEMA and PEO and mixed polymer brushes grafted on gold substrates was observed by atomic force microscopy. The results are shown in Fig. 45. In all cases, only the roughness of the gold grains can be seen. Pure gold was not analyzed in this study, but previous works often report such rough surfaces. The actual presence of polymer brushes was however confirmed by XPS, streaming potential and QCM measurements. Therefore, it can be assumed that the polymer brushes are very thin, and that no aggregates are present.

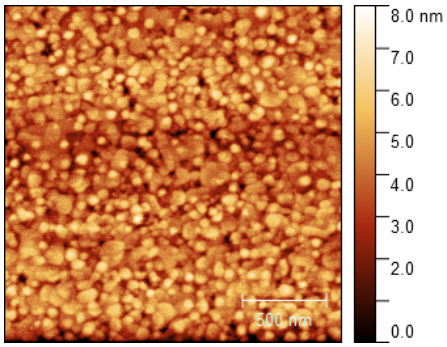

(a) PDMAEMA on gold.

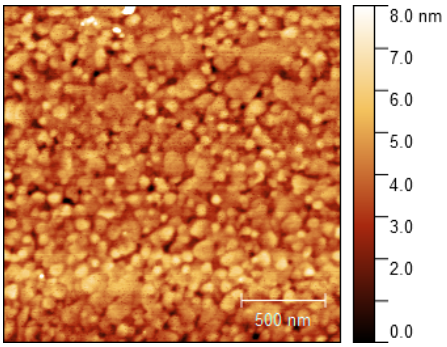

(b) Mixed PDMAEMA/PEO 30/70 on gold.

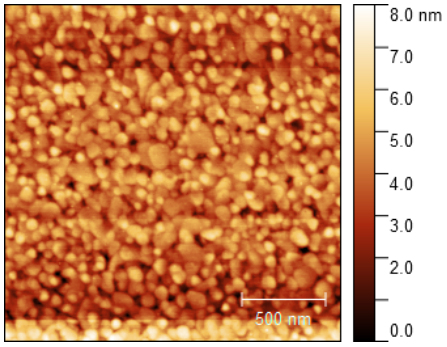

(c) PEO on gold.

Fig. 45. Topography of polymer brushes on a gold substrate by AFM.

5.3 Wettability

Static water contact angle measurements were performed in order to determine the wetting properties of the coatings, at natural pH. The results are shown on the chart in Fig. 46.

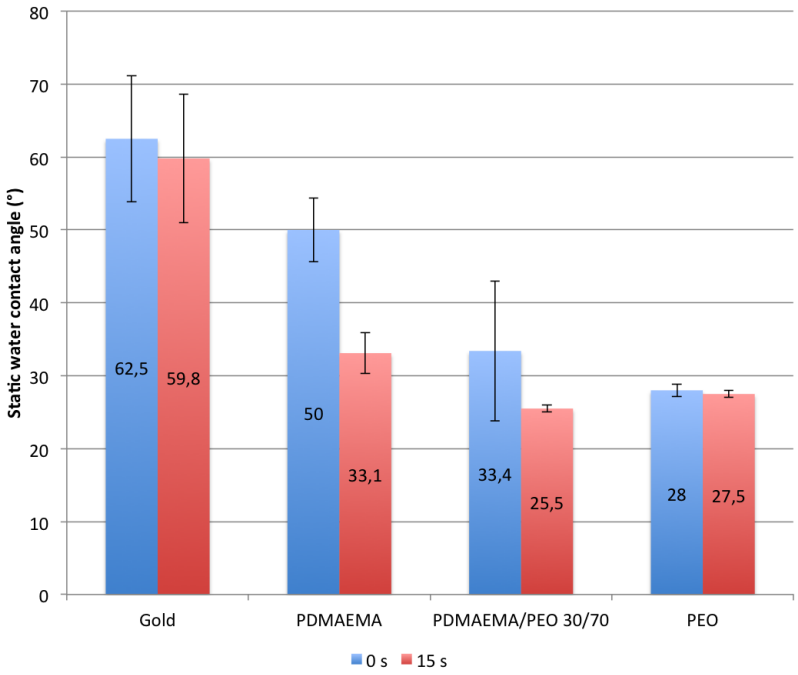

Fig. 46. Static water contact angles [degree] measured for surfaces of gold, brushes of PDMAEMA, PDMAEMA/PEO 30/70, and PEO, right after the sessile drop deposition (0 s - blue) and after 15 seconds (red).

Droplets with lower contact angles were formed on more hydrophilic surfaces. The unmodified gold substrate showed a water contact angle around 60°. After modification with PDMAEMA brushes, the contact angle decreased to ~33.1°, 15 s after deposition. As expected, PEO showed the lowest contact angles due to its highly hydrophilic nature, which forms a hydration barrier to the binding of proteins. The results obtained on mixed polymer brushes of PDMAEMA/PEO 30/70 are very close to the ones of pure PEO, suggesting that the presence of PEO affects their wetting properties by making the surface more hydrophilic, which can help to reach more protein desorption.

5.4 Surface charge

The streaming potential E_S was measured for surfaces of PDMAEMA, mixed PDMAEMA/PEO 30/70 and PDMAEMA/PEO 30/70 with adsorbed HSA, at I= 10^{-3} and pH 7.4. From graphs of the dependence of E_S and the hydrostatic pressure ΔP, the ζ potential can be calculated from the Smoluchowski equation. The results are plotted in Fig. 47. The potential on PDMAEMA shows a positive value, and the change is negligible for mixed PDMAEMA/PEO brushes. As expected, protonation of PDMAEMA gives a positive surface potential, and this may allow for negatively charged proteins to be adsorbed on the surface.

After adsorption of HSA, the ζ potential changes from 37 mV for the brush to −13 mV. This shows that HSA is effectively adsorbed on the brush, and that the resulting layer is negatively charged.

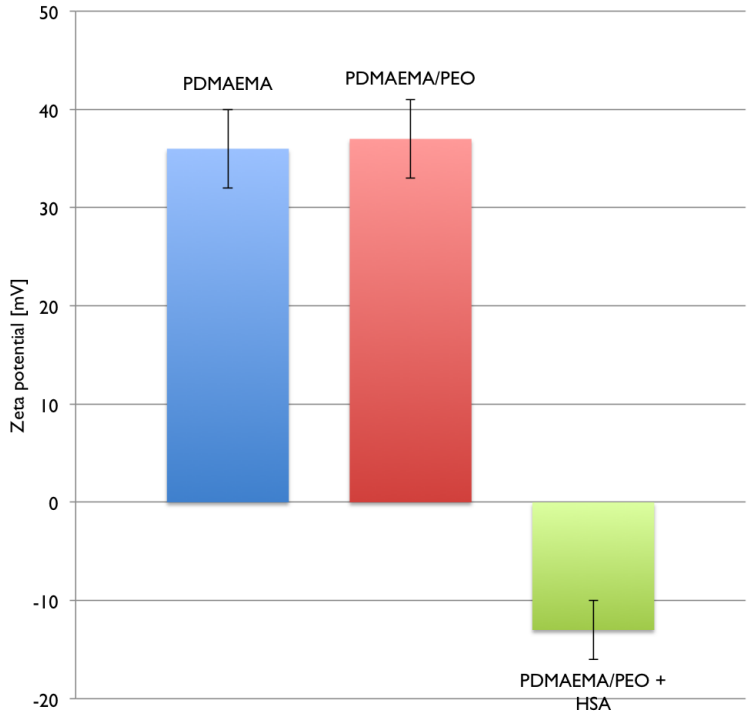

Fig. 47. Zeta potential [mV] measured for brushes of PDMAEMA (blue), PDMAEMA/PEO (red) and PDMAEMA/PEO with adsorbed HSA (green).

5.5 ToF-SIMS

Gold surfaces coated with PEO, PDMAEMA, and PDMAEMA/PEO 90/10 were analyzed by ToF-SIMS in order to find their specific peaks. They are also compared with a sample of pure gold. Each peak obtained with ToF-SIMS corresponds to the presence of a molecule fragment or a compound of specific mass on the surface. Tables 5.3 and 5.4 show the principal positive peaks attributed to PEO and PDMAEMA found in the literature [56, 55].

Table 5.3. PEO positive fingerprints [56].

Fragment	m/z
CH_3O^+	31
$C_2H_3O^+$	43
$C_2H_5O^+$	45
$C_3H_3O^+$	55
$C_3H_5O^+$	57
$C_3H_7O^+$	59
$C_4H_7O^+$	71
$C_3H_5O_2^+$	73
$C_4H_9O^+$	73
$C_4H_7O_2^+$	87
$C_4H_9O_2^+$	89

Table 5.4. PDMAEMA positive fingerprints [55].

Fragment	m/z
$(CH_3)_2N^+$	44
$(CH_3)_2NCH_2^+$	58
$(CH_3)_2NCH_2CH_2^+$	72

A principal component analysis was first run for a pure gold surface, PEO, PDMAEMA and PDMAEMA/PEO 90/10, based on a list of 317 positive peaks in order to minimize the loss of information. The scores plot of PC1 and PC2 is shown in Fig. 48.

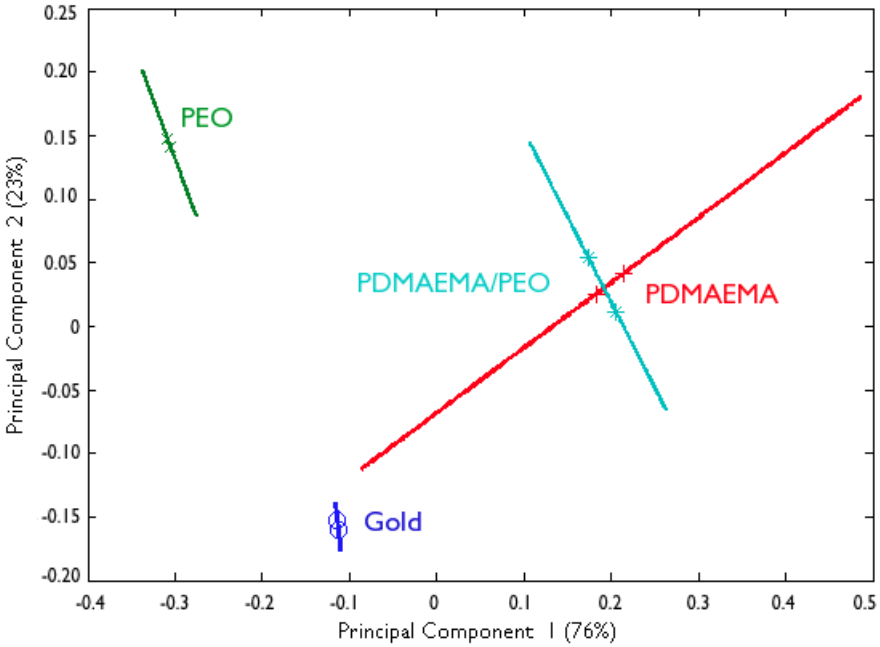

Fig. 48. Scores plot of gold surfaces coated with PEO, PDMAEMA, PDMAEMA/PEO 90/10 and a pure gold substrate.

76% of the total variability is described by the first principal component. PC1 allows to distinguish surfaces containing PDMAEMA (positive score) from gold and gold covered by PEO (negative score). The predominance of PDMAEMA (90% in the grafting solution) in the mixed polymer brush explains the presence of both brushes in the same region. PC2 collects 23% of the data variance and permits to differentiate pure gold from PEO. There is thus a marked difference in their signals, further inves-

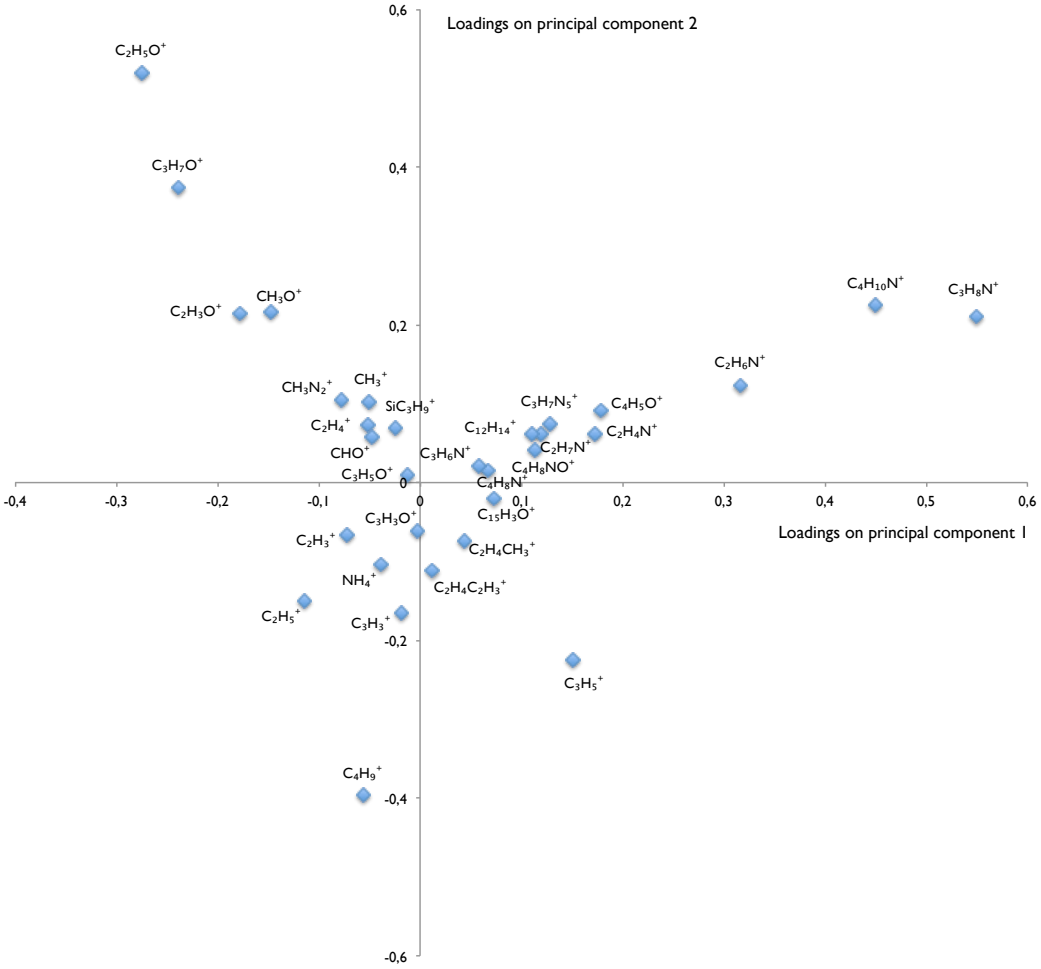

Fig. 49. PC1 and PC2 loading plots for gold surfaces coated with PEO, PDMAEMA, PDMAEMA/PEO 90/10 and a pure gold substrate.

tigated by looking at the loadings.

Fig. 49 presents the loadings of PC1 and loadings of PC2, which show the contribution of each peak to a principal component. Fragments present in a significantly higher amount in one of the samples will be located in the loadings plot as the corresponding polymers in the scores plot. Conversely, peaks that are close to the center of the graph do not contribute to the variation in any of the principal components. Those ones were removed from the plot and 31 peaks were left for analysis. They are presented in Table 5.5 and attributed to one or several of the analyzed surfaces according to the PCA. Characteristic peaks found in the literature (tables 5.3 and 5.4) are indicated in bold in the following table. The PEO peaks associated to $C_4H_7O_2^+$, $C_3H_5O_2^+$ and $C_4H_9O_2^+$ at m/z equal to 71.05, 73.03 and 89.07 g mol^{-1} respectively were found in the 317 original peaks as well.

Table 5.5. Characteristic peaks of the gold surface, PEO and PDMAEMA obtained by ToF-SIMS.

m/z	Fragments	Surfaces
15.02	CH_3^+	PEO
18.03	NH_4^+	Gold
27.02	$C_2H_3^+$	Gold, PEO, PDMAEMA
28.03	$C_2H_4^+$	PEO
29.00	CHO^+	PEO
29.04	$C_2H_5^+$	Gold, PEO, PDMAEMA
31.02	$\mathbf{CH_3O^+}$	**PEO**
39.02	$C_3H_3^+$	Gold, PEO, PDMAEMA
41.04	$C_3H_5^+$	Gold, PDMAEMA
42.03	$C_2H_4N^+$	PDMAEMA
43.02	$\mathbf{C_2H_3O^+}$	**PEO**
43.03	$CH_3N_2^+$	PEO
43.05	$C_2H_4CH_3^+$	Gold, PEO, PDMAEMA
44.05	$\mathbf{C_2H_6N^+}$	**PDMAEMA**
45.03	$\mathbf{C_2H_5O^+}$	**PEO**
45.06	$C_2H_7N^+$	PDMAEMA
55.02	$\mathbf{C_3H_3O^+}$	**PEO**
55.05	$C_2H_4C_2H_3^+$	Gold, PDMAEMA
56.05	$C_3H_6N^+$	PDMAEMA
57.03	$\mathbf{C_3H_5O^+}$	**PEO**
57.07	$C_4H_9^+$	Gold
58.07	$\mathbf{C_3H_8N^+}$	**PDMAEMA**
59.05	$\mathbf{C_3H_7O^+}$	**PEO**
69.04	$C_4H_5O^+$	PDMAEMA
70.07	$C_4H_8N^+$	PDMAEMA
72.09	$\mathbf{C_4H_{10}N^+}$	**PDMAEMA**
73.04	$SiC_3H_9^+$	PEO, PDMAEMA
86.07	$C_4H_8NO^+$	PDMAEMA
113.06	$C_3H_7N_5^+$	PDMAEMA
158.13	$C_{12}H_{14}^+$	PDMAEMA
219.18	$C_{15}H_3O^+$	Gold, PDMAEMA

5.6 Conclusions

XPS was performed on mixed PDMAEMA/PEO 90/10 brushes, and its composition was almost identical to the one of pure PDMAEMA, suggesting a predominance of PDMAEMA on the surface. ToF-SIMS measurements on the same brushes also revealed the same characteristic peaks for both samples, confirming that the same fragments can be found in the mixed polymer brushes.

On the other hand, when less PDMAEMA is present in the grafting solution for the mixed brushes, that is, for PDMAEMA/PEO 30/70, the brushes exhibited some PEO properties. Measurements of the static water contact angle showed that the mixed brushes were as hydrophilic as pure PEO. This confirms that not only PDMAEMA gets grafted from the grafting solution, and suggests an influ-

ence of the amount of PEO present in the grafting solution on the final properties of the mixed brushes.

Furthermore, thin film layers of polymer brushes form on the substrate, as confirmed by topography characterization using AFM. No aggregates were distinguished on the surface
However, streaming potential measurements confirmed that PDMAEMA homobrushes are positively charged, and PDMAEMA/PEO 30/70 brushes showed no significant difference, suggesting that PEO, which is a neutral molecule, does not influence significantly the charge of the brushes. On the other hand, measurements after HSA adsorption showed a change of ζ potential to negative values, indicating effective adsorption.

In conclusion, mixed PDMAEMA/PEO brushes were successfully created by simultaneous grafting onto gold substrates, from polymer chains functionalized with a thiol or disulfide group. Their properties were characterized by various methods, which confirm their ability to present a stimuli-responsive behavior to control protein adsorption.

6 | Switchable properties of polymer brushes toward protein adsorption

The objective of this chapter is to study protein adsorption from single-protein solutions, on stimuli-responsive PDMAEMA/PEO 30/70 brushes at pH 7.4 and ionic strength 10^{-3}M, and to achieve a total desorption by changing these conditions. Then, the obtained QCM results will be presented as a function of the PEO content in the grafting solution.

6.1 Switchable behavior of polymer brushes

PDMAEMA is subjected to conformational changes upon pH and ionic strength changes, and it is important to predict them and choose suitable conditions to optimize protein adsorption and desorption. In low I conditions (10^{-3}M), PDMAEMA chains are protruding for all pH conditions because less counterions can participate to charge screening. PDMAEMA is then positively charged for the whole range of pH until pH 9.0, and therefore is expected to interact with negatively charged proteins at pH 7.4, chosen for protein adsorption.

Upon raising I, PDMAEMA chains are screened by ions from the solution, resulting in a shrunk conformation. In these conditions, PEO chains are believed to be exposed to the outermost surface and repel proteins. Therefore, the chosen adsorption conditions are pH 7.4 and I= 10^{-3}M, and the desorption was be performed at pH 9.0 and I= 0.15M. A scheme in Fig. 50 illustrates these expected PDMAEMA conformational changes upon pH and ionic strength variation, and the resulting brush behavior.

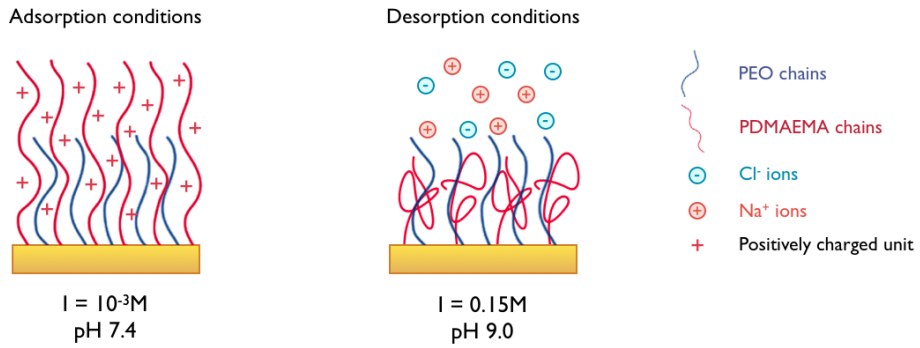

Fig. 50. Scheme of expected PEO and PDMAEMA conformation in the adsorption and desorption conditions of the surrounding medium.

6.2 Protein adsorption and desorption

Protein adsorption on mixed polymer brushes was monitored by QCM-D for HSA, fibrinogen (Fb), lysozyme (Lym) and avidin (Avi). Mixed polymer brushes containing PDMAEMA/PEO 30/70 were used. The time dependence of changes in frequency during the experiments is shown in Fig. 51.

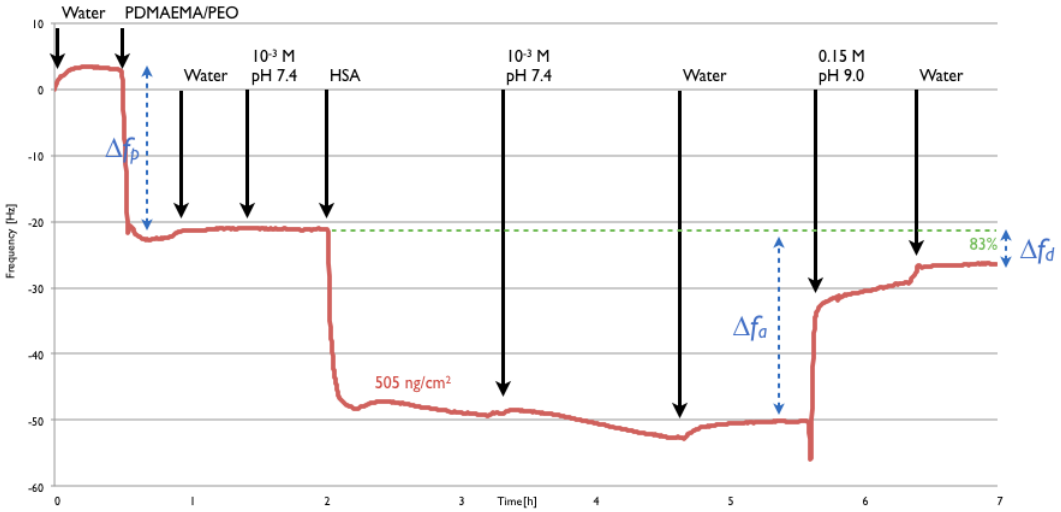

(a) HSA

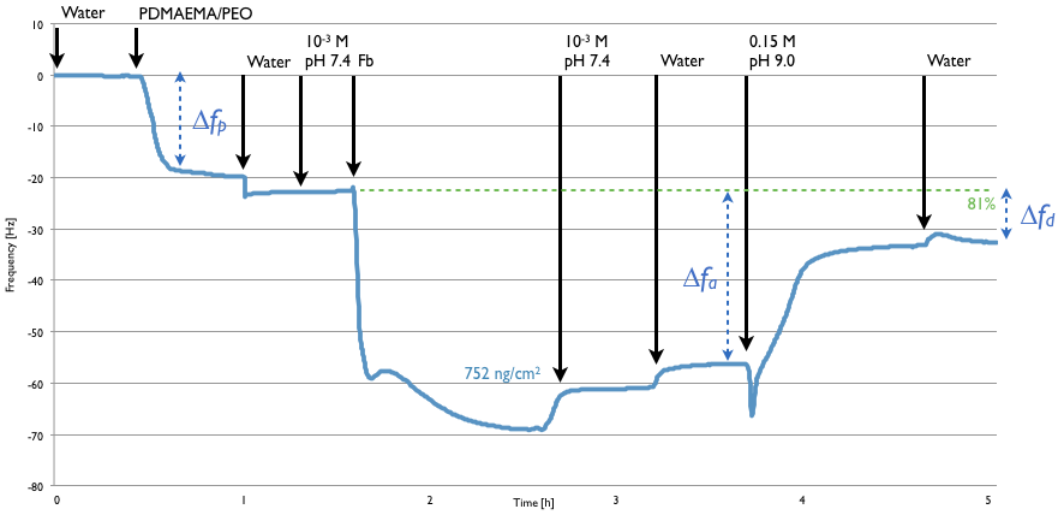
Water
PDMAEMA/PEO
Water
10-3 M pH 7.4 Fb
10-3 M pH 7.4
Water
0.15 M pH 9.0
Water
Δfp
Δfa
Δfd
81%
752 ng/cm²
Frequency [Hz]
Time [h]

(b) Fb

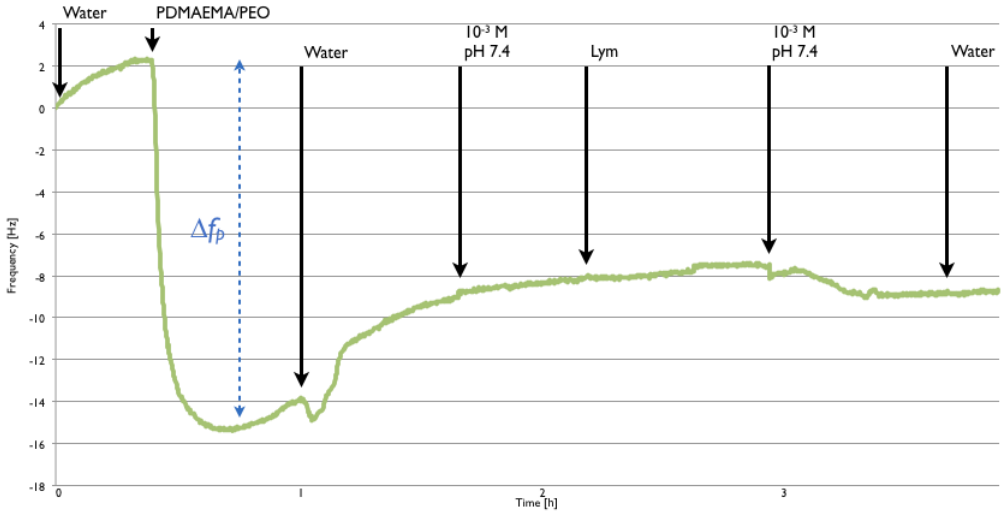
Water
PDMAEMA/PEO
Water
10-3 M pH 7.4
Lym
10-3 M pH 7.4
Water
Δfp
Frequency [Hz]
Time [h]

(c) Lym

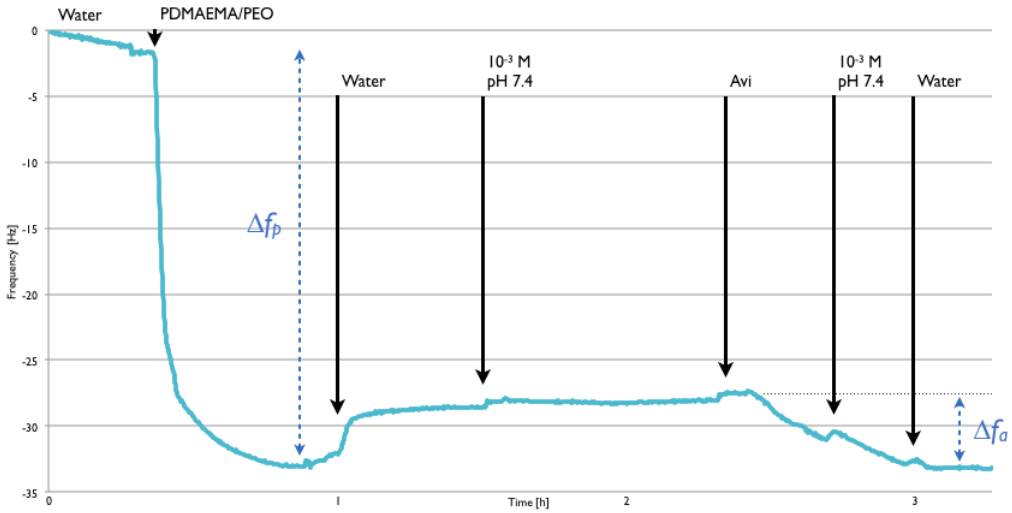

(d) Avi

Fig. 51. QCM graph of PDMAEMA/PEO 70/30 brushes formed on gold surfaces followed by steps of adsorption (I = 10^{-3}M, pH 7.4), and desorption (I = 0.15M, pH 9.0) of adsorbed proteins (cont.).

The first rapid frequency drop (Δf_P) indicates the formation of polymer brushes on the gold-coated crystal. A small subsequent increase is possible, showing the removal of loosely bound chains by rinsing with water. The hydrated mass of polymers per unit area, as estimated at this step by the Sauerbrey equation, is equal to ~473 ng cm^{-2} (this value is the average from several experiments).

At pH 7.4, HSA (iep 4.8) and Fb (iep 5.8) are negatively charged, so they are expected to adsorb on positively charged polymer brushes. On the other hand, Lym (iep 11) and Avi (iep 10.5) are then positively charged and electrostatic repulsion should prevent them from adsorbing on the positively charged surface. The average values of adsorbed masses of proteins after rinsing with NaCl and water are shown in table 6.1, also calculated by the Sauerbrey equation with the frequency shift Δf_a. These results confirm that PDMAEMA brushes are well suited to adsorb large amounts of HSA and Fb, while the adsorption of Lym and Avi is negligible, as expected.

Table 6.1. Average adsorbed mass of proteins on polymer brushes per unit area ($\Delta m_{adsorption}$) and percentage of desorption.

Protein	$\Delta m_{adsorption}$ [ng/cm^2]	$\%_{desorption}$ [%]
HSA	494	83
Fb	1745	81
Lym	25	N/A
Avi	55	N/A

Table 6.1 also presents the desorption percentage ($\%_{desorption}$), calculated as :

$$\%_{desorption} = \left(1 - \frac{\Delta m_{desorption}}{\Delta m_{adsorption}}\right) \times 100 \tag{6.1}$$

where $\Delta m_{desorption}$ is the remaining mass of proteins after the desorption steps, calculated from the

frequency shift Δf_d. The achieved desorption was not total, neither for HSA (83%) nor for fibrinogen (81%), but as protein adsorption is a largely irreversible phenomenon, these values show a good degree of reversibility of adsorption on PDMAEMA/PEO brushes.

6.3 PEO repellent properties

In order to demonstrate PEO repellent properties, QCM-D was also used to analyze the dependence of its amount in the grafting solution on protein adsorption and desorption. Polymer brushes with various proportions of PEO and PDMAEMA in the grafting solution were grafted on the QCM quartz crystal, and adsorption of HSA and Fb was performed from single protein solutions on each polymer brush. Charts in Fig. 52a and 52b show the results from these experiments. As the percentage of PEO in the grafting solution increases, the adsorbed masses of both proteins decrease, with an almost linear trend for HSA. The percentage of desorbed proteins increases with increasing PEO fraction in the grafting solution. It can be assumed that the more PEO is contained in the grafting solution, the more PEO is present in the mixed brushes. Moreover, previous studies on PEO have shown that pure PEO inhibits protein adsorption.

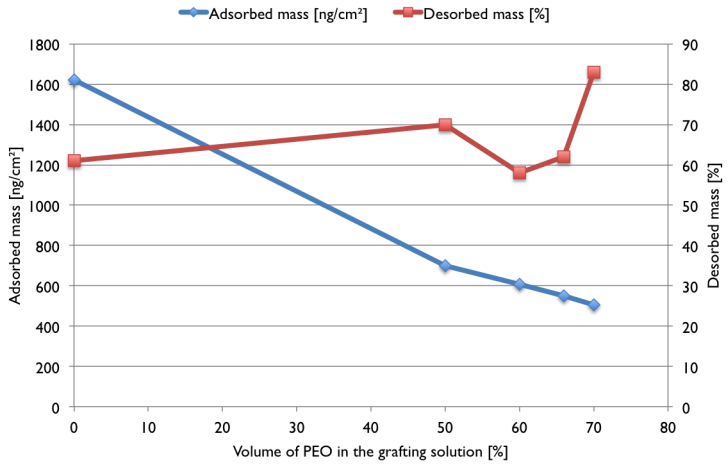

(a) HSA

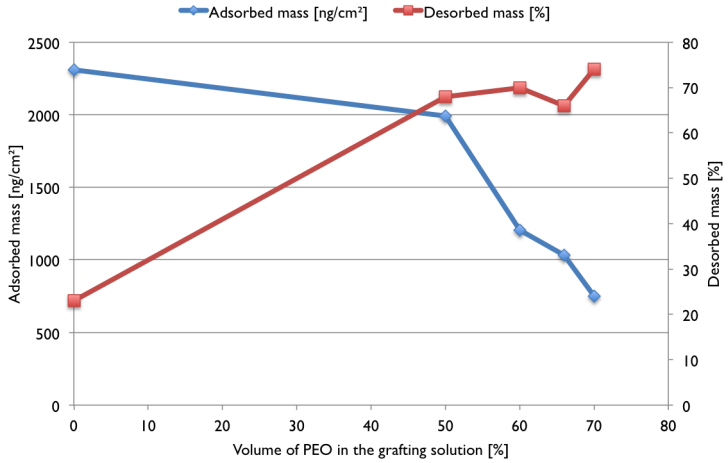

(b) Fb

Fig. 52. Adsorbed mass per unit area and desorption percentage of proteins in function of the volume proportions in the grafting solution.

This is why for all desorption experiments, mixed polymer brushes containing PDMAEMA/PEO 30/70 were used. They will also be used for all subsequent experiments, unless otherwise stated.

6.4 Conclusion

In conclusion, this chapter confirmed that positively charged polymer brushes indeed only interact with negatively charged proteins. It was also demonstrated that HSA and Fb adsorption can be tuned by controlling the switchable properties of mixed PDMAEMA/PEO brushes, through modifications of the pH and the ionic strength of the solution. The desorption of these proteins increases with increasing PEO volume in the grafting solution.

7 | Selectivity of protein adsorption on stimuli-responsive polymer brushes

The aim of this chapter is to test the selectivity of the designed polymer brushes. First, characteristic fragments of the different proteins will be determined. Then, the adsorption of protein mixtures was monitored by QCM-D and will be discussed in this chapter, and the surfaces were analyzed by ToF-SIMS with PCA in order to detect and identify the adsorbed species.

7.1 Protein fingerprints by PCA

In order to identify proteins adsorbed on PDMAEMA/PEO brushes, ToF-SIMS was used with principal component analysis. First, PCA was conducted on proteins adsorbed from single solutions (HSA and Fb on polymer brushes, Lys and Avi on gold) in order to identify the most characteristic fragments of each protein. These are called *fingerprints*. Table 7.1 gives the ToF-SIMS peaks of the different amino acids, which are the building blocks of proteins. It will allow to attribute fragments and amino acids to the identified peaks.

Only the positive peaks were analyzed in this study because they are efficient to determine the nature of adsorbed proteins on the surface. The PCA was performed on a list of 55 protein peaks, that can be found in Appendix B.1.

7.1.1 General approach

Proteins on the gold substrate

First, samples of gold with adsorbed Lym, Avi, HSA, and Fb were analyzed by PCA. The obtained scores (Fig. 53) allow to distinguish the different proteins. A first look at the scores shows that HSA and Lym are very close to each other, suggesting that the fragments are similar. PC1 collects 95% of the data variance and separates HSA and Lym (negative scores) from Fb and Avi (positive scores). PC2 captures 4% of the variability and allows to distinguish Avi (positive scores) and Fb (negative scores). The loadings are shown in Fig. 54. As the loadings for PC1 show, no peaks can be found in the positive semi-plane, for Avi and Fb. PC2 loadings however bring out some peaks. However, the distinction between HSA and Lym is still not clear and needs further comparison between their peaks.

Table 7.1. ToF-SIMS fingerprints of the different amino acids.

Amino acid	**m/z**	**Fragments**
Alanine (Ala)	44.05 ; 72.05	$C_2H_6N^+$; $C_3H_6NO^+$
Arginine (Arg)	43.03 ; 59.05 ; 73.06 ; 100.14 ;101.15 ; 110.07 ; 127.17	$CH_3N_2^+$; $CH_5N_3^+$; $C_2H_7N_3^+$; $C_4H_{10}N_3^+$; $C_4H_{11}N_3^+$; $C_5H_8N_3^+$; $C_5H_{11}N_4^+$
Asparagine (Asn)	44.01 ; 70.03 ; 87.06 ; 88.06 ; 98.02	CH_2NO^+ ; $C_3H_4NO^+$; $C_3H_7N_2O^+$; $C_3H_6NO_2^+$; $C_4H_4NO_2^+$
Aspartic acid (Asp)	38 ; 86 ; 88.06	CH_3Na^+ ; $C_3H_4NO_2^+$; $C_3H_6NO_2^+$
Cysteine (Cys)	45.00 ; 76.14	CHS^+ ; $C_2H_6NS^+$
Glutamine (Gln)	84.05	$C_4H_6NO^+$
Glutamic acid (Glu)	43 ; 58 ; 84.05 ; 102.06	$C_2H_3O^+$; $C_3H_8N^+$; $C_4H_6NO^+$; $C_4H_8NO_2^+$
Glycine (Gly)	28 ; 30.03 ; 42 ; 115 115	CH_2N^+ ; CH_4N^+ ; $C_2H_4N^+$; $C_4H_7N_2O_2^+$
Histidine (His)	42 ; 54 ; 81.05 ; 82.10 ; 108 ; 110.07	$C_2H_4N^+$; $C_3H_4N^+$; $C_4H_5N_2^+$; $C_4H_6N_2^+$; $C_5H_6N_3^+$; $C_5H_8N_3^+$
Isoleucine (Ile)	86.10	$C_5H_{12}N^+$
Leucine (Leu)	42 ; 44 ; 84.08 ; 86.10	$C_2H_4N^+$; $C_2H_6N^+$; $C_5H_{10}N^+$; $C_{H12}N^+$
Lysine (Lys)	30 ; 56.05 ; 68 ; 84.08	CH_4N^+ ; $C_3H_6N^+$; $C_4H_6N^+$; $C_5H_{10}N^+$
Methionine (Met)	56 ; 61.01 ; 102 ; 104 ; 150	$C_3H_6N^+$; $C_2H_5S^+$; $C_4H_8NS^+$; $C_4H_{10}NS^+$; $C_5H_{12}NO_2S^+$
Phenylalanine (Phe)	77 ; 91 ; 118 ; 120.08 ; 131 ; 166	$C_6H_5^+$; $C_7H_7^+$; $C_8H_8N^+$; $C_8H_{10}N^+$; $C_9H_8O^+$; $C_9H_{12}NO_2^+$
Proline (Pro)	68.05 ; 70.07	$C_4H_6N^+$; $C_4H_8N^+$
Serine (Ser)	42 ; 58 ; 60.05 ; 71	$C_2H_4N^+$; $C_2H_4NO^+$; $C_2H_6NO^+$; $C_3H_3O_2^+$
Threonine (Thr)	69 ; 74.06	$C_4H_5O^+$; $C_3H_8NO^+$
Tryptophan (Trp)	102 ; 130.17 ; 159 ; 170	$C_6H_{16}N^+$; $C_9H_8N^+$; $C_{10}H_{11}N^+$; $C_{11}H_8NO^+$
Tyrosine (Tyr)	77 ; 91 ; 107.05 ; 134 ; 136.07	$C_6H_5^+$; $C_7H_7^+$; $C_7H_7O^+$; $C_8H_8NO^+$; $C_8H_{10}NO^+$
Valine (Val)	56 ; 70 ; 72.08 ; 83	$C_3H_6N^+$; $C_4H_8N^+$; $C_4H_{10}N^+$; $C_5H_7O^+$

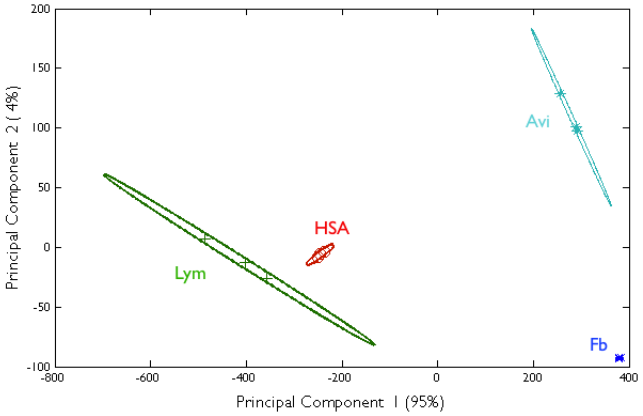

Fig. 53. Scores of PC1 and PC2 for HSA, Fb, Lym and Avi.

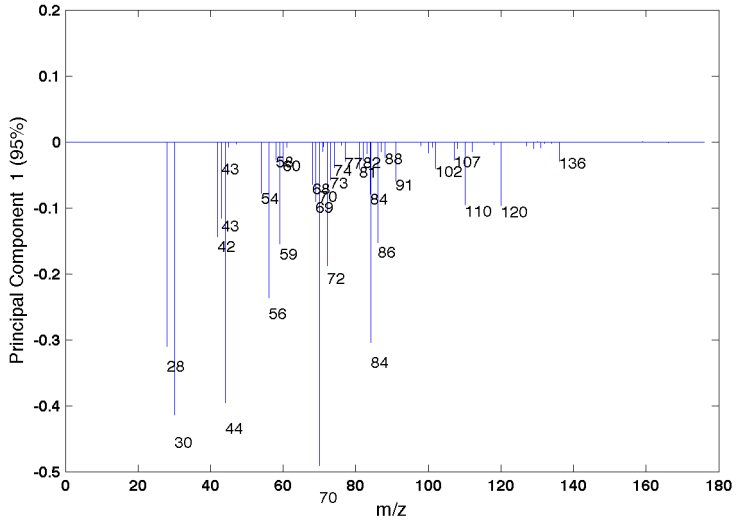

(a) PC1

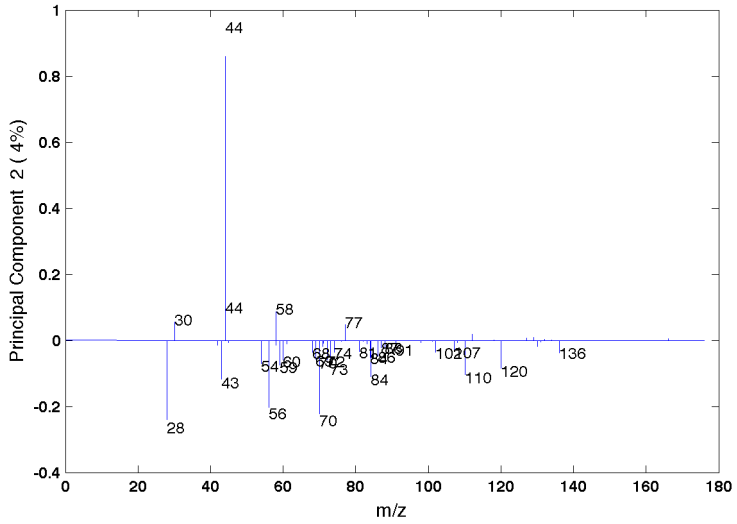

(b) PC2

Fig. 54. Loadings for HSA, Fb, Lym and Avi on gold.

Comparing all proteins between each other when adsorbed on pure gold can remove doubts about the presence of characteristic peaks of PDMAEMA or PEO. The fingerprints were however not characteristic of the studied system. Indeed, fingerprints determined from adsorption on gold, or on polymer brushes, differ significantly. The reason is that proteins do not adsorb in the same way on the pure gold substrate and on polymer coatings, they can adsorb in a preferential conformation. It is typically well-known in the case of fibrinogen. Fibrinogen is a large protein (47.5 nm) that is highly anisotropic (Fig. **??**). It consists in an elongated rod, whose extremities bear extended chains from the core of the molecule, forming two polar appendages. Indeed, at pH 7.4, the core of the molecule is negatively charged and these "arms" bear positive charges which play an important role in Fb adsorption on

solid surfaces. Therefore, it is possible that Fb adsorbs on the positively charged polymer brushes in a preferential conformation, revealing its positively charged "arms" to the primary ions from the ToF-SIMS instrument. Since the sampling depth of ToF-SIMS does not exceed 2 nm, only this part of the molecule is then analyzed. On the other hand, when adsorbed on gold, the molecule may not exhibit the same conformation as when adsorbed on PDMAEMA/PEO brushes, and the ToF-SIMS fingerprints may differ. This is why in order to identify proteins adsorbed on the mixed brushes from a mixture, HSA and Fb samples obtained from adsorption on the same brushes were further used for PCA analysis.

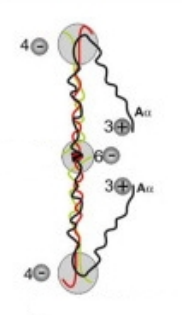

Fig. 55. Anisotropic structure of fibrinogen

Lym and Avi on the gold substrate, HSA and Fb on polymer brushes

PCA was then performed on ToF-SIMS data acquired on samples of HSA and Fb on PDMAEMA/PEO 30/70 brushes, and Lys and Avi on the gold substrate (which do not adsorb on PDMAEMA/PEO), after single protein adsorption. The scores of the first two principal components are shown in Fig. 56. PC1 captures 79% and PC2 captures 18% of the data variance. The four proteins lie in different quadrants of the plot, and are thus easily distinguished from each other. PC1 allows to separate HSA and Fb in the negative values, from Lys and Avi in the positive values, while PC2 distinguishes HSA and Lym in the negative scores, from Fb and Avi in the positive scores. In the same way as for the polymers in Sec. 5.5, the loadings were plotted in Fig. 57. However, peaks close to zero were removed because they do not contribute significantly to the variation of the principal components and, therefore, 23 peaks were chosen for further analysis. Fig. 57 is presented with these 23 peaks only for better visibility. They are listed in Table 7.2, and attributed to the proteins by analysis of the loadings. However, no characteristic peaks were found for Avi in this analysis. Moreover, detected fingerprints for HSA are also highly present in Lym, so that they cannot be distinguished from each other. It is thus difficult to distinguish characteristic protein fragments from the study of all four proteins at once. In order to precisely identify each protein, PCAs were performed in pairs for all studied proteins (6 combinations), but only the three relevant pairs will be presented further in this chapter.

Some peaks associated to PEO and PDMAEMA can also be seen in this list (indicated by arrows in Table 7.2). The possibility of them to result from polymers is however not likely. Indeed, previous QCM experiments have shown that when proteins adsorb on the brushes, they reach a stable signal (a plateau), which means that proteins are no longer adsorbed, and a dense layer of proteins covers the

brushes. The sampling depth of ToF-SIMS does not exceed 2 nm, while the proteins of interest have dimensions between 4 and 45 nm, which should prevent primary ions to reach PDMAEMA and PEO.

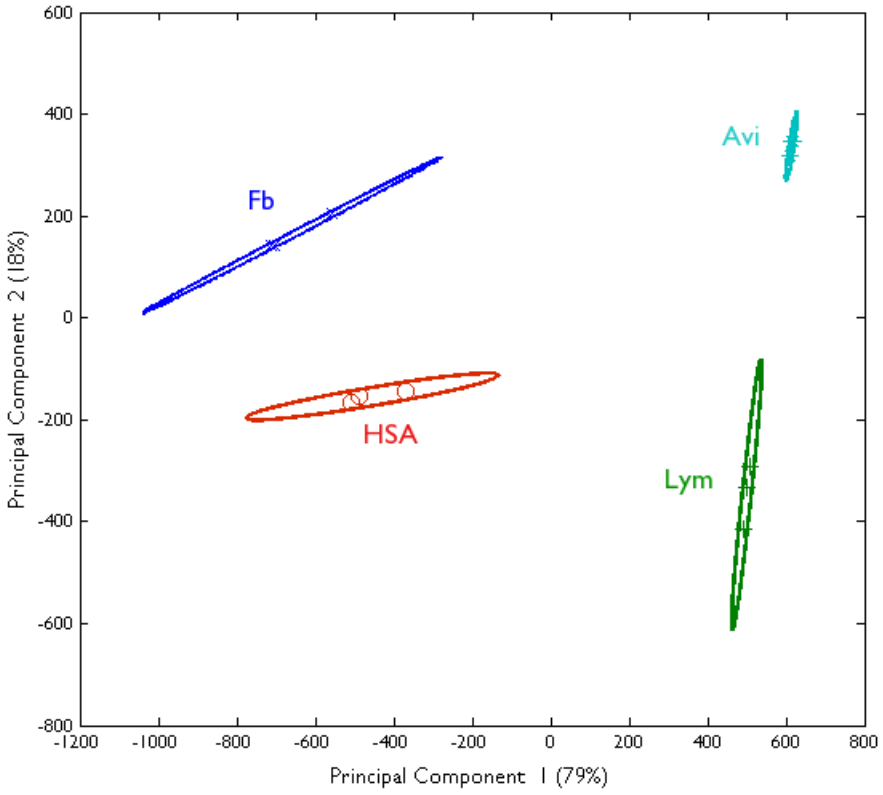

Fig. 56. Scores of PC1 and PC2 for HSA and Fb on PDMAEMA/PEO brushes, and Lym and Avi on gold.

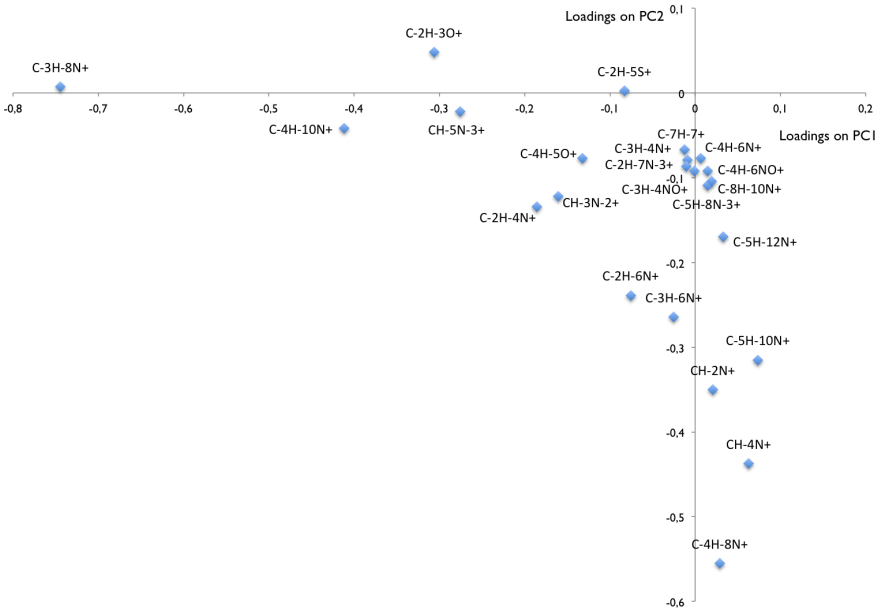

Fig. 57. Loadings on PC2 in function of loadings on PC2, for HSA, Fb, Lym and Avi.

Table 7.2. Characteristic positive peaks from protein samples.

m/z	Fragments	Attributed proteins	
28.02	CH_2N^+	Lym, HSA	
30.04	CH_4N^+	Lym, HSA	
42.03	$C_2H_4N^+$	HSA, Fb	$\longrightarrow$ PDMAEMA
43.02	$C_2H_3O^+$	Fb, HSA	$\longrightarrow$ PEO
43.03	$CH_3N_2^+$	HSA, Fb	
44.05	$C_2H_6N^+$	HSA, Fb, Lym, Avi	$\longrightarrow$ PDMAEMA
54.03	$C_3H_4N^+$	Lym, HSA	
56.05	$C_3H_6N^+$	Lym, HSA	
58.07	$C_3H_8N^+$	Fb, HSA	$\longrightarrow$ PDMAEMA
59.05	$CH_5N_3^+$	Fb	
61.01	$C_2H_5S^+$	Fb, HSA	
68.05	$C_4H_6N^+$	Lym, HSA	
69.03	$C_4H_5O^+$	Fb, HSA	$\longrightarrow$ PDMAEMA
70.03	$C_3H_4NO^+$	Lym, HSA	
70.07	$C_4H_8N^+$	Lym, HSA	$\longrightarrow$ PDMAEMA
72.08	$C_4H_{10}N^+$	Fb, HSA	$\longrightarrow$ PDMAEMA
73.06	$C_2H_7N_3^+$	Lym, HSA	
84.04	$C_4H_6NO^+$	Lym, HSA	
84.09	$C_5H_{10}N^+$	Lym, HSA	
86.10	$C_5H_{12}N^+$	Lym, HSA	
91.05	$C_7H_7^+$	HSA, Lym	
110.07	$C_5H_8N_3^+$	Lym, HSA	
120.08	$C_8H_{10}N^+$	Lym, HSA	

7.1.2 Comparisons between two proteins

In order to precisely identify proteins in mixtures, fingerprints were investigated for each pair of proteins that follows :

- HSA on PDMAEMA/PEO, and Lys on gold ;
- HSA on PDMAEMA/PEO, and Avi on gold ;
- HSA on PDMAEMA/PEO, and Fb on PDMAEMA/PEO ;

The results from comparisons between pairs of proteins adsorbed on gold exclusively are described in Appendice B (sections B.2, B.2 and B.2 for each pair of proteins, respectively).

HSA/Lym

In this section, PCA was performed on protein fragments detected after adsorption of HSA and Lym from single protein solutions. The scores on PC1 and PC2 are shown in Fig. 58. PC1 captures 99% of the variance and allows to distinguish both proteins. PC1 is negative for HSA and positive for Lym. This plot was further investigated with PC1 and PC2 loadings (that can be found in Appendice B.5), and Fig. 59 shows the correlation between them. Peaks close to zero were removed because they do not contribute significantly to the PC variability.

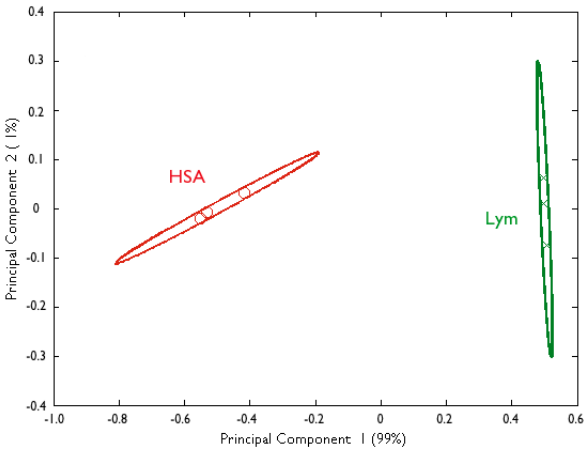

Fig. 58. Scores on PC1 and PC2 for HSA and Lym.

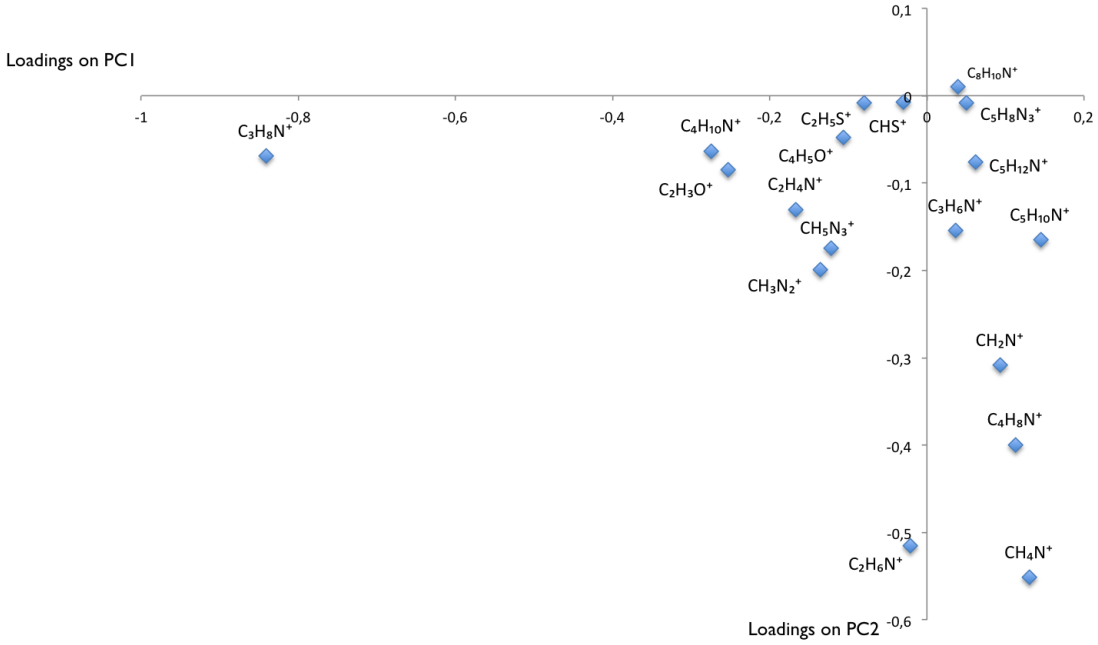

Fig. 59. Loadings on PC2 in function of loadings on PC2, for HSA and Lym.

The peaks located in areas of the loadings plot represent amino acids that are in significantly higher concentration in the protein that is in the same area in the scores plot. In the case of HSA, the most negative loadings correspond to the five most negative peaks, while for Lym they correspond to the three fragments with the most positive loadings. Table 7.3 summarizes all selected peaks, next to attributed proteins according to the relative intensities of the loadings. Peaks shown in bold characters are the fingerprints of HSA or Lym.

Table 7.3. Positive fingerprints of HSA and Lym.

m/z	Fragments	Corresponsing amino acids	Proteins
28,02	CH_2N^+	Ala, Arg, Asn, Glu, Gly, Leu, Ser, Trp	Lym
30,04	CH_4N^+	Gly, Arg, Asn, Glu, Leu, Lys, Ser	Lym
42,03	$C_2H_4N^+$	Ala, Gly, His, Leu, Ser	HSA
43,02	$\mathbf{C_2H_3O^+}$	**Glu**	**HSA**
43,03	$CH_3N_2^+$	Arg	HSA
44,05	$C_2H_6N^+$	Ala, Asn, Leu	HSA, Lym
44.98	$\mathbf{CHS^+}$	**Cys**	**HSA**
56,05	$C_3H_6N^+$	Lys, Met, Val	Lym, HSA
58,07	$\mathbf{C_3H_8N^+}$	**Glu**	**HSA**
59,05	$CH_5N_3^+$	Arg	HSA
61,01	$\mathbf{C_2H_5S^+}$	**Met**	**HSA**
69,03	$C_4H_5O^+$	Thr	HSA
70,07	$C_4H_8N^+$	Pro, Val	Lym, HSA
72,08	$\mathbf{C_4H_{10}N^+}$	**Val**	**HSA**
84,09	$\mathbf{C_5H_{10}N^+}$	**Lys, Leu**	**Lym**
86,10	$C_5H_{12}N^+$	Ile, Leu	Lym
110,07	$\mathbf{C_5H_8N_3^+}$	**His, Arg**	**Lym**
120,08	$\mathbf{C_8H_{10}N^+}$	**Phe**	**Lym**

HSA/Avi

The same procedure was applied to samples of HSA and Avi. The scores on PC1 and PC2 are shown in Fig. 70. PC1 captures 100% of the variance in the data set, and allows to differentiate HSA from Avi. PC1 is negative for HSA, and positive for Avi. PC1 and PC2 loadings are presented in Fig. 61. A list of 20 peaks is selected. Several fingerprints are found for HSA and listed in bold characters in Table 7.4. However, no peak for Avi could be determined. It is confirmed by the complete PC1 loadings spectrum found in Appendice B.5, which does not show any peak in the positive semi-plane.

In fact, all loadings relative intensities (attached in Appendice B.6) show quite negligible signals from the Avi sample compared to HSA, except for some peaks indicated in Table 7.4. Different normalization methods were also used, but did not bring any better solutions.

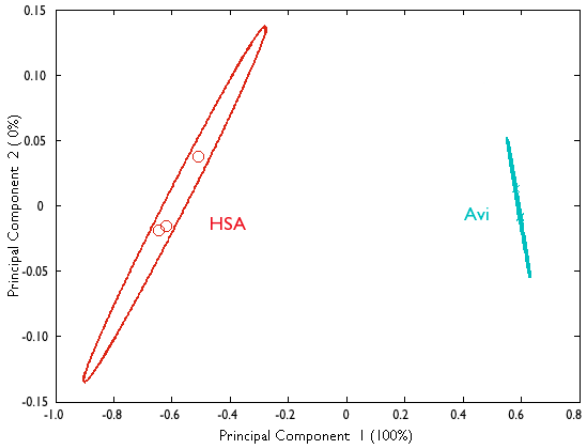

Fig. 60. Scores on PC1 and PC2 for HSA and Avi.

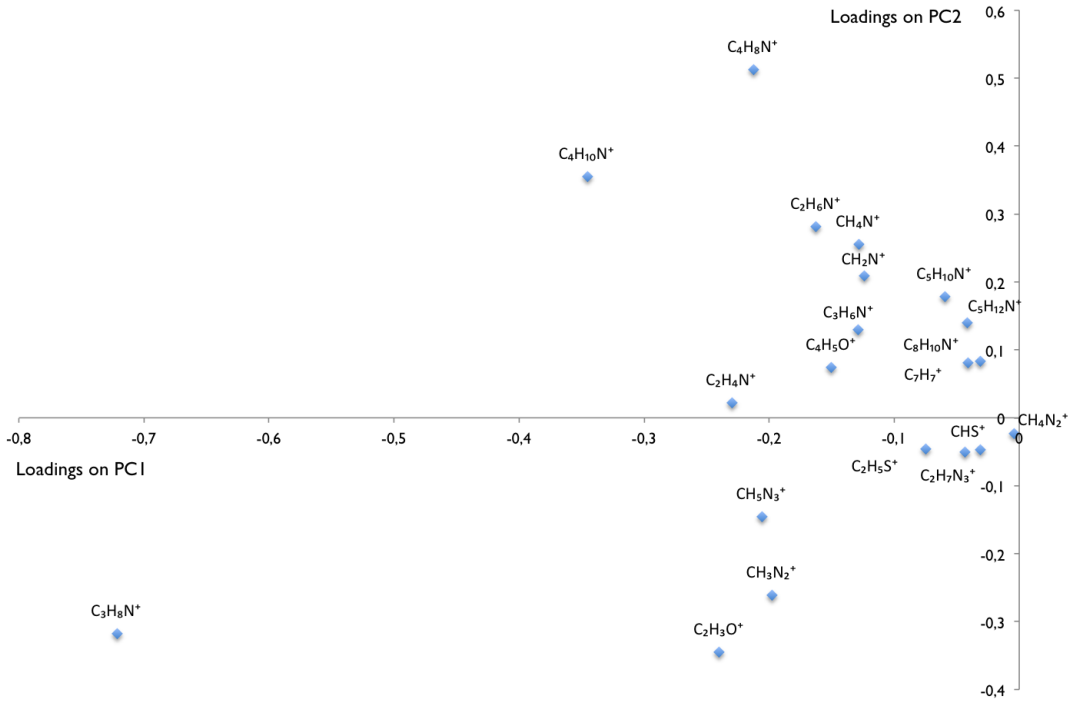

Fig. 61. Loadings on PC2 in function of loadings on PC2, for HSA and Avi.

Table 7.4. Positive fingerprints of HSA and Avi.

m/z	Fragments	Proteins
28,02	CH_2N^+	HSA
30,04	CH_4N^+	HSA, Avi
42,03	$C_2H_4N^+$	HSA
43,02	$\mathbf{C_2H_3O^+}$	**HSA**
43,03	$\mathbf{CH_3N_2^+}$	**HSA**
44,04	$CH_4N_2^+$	HSA, Avi
44,05	$C_2H_6N^+$	HSA, Avi
44.98	CHS^+	HSA
56,05	$C_3H_6N^+$	HSA
58,07	$\mathbf{C_3H_8N^+}$	**HSA**
59,05	$\mathbf{CH_5N_3^+}$	**HSA**
61.01	$C_2H_5S^+$	HSA
69.04	$C_4H_5O^+$	HSA
70,07	$C_4H_8N^+$	HSA, Avi
72,08	$\mathbf{C_4H_{10}N^+}$	**HSA**
73,06	$C_2H_7N_3^+$	HSA
84,09	$C_5H_{10}N^+$	HSA, Avi
86,10	$C_5H_{12}N^+$	HSA, Avi
91.05	$C_7H_7^+$	HSA
120,08	$C_8H_{10}N^+$	HSA

HSA/Fb

The scores on PC1 and PC2 are shown in Fig. 73. PC1 collects 91% of the data variability and clearly separates HSA (negative score) from Fb (positive score). The plot of the loadings of PC1 and PC2 (Fig. 63) allows to determine 17 characteristic peaks presented in Table 7.5. The amino acid fragments with negative loadings in PC1 are exposed at the outermost surface after HSA adsorption, while the amino acid fragments with positive loadings are present at the surface after Fb adsorption. The peaks shown in bold characters are those showing the largest differences in relative intensities between both proteins when analyzing each loading separately.

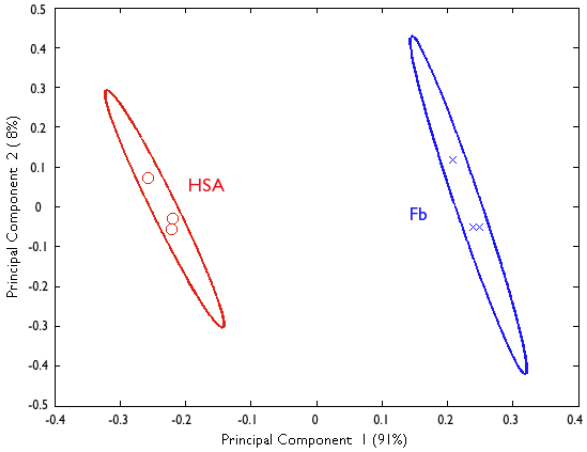

Fig. 62. Scores on PC1 and PC2 for HSA and Fb.

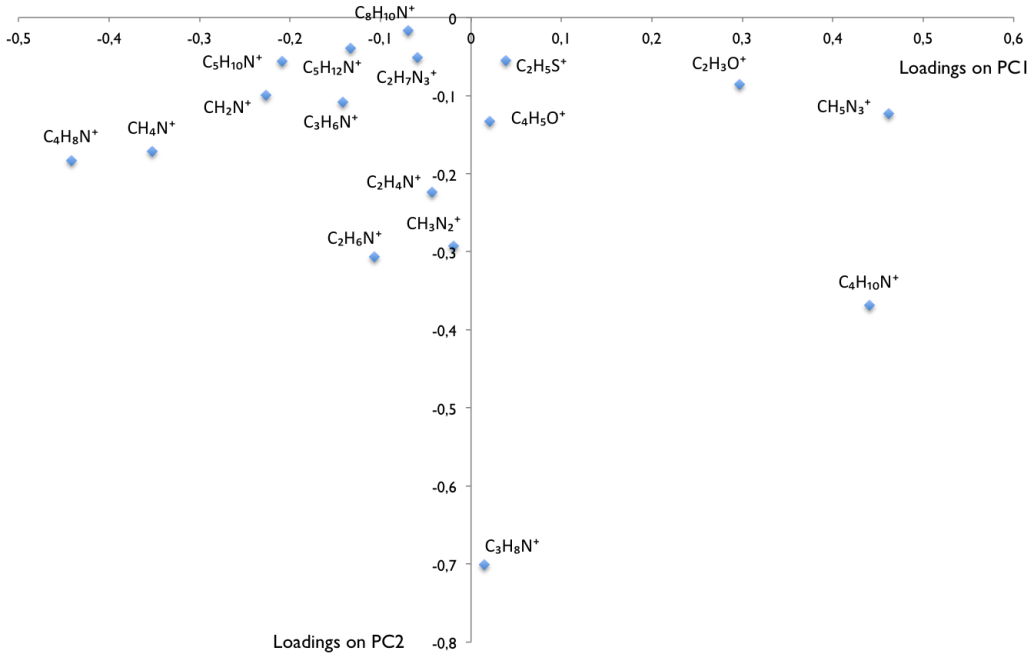

Fig. 63. Loadings on PC2 in function of loadings on PC2, for HSA and Fb.

Table 7.5. Positive fingerprints of HSA and Fb.

m/z	Fragment	Protein
28,0190	CH_2N^+	HSA
30,0352	CH_4N^+	HSA
42,0336	$C_2H_4N^+$	HSA, Fb
43,02	$\mathbf{C_2H_3O^+}$	**Fb**
43,0277	$CH_3N_2^+$	HSA, Fb
44,0514	$C_2H_6N^+$	HSA, Fb
56,0492	$C_3H_6N^+$	HSA, Fb
58,0658	$C_3H_8N^+$	HSA, Fb
59,0484	$\mathbf{CH_5N_3^+}$	**Fb**
61,0091	$\mathbf{C_2H_5S^+}$	**Fb**
69,0339	$\mathbf{C_4H_5O^+}$	**Fb**
70,0707	$\mathbf{C_4H_8N^+}$	**HSA**
72,08	$\mathbf{C_4H_{10}N^+}$	**Fb**
73,0625	$C_2H_7N_3^+$	HSA
84,0860	$\mathbf{C_5H_{10}N^+}$	**HSA**
86,1010	$\mathbf{C_5H_{12}N^+}$	**HSA**
120,0824	$\mathbf{C_8H_{10}N^+}$	**HSA**

7.1.3 Conclusion

While these lists found by data treatment on PCA give some insights into fragments that can distinguish them, they are not exhaustive. The results do not always correlate with data found in the literature about amino acid composition of proteins. They may differ due to different substrates, concentrations and experimental conditions and treatments of the gold crystals.

7.2 Adsorption and desorption of protein mixtures by QCM-D

Adsorption and desorption of mixtures containing two different proteins (HSA/Lym, HSA/Avi and HSA/Fb) on PDMAEMA/PEO 70/30 brushes were monitored by QCM-D. These results are presented and discussed in this section.

7.2.1 HSA/Lym

The QCM graph presenting protein adsorption from a mixture of HSA and Lym on PDMAEMA/PEO 30/70 brushes is shown in Fig. 64. It has similar kinetics to the one of single HSA adsorption, suggesting that HSA is adsorbed from the mixture. It should however be noted that QCM does not enable to distinguish protein nature, so the same shift in frequency can arise from a pure HSA layer or from a mixed HSA/Lym layer. The adsorbed mass of proteins per unit area based on the Δf_a shift after protein adsorption, was around $315\,\mathrm{ng\,cm^{-2}}$, which was less than for single HSA due to lower

concentration in HSA in the mixed solution (0.1 mg ml^{-1}). The achieved desorption percentage was 94%.

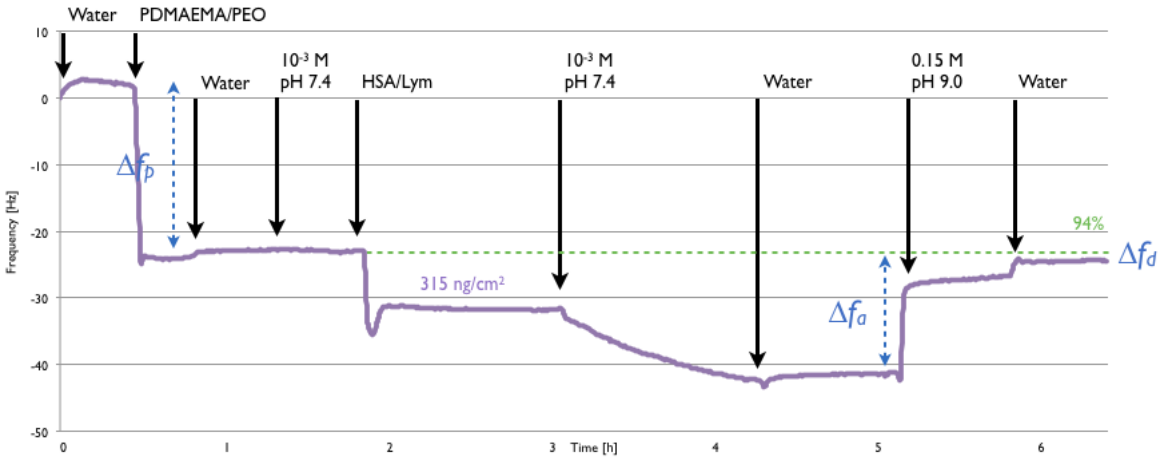

Fig. 64. Time dependence of the changes in QCM-D frequency (7th overtone) upon PDMAEMA/PEO brush formation and introduction of the HSA/Lym mixture.

7.2.2 HSA/Avi

Fig. 65 shows the QCM graph obtained for HSA/Avi adsorption and desorption. The frequency shift decreased linearly during the proteins adsorption step because the concentration of both proteins used was 0.1 mg ml^{-1} in this case, instead of 0.2 mg ml^{-1} in all other experiments, which may not be enough for the system to reach a plateau within the time of the experiment. After one hour and a half of adsorption, the adsorbed mass per unit area was around 575 ng cm^{-2}. This value is very close to the sum of the average masses adsorbed of HSA and Avi from single protein solutions (see Sec. 6.2). Nearly all proteins were desorbed after the rinsing steps (98%).

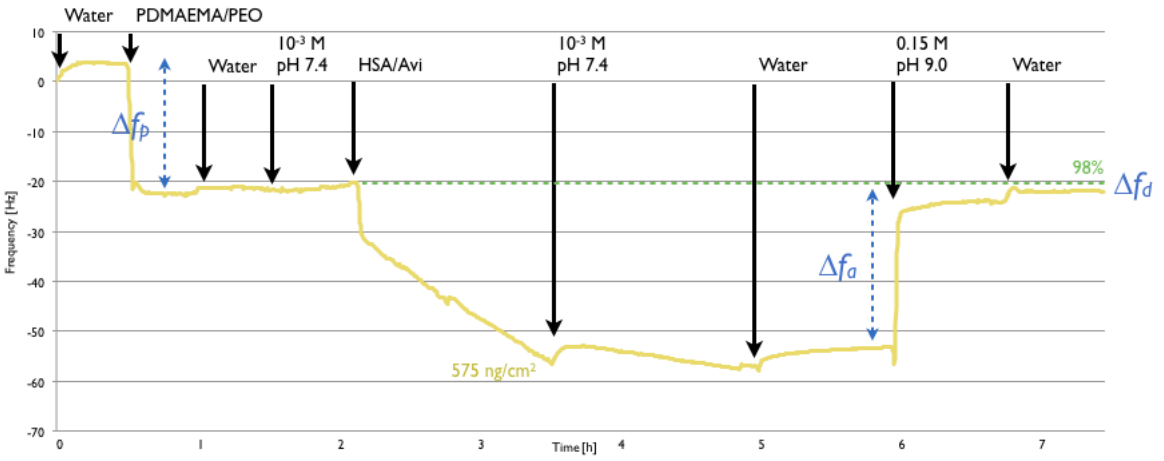

Fig. 65. Time dependence of the changes in QCM-D frequency (7th overtone) upon PDMAEMA/PEO brush formation and introduction of the HSA/Avi mixture.

7.2.3 HSA/Fb

A typical QCM graph presenting adsorption and desorption of protein from a mixture of HSA and Fb, both negatively charged at pH 7.4, is shown in Fig. 66. The average adsorbed mass per unit area was 1442 ng cm^{-2}. This value is close to the mass of fibrinogen adsorbed from single adsorption (1745 ng cm^{-2}) and the QCM graph has a similar appearance. 93% of proteins were then desorbed.

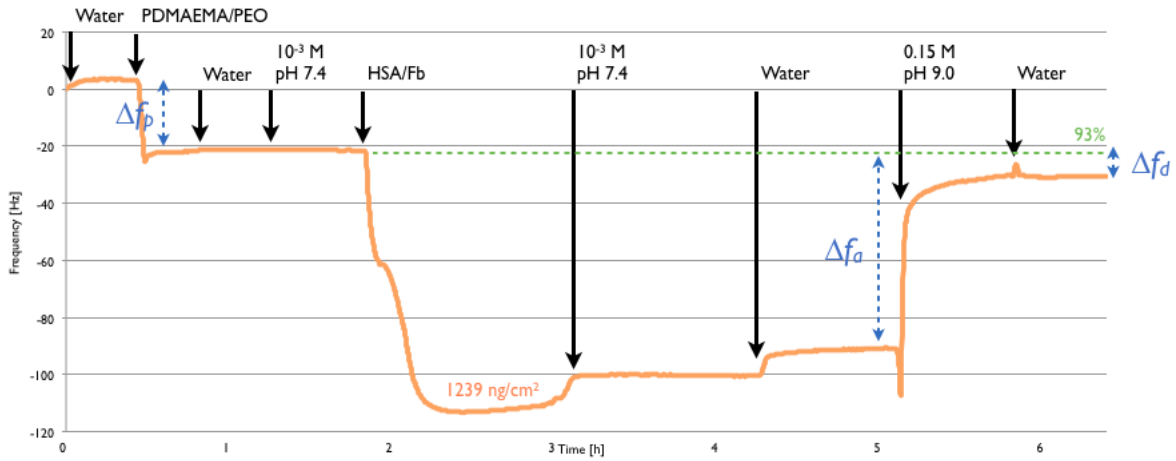

Fig. 66. Time dependence of the changes in QCM-D frequency (7th overtone) upon PDMAEMA/PEO brush formation and introduction of the HSA/Fb mixture.

7.2.4 Conclusions

These QCM experiments allowed to observe a significant adsorption of proteins from mixtures of HSA/-Lym, HSA/Avi, and HSA/Fb, on the designed PDMAEMA/PEO 30/70 brushes. The stabilized signal during adsorption suggests that no multiple layers are formed by alternation of oppositely charged proteins.

Moreover, the adsorbed proteins were almost completely removed from the brushes after rinsing with salt and water, demonstrating the switchable nature of the polymer brushes.

QCM only provides information about the adsorbed mass and it cannot be used to identify proteins adsorbed from mixtures. Selective adsorption can be suspected, but other techniques are necessary to confirm this statement. One of them is ToF-SIMS, a very sensitive technique which allows to precisely distinguish the different proteins, with the help of principal component analysis. The obtained results from ToF-SIMS will be discussed in the next section.

7.3 Selectivity of protein adsorption by PCA

In order to obtain more information concerning the protein layer composition after adsorption from mixtures of proteins, and to test the selectivity of polymer brushes, ToF-SIMS with principal component analysis of the protein fragments were applied. This section provides the results for each proteins pair of interest.

7.3.1 HSA/Lym

PCA was performed on spectra from samples of HSA adsorbed on PDMAEMA/PEO, Lym on pure gold, and the mixture of both proteins on PDMAEMA/PEO, using the list of 18 peaks found in Sec. 7.1.2, characteristic of HSA and Lym. Fig. 67 represents the resulting scores on PC1 and PC2. Three populations can be distinguished, separated by both principal components.

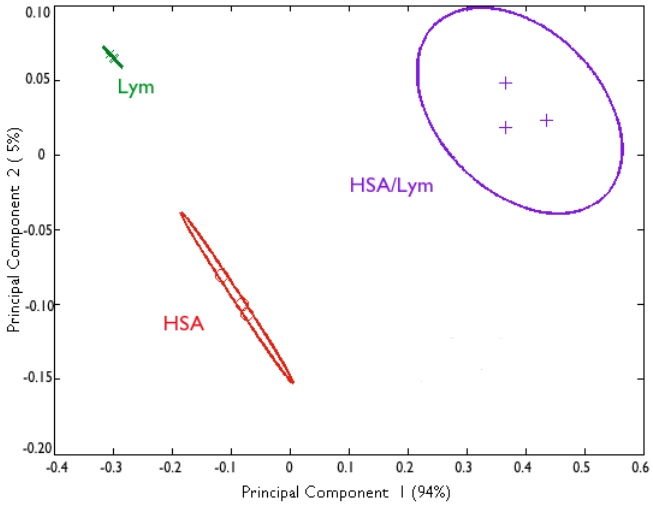

Fig. 67. Scores HSA/Lym

PC1 captures 94% of the variability, and distinguishes HSA and Lym (negative score) from the mixture (positive score). PC1 loadings are presented in Fig. 68a. Positive loadings in PC1 contain fingerprints of HSA (43.02 Glu, 58.07 Glu, 61.01 Met, 72.08 Val), but present no fingerprints of Lym. PC2 captures 5% of the data variance, and separates Lym and the mixture (positive score), from HSA (negative score), but the distinction is less clear. In the PC2 loadings (Fig. 68b), one characteristic peak of HSA has a positive score (43.02 Glu), whereas other peaks from HSA lie in the negative semi-plane, as well as one fingerprint of Lym (110.07 His, Arg).

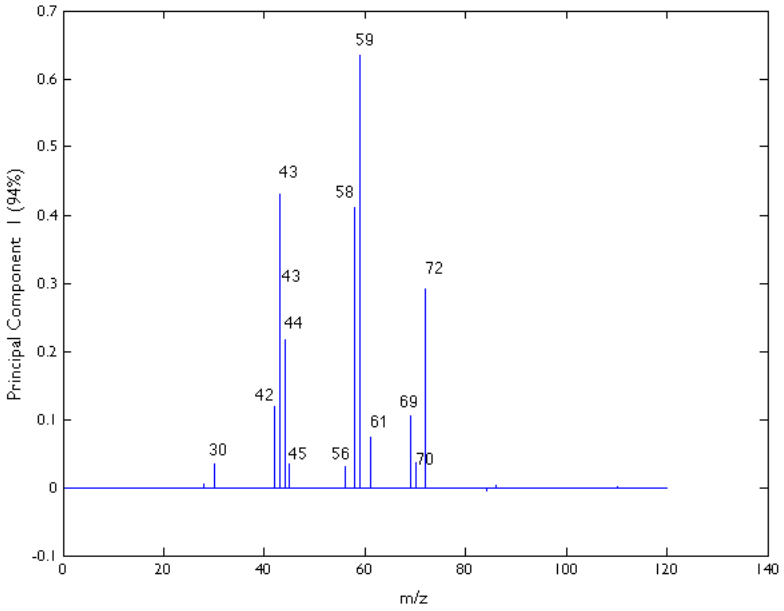

(a) PC1

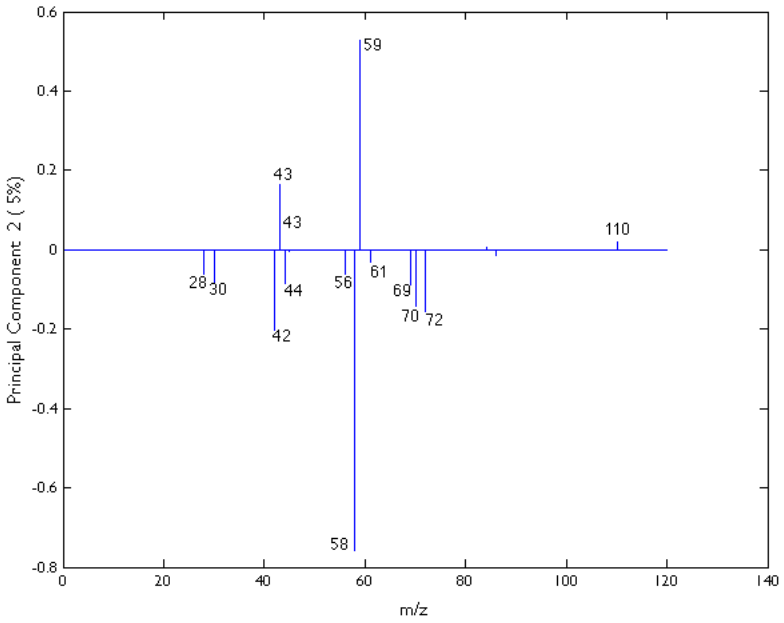

(b) PC2

Fig. 68. Loadings for HSA on PDMAEMA/PEO 70/30, Lym on pure gold, and HSA/Lym on PDMAEMA/PEO 30/70 : (a) PC1 ; (b) PC2.

However, all principal component loadings represent relative intensities of amino acid fragments detected by ToF-SIMS. The trends obtained by their analysis are thus not quantitative. To obtain at

least semi-quantitative information, one approach consists in calculating the ratios of relative intensities between a fragment in a significantly higher amount in one proteins and a fragment less represented in the same protein but, at the same time, more significant for the second protein. Fig. 69 shows such ratios based on HSA and Lym fingerprints, r_1, r_2 and r_3, defined as :

$$r_1 = \frac{I_{rel}(58.07)}{I_{rel}(70.07)}$$
$$r_2 = \frac{I_{rel}(72.08)}{I_{rel}(110.07)}$$
$$r_3 = \frac{I_{rel}(61.01)}{I_{rel}(110.07)}$$

where $I_{rel}(x)$ represent the relative intensities of peaks x. It can be directly seen that the values for the mixture are similar to the ones of HSA, suggesting that their compositions are close. The presence of adsorbed Lym from the HSA/Lym mixture can however not be excluded.

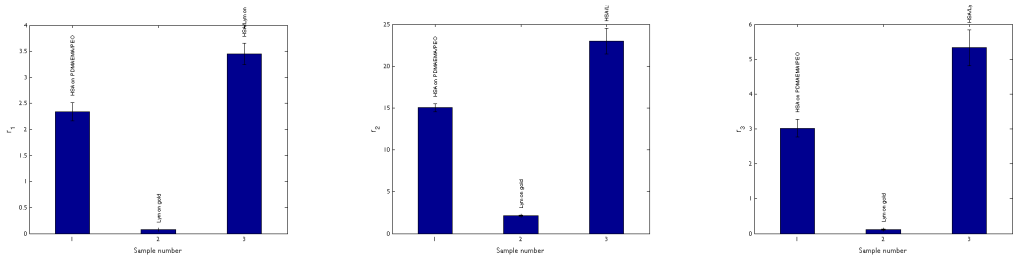

(a) r_1 **(b)** r_2 **(c)** r_3

Fig. 69. Plots of relative intensities ratios between two fingerprints of HSA and Lym, for HSA on PDMAEMA/PEO, Lym on gold, and HSA/Lym on PDMAEMA/PEO.

Indeed, Lym proteins are small and compact molecules, that could be hidden between HSA molecules, which are oppositely charged, and adsorbed with them.

Lym being adsorbed on pure gold, the similarity between HSA and HSA/Lym samples could also arise from the effect of polymer brushes. All protein fingerprints are indeed fragments largely present in PEO, and/or PDMAEMA. However, the sampling depth of ToF-SIMS does not exceed 2 nm. It was seen that the formed polymer brushes did not segregate into patches, and it is assumed that, once a stable signal for proteins adsorption was obtained on QCM, the brushes were covered with a protein layer, preventing further adsorption. Owing to the large dimensions of proteins (at least 6 nm for HSA), their packing in a monolayer and their conformation, the primary ions in ToF-SIMS should then not reach the polymer brushes.

However, the mixture does not lie near HSA in the scores plot, suggesting that Lym can also be adsorbed on the surface. Due to the ToF-SIMS sampling depth, the shape and the orientation of the adsorbed proteins have also a direct effect on the ions generated during ToF-SIMS measurements, and on the obtained data. It is for example possible that HSA adsorbs with preferential orientations when adsorbed from a single solution, while it would expose other patches on its surface when it is mixed

with Lym, revealing peaks that were not observed while identifying fragments on HSA from single protein solution.

7.3.2 HSA/Avi

The PCA results obtained for a mixture of HSA/Avi, HSA, and Avi on gold, are presented in this section. The PCA was based on the peak list determined in Sec. 7.1.2. The scores are plotted in Fig. 70. PC1 collects 97% of the data variability and clearly distinguishes two groups : HSA and the mixture of HSA/Avi in the negative values, and Avi in the positive values. PC2 will not be discussed in this section.

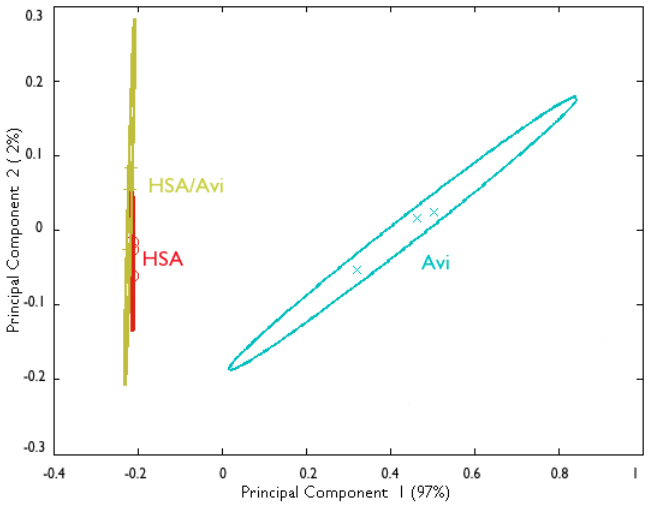

Fig. 70. Scores HSA/Avi

As a first approximation, it seems rather obvious that the composition of the adsorbed mixtures is similar to the one of single HSA, and that no Avi was adsorbed, as expected. A closer look at the loadings on PC1 in Fig. 71 shows several peaks in the positive area, which were not negligible for Avi in the determination of fingerprints (44.05, 70.07, 84.09, 86.1). It can then be assumed that they are indeed characteristic of Avi. The negative loadings only show three HSA fingerprints (43.03, 58.07, 72.08).

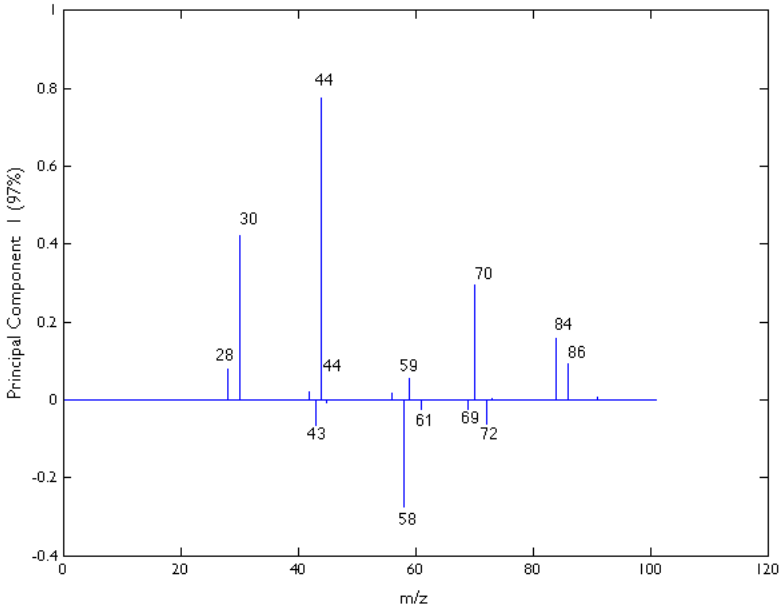

Fig. 71. PC1 loadings for HSA, Avi and HSA/Avi on PDMAEMA/PEO 70/30.

The relative intensities of representative peaks of HSA and Avi are also compared in Fig. 72, where :

$$r_1 = \frac{I_{rel}(72.08)}{I_{rel}(84.09)}$$
$$r_2 = \frac{I_{rel}(58.07)}{I_{rel}(70.07)}$$
$$r_3 = \frac{I_{rel}(61.01)}{I_{rel}(86.10)}$$

A strong similarity between the ratios for HSA and the mixture can be observed, confirming the first hunch.

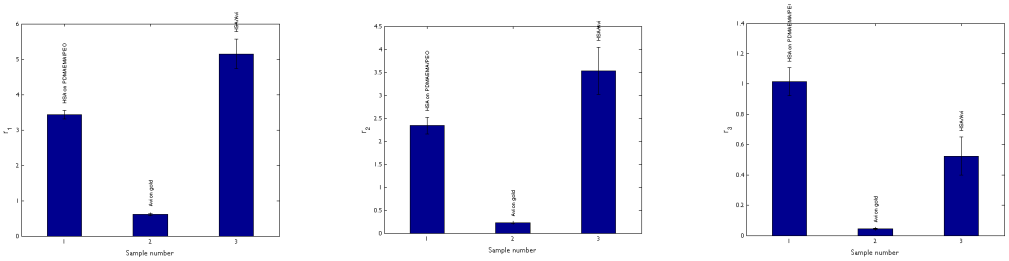

(a) r_1 **(b)** r_2 **(c)** r_3

Fig. 72. Plots of relative intensities ratios between two fingerprints of HSA and Avi, for HSA on PDMAEMA/PEO, Avi on gold, and HSA/Avi on PDMAEMA/PEO.

However, these results do not provide enough information to confirm that the brushes did not adsorb

any avidin. It was also seen during the QCM experiments, that the mixture of HSA and Avi was not concentrated enough to reach a stable signal within the time of the experiment. Therefore, a dense layer of proteins may have not been achieved, and ToF-SIMS primary ions may have reached the polymer brushes, biasing the obtained results.

7.3.3 HSA/Fb

Samples of HSA, Fb and HSA/Fb adsorbed on PDMAEMA/PEO were analyzed with PCA, using the 17 significant peaks determined in Sec. 7.1.2. Fig. 73 shows the three well-defined groups.

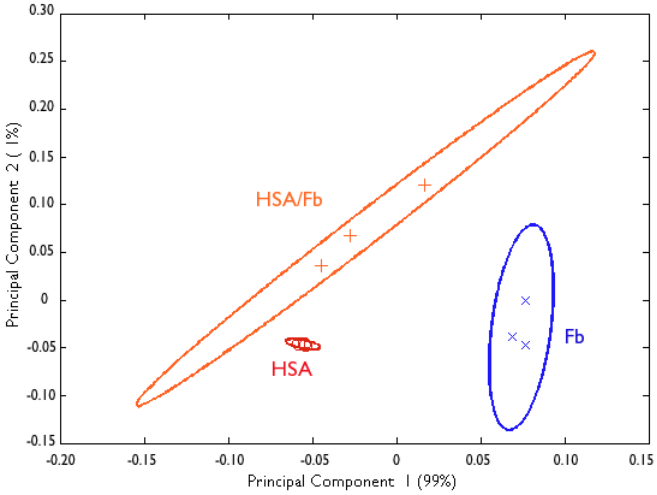

Fig. 73. Scores HSA/Fb

PC1 collects 99% of the data variance and separates HSA (negative score) from Fb (positive score). The mixture seems to be closer to HSA. The main contribution in PC1 loadings (Fig. **??**) is given by positive values, particularly by Fb fingerprints (59.05, 61.01, 69.03, 72.08). This reflects the fact that most of the signal in the spectra is represented by Fb, meaning that most of the variance is contained in the peaks belonging to Fb. Some relevant peaks may have been lost in the prior selection that was made for this study, or the normalization method could have degraded some information.

PC2 separates HSA (negative score) from the mixture (positive score), but the distinction is not very clear, and PC2 collects only 1% of the data variance. According to the loadings on PC2 (Fig. **??**), two fingerprints of Fb can be found among the positive peaks (43.02, 59.05), while negative peaks represent both Fb (Lys, Met, Val : 56.05, 69.03, 72.08) and HSA fingerprints (70.07, 84.10). Unfortunately, this inspection of the spectrum is not enough to obtain information about the content of the mixed sample.

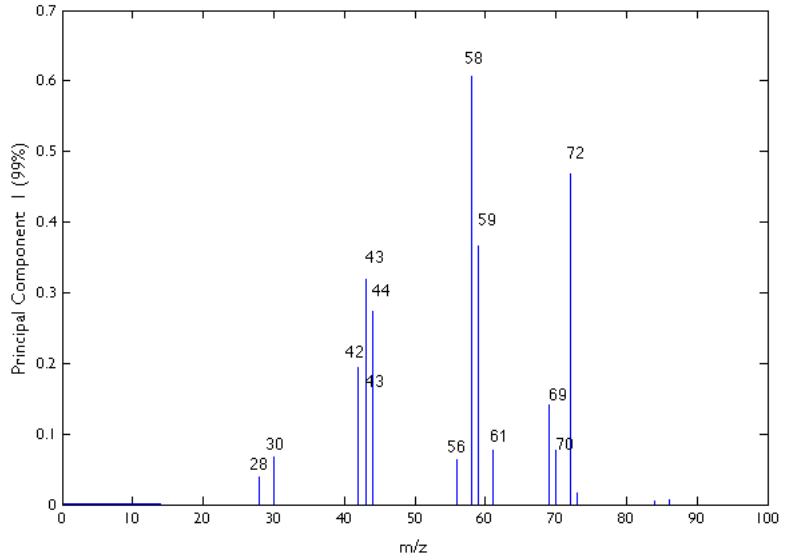

(a) PC1 loadings for HSA, Fb and HSA/Fb on PDMAEMA/PEO 70/30.

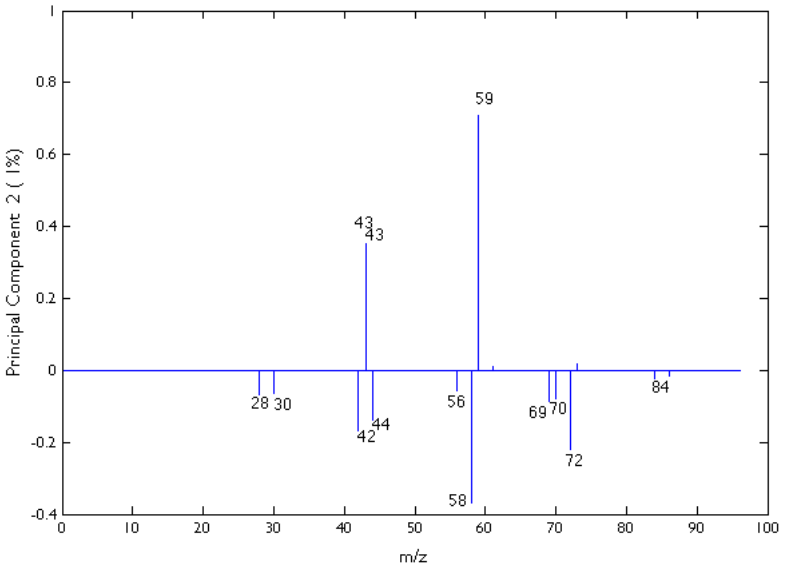

(b) PC2 loadings for HSA, Fb and HSA/Fb on PDMAEMA/PEO 70/30.

Similarly to the previous cases, the ratios of relative intensities between a fragment in a significantly higher amount in one of the proteins and a fragment less represented were calculated and presented in Fig. 75 to obtain some semi-quantitative information. The ratios are as follows :

$$r_1 = \frac{I_{rel}(59.05)}{I_{rel}(70.07)}$$
$$r_2 = \frac{I_{rel}(72.08)}{I_{rel}(84.09)}$$
$$r_3 = \frac{I_{rel}(59.05)}{I_{rel}(84.09)}$$

The ratios of relative intensities of Fb and the mixture are fairly similar, suggesting the presence of Fb adsorbed from HSA/Fb. However, there is not enough information to exclude the presence of HSA.

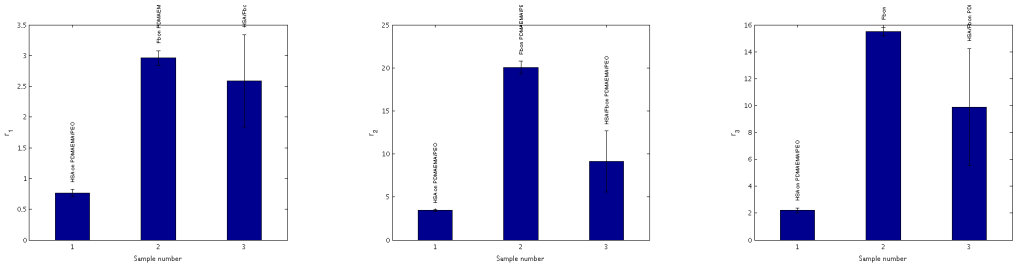

(a) r_1 **(b)** r_2 **(c)** r_3

Fig. 75. Plots of relative intensities ratios between two fingerprints of HSA and Fb, for HSA, Fb, and HSA/Fb on PDMAEMA/PEO.

7.3.4 Conclusion

Principal component analysis allowed to give some evidence of selective protein adsorption on PDMAEMA/PEO brushes. ToF-SIMS is a very sensitive technique that provides a good qualitative insight into the adsorbed species from mixtures. Analysis of the scores and the loadings with PCA first allowed to distinguish the different samples from each other. Studying the loadings and comparing their relative intensities ratios gave semi-quantitative information about adsorbed proteins. Negatively charged HSA would adsorb from a mixture with positively charged Lym, or Avi, while Fb, due to its larger size, would adsorb from a mixture with HSA. However, many hypotheses were made to obtain these results, and could have altered the real composition of the samples. First, the analysis is made on peaks from a pre-selected list. The normalization procedure can also degrade the information contained in the spectra.

Moreover, oppositely charged molecules are attracted to each other, so that smaller molecules can be carried by larger ones. They can then be involved in building the adsorbed layer on the brushes, and not being detected by ToF-SIMS. In fact, a similar phenomenon (hiding) may be the cause of a lack of adsorption of the mixture Fb/Lym (not presented here). On multiple occurrences, this mixture presented a QCM graph without any changes upon introduction of the solution ($\Delta f_a \approx 0$). Fibrinogen is an anisotropic large molecule (47.5 nm), while Lym is small and compact. Although no aggregation was observed in the solution, some Lym molecules could be attracted to Fb molecules, preventing adsorption through its negatively charged sites, on the positively charged polymer brushes.

ToF-SIMS only analyzes the outermost 2 nm of the surface. However, the proteins of interest have dimensions between 4 and 47.5 nm. The orientation preferences of proteins on polymer brushes have therefore a direct impact on the ions generated. This is also why determined fingerprints vary upon a change of substrate. ToF-SIMS is also very sensitive to sample preparation treatments. Contaminants from the atmosphere, or from the washing steps of the gold substrates can alter the resulting spectra.

Part IV

Conclusions and perspectives

8 | Conclusions

The goal of this work was to design mixed stimuli-responsive polymer brushes, in order to tune their properties toward selective protein adsorption.

The first step consisted in fabricating the mixed PDMAEMA/PEO brushes, and characterizing them using X-ray photoelectron spectroscopy (XPS), time-of-flight secondary ion mass spectrometry (ToF-SIMS), atomic force microscopy (AFM), water contact angle and streaming potential measurements. The presence of both polymers on the surface was revealed. It was shown that their properties changed depending on the volume proportions of both polymers in the grafting solution. Finally, PDMAEMA/PEO 30/70 were chosen for the ability of proteins to reversibly adsorb onto them. Indeed, adsorption is generally a highly irreversible process, while desorptions of at least 83% were observed in this study.

Protein adsorption and desorption from solutions containing one protein were then studied using QCM. The switchable behavior of the polymer brushes depending on the conditions allowed to demonstrate partial reversibility of protein adsorption.

Finally, selectivity of the developed polymer brushes was tested using ToF-SIMS and principal component analysis, to identify the adsorbed proteins from mixed solutions. Selectivity of polymer brushes could be evidenced for one of the mixes (HSA/Avi), but was less clear for the others. First, ToF-SIMS only provides semi-quantitative results, and has a sampling depth of no more than 2 nm, which is smaller than most of the proteins of interest. It means only a small portion of the molecules surface is analyzed. Some small proteins may be trapped under larger ones, and may not be detected by ToF-SIMS. Moreover, as ToF-SIMS is a very sensitive technique, contaminants for pre-treatments of the samples or from the atmosphere may bias the signal of proteins. This is why other techniques are needed to investigate the selectivity of protein adsorption on the brushes.

9 | Perspectives

Interesting perspectives emerge from the conclusions of this study, to investigate selective protein adsorption on stimuli-responsive polymer brushes.

Regarding ToF-SIMS, a better investigation of characteristic peaks for proteins would allow to provide more accurate results. Moreover, a comparison for HSA and Fb samples between the proteins adsorbed on gold and on PDMAEMA/PEO brushes could give some information about the influence of the substrate on their fingerprints.

The most important perspective consists in the use of ToF-SIMS and PCA, which may not be the most appropriate technique to detect proteins. This is why fluorescence microscopy with dyes, as well as gel electrophoresis, are suggested, two more suitable techniques for proteins.

Other mixtures can also be investigated, particularly those containing fibrinogen, as this protein presents interesting structure features that have a direct effect on its conformation when adsorbed on a surface.

The result of streaming potential measurements on polymer brushes showed a significant change of the sign of the surface charge upon protein adsorption. Furthermore, if a mixture of two oppositely charged proteins is introduced onto the gold substrate, it can be investigated whether multi-layers of alternating proteins could be formed on the surface.

This study was performed only at one particular pH and ionic strength. However, it was seen that polymer brushes undergo strong conformational changes depending on these conditions, and the behavior of proteins also undergoes changes. It would then be interesting to analyze the systems for full ranges of pH and ionic strengths.

Bibliography

Books and Journals

[1] H. F. Mark. *Encyclopedia of Polymer Science and Technology.* 4th Edition. Wiley, 2013.

[2] L. Börjesson et al. "Protein folding : Implementation of the Simulated Annealing Algorithm on Simple Three-Dimensional Models". PhD thesis. Department of Computer Science and Engineering, SE-412 96 Gothenburg (Sweden): University of Gothenburg, 2014.

[4] B. D. Ratner et al. *Biomaterials Science : An Introduction to Materials in Medicine.* Academic Press, 1996.

[5] F. Poncin-Epaillard et al. "Surface Treatment of Polymeric Materials Controlling the Adhesion of Biomolecules". In: *Journal of Functional Biomaterials* 3 (2012), pp. 528–543.

[7] B. Li and Q. Ye. "Antifouling Surfaces of Self-assembled Thin Layer". In: *Antifouling Surfaces and Materials* 9 (2015), pp. 31–40.

[8] G. D. Bixler and B. Bhushan. "Biofouling : lessons from nature". In: *Philosophical Transactions of the Royal Society A* 370 (2012), pp. 2381–2417.

[9] J. Wang. "Electrochemical biosensors: Towards point-of-care cancer diagnostics". In: *Biosensors and Bioelectronics* 21 (2006), pp. 1887–1892.

[10] M. Welch, A. Rastogia, and C. Ober. "Polymer brushes for electrochemical biosensors". In: *Soft Matter* 7 (2011), pp. 297–302.

[12] M. Wahlgren and T. Arnebrant. "Protein adsorption to solid surfaces". In: *Elsevier Science Publishers Ltd* 9 (1991), pp. 201–208.

[13] M. Delcroix. "Ionic strength and pH-dependent conformation of mixed polymer brushes for cycles of protein adsorption and desorption". PhD thesis. Faculté d'ingénierie biologique, agronomique et environnementale, Institut de la matière condensée et des nanosciences, Louvain-La-Neuve (Belgium): Université catholique de Louvain, 2013.

[14] W. Norde. "My voyage of discovery to proteins in flatland ... and beyond". In: *Colloids and Surfaces B : Biointerfaces* 61 (2008), pp. 1–9.

[15] J. L. Brash and T. A. Horbett. *Proteins at Interfaces II.* American Chemical Society, 1995.

[16] M. Van Beeka, L. Jonesa, and H. Sheardown. "Hyaluronic acid containing hydrogels for the reduction of protein adsorption". In: *Biomaterials* 29 (2008), pp. 780–789.

[17] A. Halperin. “Polymer Brushes that Resist Adsorption of Model Proteins : Design Parameters”. In: *Langmuir* 15 (1999), pp. 2525–2533.

[18] Y. Inouea and K. Ishihara. “Reduction of protein adsorption on well-characterized polymer brush layers with varying chemical structures”. In: *Colloids and Surfaces B: Biointerfaces* 81 (2010), pp. 350–357.

[19] E. Österberg et al. “Protein-rejecting ability of surface-bound dextran in end-on and side-on configurations : Comparison to PEG”. In: *Journal of Biomedical Materials Research Part A* 29 (1995), pp. 741–747.

[20] X. Wang et al. “Nanopatterns of polymer brushes for understanding protein adsorption on the nanoscale”. In: *The Royal Society of Chemistry* 4 (2014), pp. 45059–45064.

[21] M. Y. Paik et al. “Patterning of Polymer Brushes. A Direct Approach to Complex, Sub-Surface Structures”. In: *Nano Letters* 10 (2010), pp. 3873–3879.

[22] W. J. Brittain and S. Minko. “A Structural Definition of Polymer Brushes”. In: *Journal of Polymer Science Part A: Polymer Chemistry* 45 (2007), pp. 3505–3512.

[23] S. P. Armes et al. “Synthesis of Well-Defined, Polymer-Grafted Silica Particles by Aqueous ATRP.” In: *Langmuir* 17 (2001), pp. 4479–4481.

[24] W. T. S. Huck et al. “Polymer Brush Coatings Regulating Cell Behavior: Passive Interfaces Turn Into Active.” In: *Langmuir* 27 (2011), p. 1251.

[25] T. Wu et al. “Light-triggered reversible phase transfer of composite colloids.” In: *Langmuir* 26 (2010), pp. 9442–9448.

[26] M. Delcroix, S Demoustier, and C. Dupont. “Quartz Crystal Microbalance Study of Ionic Strength and pH-Dependent Polymer Conformation and Protein Adsorption/Desorption on PAA, PEO, and Mixed PEO/PAA Brushes.” In: *Langmuir* 30 (2014), pp. 268–277.

[27] M. E. Welch and C. K. Ober. “Responsive and patterned polymer brushes.” In: *Journal of Polymer Science Part B* 51 (2013), pp. 1457–1472.

[28] M. Motornov et al. “Chemical gating with nanostructured responsive polymer brushes: mixed brush versus homopolymer brush.” In: *ACS Nano* 2 (2008), pp. 41–52.

[29] M. Delcroix et al. “Design of Mixed PEO/PAA Brushes with Switchable Properties Toward Protein Adsorption.” In: *Biomacromolecules* 14 (2013), pp. 215–225.

[30] L. D. Unsworth, H. Sheardown, and J. L. Brash. “Protein-resistant poly(ethylene oxide)-grafted surfaces: chain density-dependent multiple mechanisms of action.” In: *Langmuir* 24 (2008), pp. 1924–1929.

[32] M. Wasilewska and Z. Adamczyk. “Fibrinogen Adsorption on Mica Studied by AFM and in Situ Streaming Potential Measurements.” In: *Langmuir* 27 (2010), pp. 686–696.

[36] D. L. Nelson and M. M. Cox. *Lehninger Principles of Biochemistry*. 4th Edition. W. H. Freeman, 2005.

[38] J. F. Watts. “X-ray photoelectron spectroscopy”. In: *Elsevier Science Publishers Ltd* 45 (1994), pp. 653–671.

[45] Malvern Instruments Ltd. *Zetasizer Nano User Manual*. Issue 1.1. Enigma Business Park, Grovewood Road, Worcestershire, 2013.

[46] M. Zembala, Z. Adamczyk, and P. Warszyński. "Streaming potential of mica covered by latex particles". In: *Colloids and Surfaces A: Physicochem.* 222 (2003), pp. 329–339.

[52] A. M. Belu et al. "Time-of-flightsecondaryionmassspectrometry:techniquesand applications for the characterization of biomaterial surfaces." In: *Biomaterials* 24 (2003), pp. 3635–3653.

[53] B. J. Tyler, G. Rayal, and D. G. Castner. "Multivariate analysis strategies for processing ToF-SIMS images of biomaterials." In: *Biomaterials* 28 (2007), pp. 2412–2423.

[54] M. J. Genet, C. Dupont-Gillain, and P. G. Rouxhet. *Medical Applications of Colloids : XPS analysis of biosystems and biomaterials.* Springer, 2008, pp. 177–307.

[55] Q. Peng et al. "Preparation of Polymer-Silicon(100) Hybrids via Interface-Initiated Reversible Addition-Fragmentation Chain-Transfer (RAFT) Polymerization." In: *Macromolecules* 39 (2006), pp. 5577–5582.

[56] P. Kingshott et al. "Ultrasensitive probing of the protein resistance of PEG surfaces by secondary ion mass spectrometry." In: *Biomaterials* 23 (2002), pp. 4775–4785.

[61] O. Hoy. "Synthesis and Characterization of Polymer Brushes for Controlled Adsorption of Proteins". MA thesis. Department of Materials Science and Engineering: Clemson University, 2008.

Electronic Ressources

[3] Saylor Academy. *The Basics of General, Organic, and Biological Chemistry*. 2012. URL: `http://saylordotorg.github.io/text_the-basics-of-general-organic-and-biological-chemistry/index.html`.

[6] Biolin Scientific. *Protein Adsorption to Biomaterials*. 2015. URL: `http://blog.biolinscientific.com/blog/protein-adsorption-to-biomaterials`.

[11] M. Cramer. *Biofilms: Impact on the Food Industry*. 2012. URL: `http://www.foodsafetymagazine.com/magazine-archive1/junejuly-2012/biofilms-impact-on-the-food-industry/`.

[31] Inc. Base Pair Biotechnologies. *ATW0015 - Human Serum Albumin (HSA) Aptamer*. 2017. URL: `https://www.basepairbio.com/store/atw0015-human-serum-albumin-hsa-aptamer/`.

[33] 3Dciencia Visual science. *Fibrinogen structure*. 2012. URL: `http://3dciencia.com/blog/2012/02/fibrinogen-structure/`.

[34] Protein Data Bank. *Solution structure of Lysozyme at low and high pressure*. 2017. URL: `http://www.rcsb.org/pdb/explore.do?structureId=1gxv`.

[35] Wikipedia The Free Encyclopedia. *Avidin*. 2017. URL: `https://en.wikipedia.org/wiki/Avidin`.

[37] Thermo Fisher Scientific Inc. *What is X-Ray Photoelectron Spectroscopy (XPS)?* 2016. URL: `http://xpssimplified.com/whatisxps.php`.

[39] M. Laurin. *Example: Principle of X-ray photoelectron spectroscopy (XPS)*. 2009. URL: http://www.texample.net/tikz/examples/principle-of-x-ray-photoelectron-spectroscopy-xps/.

[40] K. Jacobs. *Ultra High Vacuum Lab*. 2012. URL: http://jacobs.physik.uni-saarland.de/english/instrumentation/uhvl.htm.

[41] Casa Software Ltd. *Casa XPS*. 2013. URL: http://www.casaxps.com/help_manual/manual_updates/xps_spectra.pdf.

[42] JPK Instruments. *Tutorials - Atomic Force Microscopy (AFM)*. 2017. URL: http://www.jpk.com/introduction-to-imaging-modes.433.en.html.

[43] Functional materials and photonics structures. *Contact Angle platform*. URL: https://fmps.fbk.eu/contact-angle-platform.

[44] Ramé-hart contact angle goniometers and tensiometers. *Information on Contact Angle*. URL: http://www.ramehart.com/contactangle.htm.

[47] N. Saleh. *QCM-D*. 2010. URL: http://www.caee.utexas.edu/prof/saleh/facilities2.html.

[48] M. A. Poggi. *Q-Sense QCM-D Training (University of Kentucky)*. 2009. URL: http://www.engr.uky.edu/~cense/equipment/040809_UnivKentucky_Training_FINAL.pdf.

[49] Gamry Instruments Inc. *Basics of a Quartz Crystal Microbalance*. 2012. URL: https://www.gamry.com/application-notes/physechem/basics-of-a-quartz-crystal-microbalance/.

[50] Biolin Scientific Inc. *QCM-D Technology*. 2016. URL: http://www.biolinscientific.com/q-sense/technologies/.

[51] D. W. Mogk. *Time-of-Flight Secondary Ion Mass Spectrometry (ToF-SIMS)*. 2017. URL: http://serc.carleton.edu/research_education/geochemsheets/techniques/ToFSIMS.html.

[57] Yachtandboat. *Antifouling and cleaning are vital in protecting the environment*. 2008. URL: http://www.yachtandboat.com.au/news/antifouling-and-cleaning-are-vital-in-protecting-the-environment.

[58] Food Safety Brazil. *Controle de biofilmes na indústria de alimentos*. 2015. URL: http://foodsafetybrazil.org/controle-de-biofilmes-na-industria-de-alimentos/.

[59] Particulate Systems. *Zeta Potential and Nano Particle Analyzer*. 2012. URL: http://www.particulatesystems.com/Repository/Files/NanoPlus_Brochure_Final_v8.pdf.

[60] Washington University in St. Louis (School of Engineering & Applied Science). *Dynamic Light Scattering (DLS)*. URL: http://www.nano.wustl.edu/doc/Instrument%20Manuals%20and%20Protocols/DLS%20Final.pdf.

Appendices

A | XPS results

A.1 Survey spectrum of PDMAEMA powder

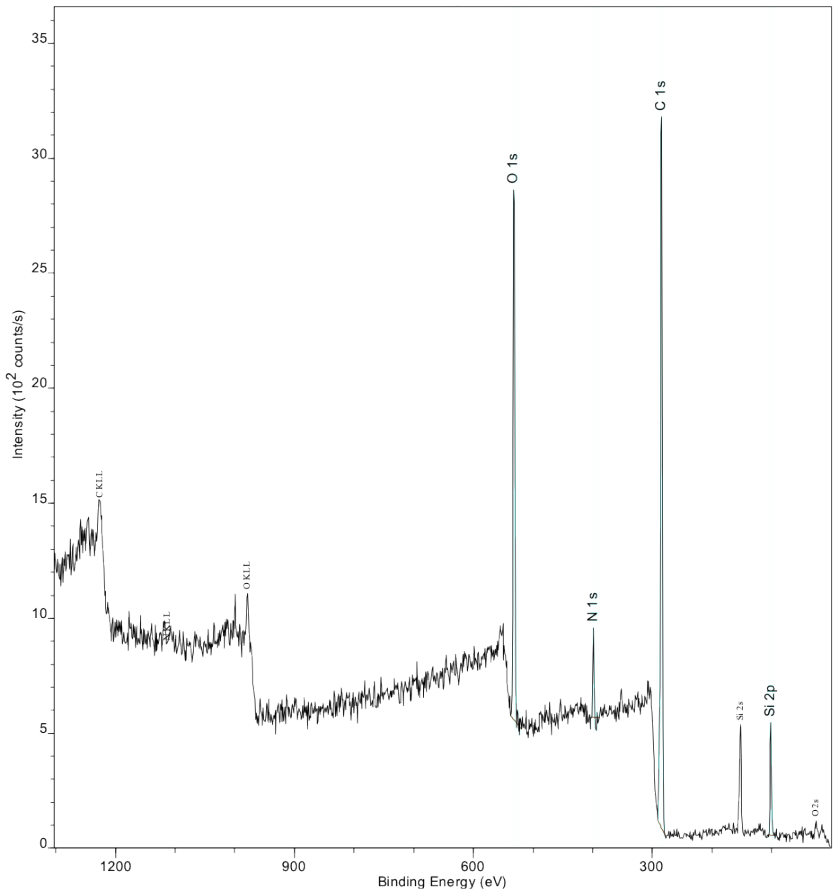

Fig. 76. Survey spectrum of PDMAEMA powder. No detection of sulfur.

A.2 Complete atomic and functional compositions of the polymer brushes

Table A.1. Atomic and functional composition of PDMAEMA powder, measured by XPS.

Element	Peak	Attribution	Binding energy*	Surface atomic fraction**
Oxygen	O 1*s*	**O**-C	533.5	3.0
		O=C, **O**-Si	532.1	11.4
		O tot.		**14.4**
Nitrogen	N 1*s*	C-**N**H+	400.9	0.4
		N-C	399.4	3.3
		N tot.		**3.7**
Carbon	C 1*s*	O-**C**=O	288.8	6.2
		C-(O,N)	286.1	19.7
		C-(C,H,Si)	284.8	46.8
		C tot.		**72.6**
Silicon	Si 2*p*	O-**Si**-C	102.1	**9.2**

*Binding energy in [eV]
**Surface atomic fraction, except hydrogen, in %

Table A.2. Atomic and functional composition of PDMAEMA brushes grafted on gold, measured by XPS.

Element	Peak	Attribution	Binding energy*	Surface atomic fraction**
Oxygen	O 1*s*	**O**-C	533.2	4.0
		O=C	531.7	5.7
		O tot.		**9.7**
Nitrogen	N 1*s*	**N**-C	399.6	**2.5**
Carbon	C 1*s*	O-**C**=O	288.5	6.6
		C-(O,N)	286.2	12.1
		C-(C,H)	284.8	28.0
		C tot.		**46.6**
Sulfur	S 2*p*	**S** 2*p* 1/2	162.5	0.2
		S 2*p* 3/2	161.3	0.4
		S tot.		**0.5**
Gold	Au 4*f*	**Au** 4*f*	83.4	**40.7**

*Binding energy in [eV]
**Surface atomic fraction, except hydrogen, in %

Table A.3. Atomic and functional composition of mixed PDMAEMA/PEO brushes grafted on gold, measured by XPS.

Element	Peak	Attribution	Binding energy*	Surface atomic fraction**
Oxygen	O 1*s*	**O**-C	533.3	3.8
		O=C	531.8	6.2
		O tot.		**10.0**
Nitrogen	N 1*s*	**N**-C	399.7	**3.1**
Carbon	C 1*s*	O-**C**=O	288.5	6.9
		C-(O,N)	286.2	11.8
		C-(C,H)	284.8	28.2
		C tot.		**46.9**
Sulfur	S 2*p*	**S** 2*p*	165	**0.3**
Gold	Au 4*f*	**Au** 4*f*	83.4	**39.7**

*Binding energy in [eV]
**Surface atomic fraction, except hydrogen, in %

A.3 High resolution nitrogen peaks

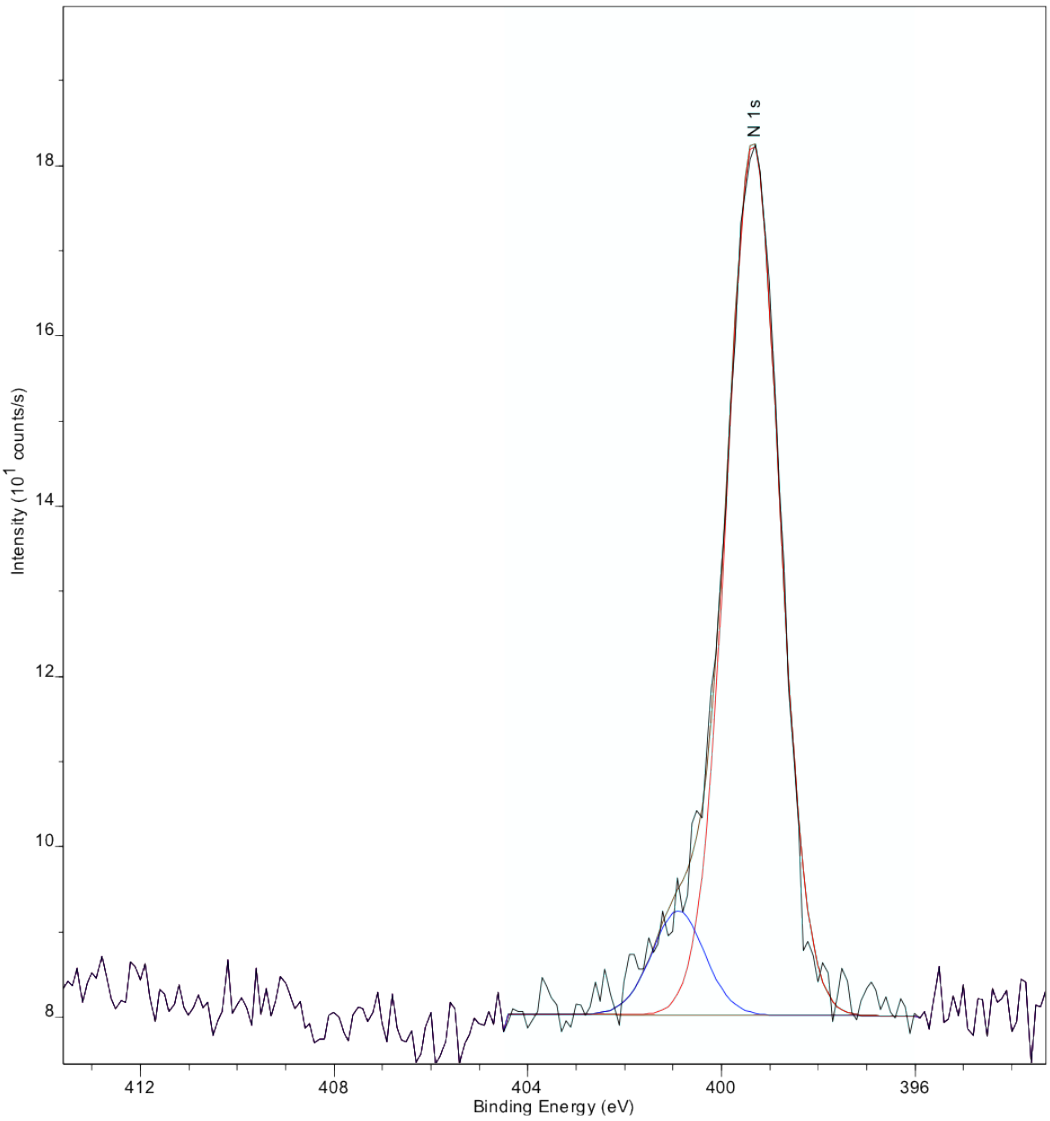

Fig. 77. PDMAEMA powder : XPS decomposition of the nitrogen peak N 1*s* into **N**−C (red) and C−**N**H^+ (blue) functions.

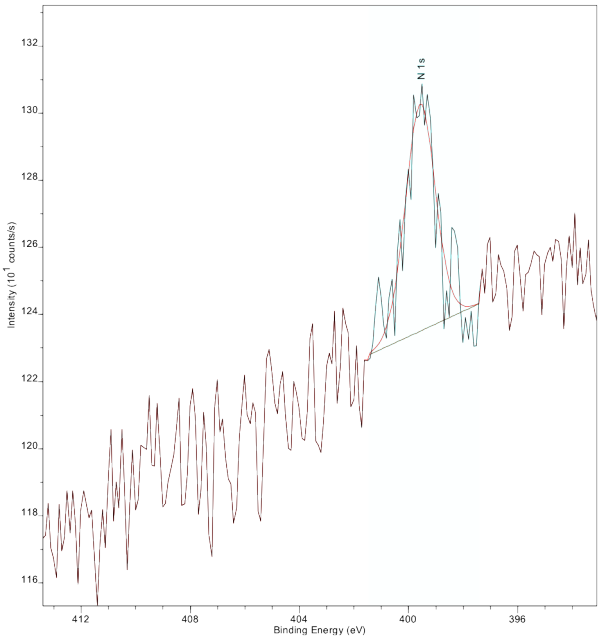

Fig. 78. PDMAEMA brush on gold : XPS nitrogen peak N 1*s*.

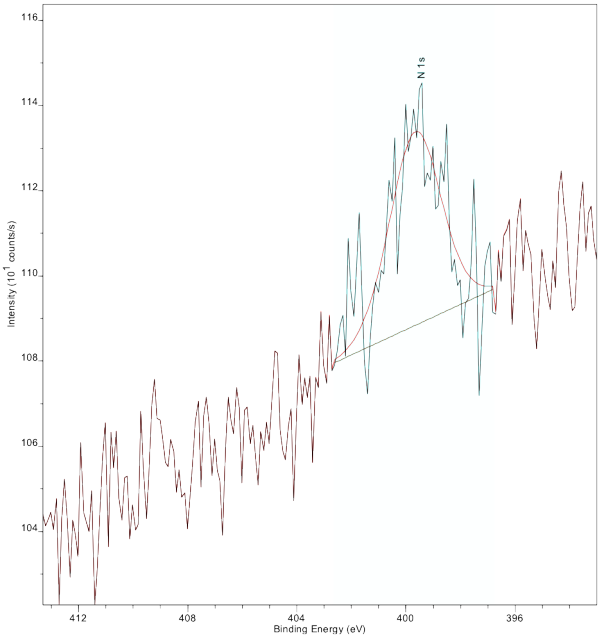

Fig. 79. PDMAEMA/PEO brush on gold : XPS nitrogen peak N 1*s*.

B | ToF-SIMS peak lists and additional results

B.1 Complete peak list for proteins

Mass	Fragments
28,02	CH_2N^+
30,04	CH_4N^+
42,03	$C_2H_4N^+$
43,02	$C_2H_3O^+$
43,03	$CH_3N_2^+$
44,04	$CH_4N_2^+$
44,05	$C_2H_6N^+$
44,98	CHS^+
46,99	CH_3S^+
54,03	$C_3H_4N^+$
56,05	$C_3H_6N^+$
58,03	$C_2H_4NO^+$
58,07	$C_3H_8N^+$
59,05	$CH_5N_3^+$
60,04	$C_2H_6NO^+$
61,01	$C_2H_5S^+$
68,05	$C_4H_6N^+$
69,03	$C_4H_5O^+$
70,03	$C_3H_4NO^+$
70,07	$C_4H_8N^+$
71,01	$C_3H_3O_2^+$
72,08	$C_4H_{10}N^+$
73,06	$C_2H_7N_3^+$
74,06	$C_3H_8NO^+$
76,02	$C_2H_6SN^+$
77,04	$C_6H_5^+$
81,04	$C_4H_5N_2^+$
82,05	$C_4H_6N_2^+$

Mass	Fragments
83,05	$C_5H_7O^+$
84,04	$C_4H_6NO^+$
84,09	$C_5H_{10}N^+$
86,10	$C_5H_{12}N^+$
87,06	$C_3H_7N_2O^+$
88,04	$C_3H_6NO_2^+$
91,05	$C_7H_7^+$
98,02	$C_4H_4NO_2^+$
100,09	$C_4H_{10}N_3^+$
101,09	$C_4H_{11}N_3^+$
102,04	$C_4H_8NS^+$
102,06	$C_4H_8NO_2^+$
107,05	$C_7H_7O^+$
108,05	$C_5H_6N_3^+$
110,07	$C_5H_8N_3^+$
112,08	$C_5H_{10}N_3^+$
118,06	$C_8H_8N^+$
120,08	$C_8H_{10}N^+$
127,10	$C_5H_{11}N_4^+$
129,11	$C_5H_{13}N_4^+$
130,06	$C_9H_8N^+$
131,05	$C_9H_7O^+$
132,05	$C_9H_8O^+$
134,06	$C_8H_8NO^+$
136,08	$C_8H_{10}NO^+$
159,09	$C_{10}H_{11}N_2^+$
166,07	$C_{11}H_6N_2^+$

B.2 PCA on HSA and Lym on pure gold

Pure gold samples coated with HSA and Lym were compared by PCA to determine their fingerprints. Table B.1 summarizes the determined characteristic peaks. The peaks shown in bold characters are those showing the largest differences in relative intensities between both proteins when analyzing each loading separately.

Table B.1. List of positive fingerprints of HSA and Lym, on gold.

m/z	Fragments	Proteins
28,02	CH_2N^+	Lym
30,04	CH_4N^+	Lym
42,03	$C_2H_4N^+$	Lym, HSA
43,02	$C_2H_3O^+$	HSA, Lym
43,03	$CH_3N_2^+$	HSA
44,05	$C_2H_6N^+$	Lym, HSA
54.03	$\mathbf{C_3H_4N^+}$	**Lym**
56,05	$\mathbf{C_3H_6N^+}$	Lym
58,07	$\mathbf{C_3H_8N^+}$	**HSA**
59,05	$CH_5N_3^+$	HSA, Lym
61,01	$\mathbf{C_2H_5S^+}$	**HSA**
68,05	$\mathbf{C_4H_6N^+}$	**Lym**
69,03	$C_4H_5O^+$	Lym, HSA
70,03	$\mathbf{C_3H_4NO^+}$	**Lym**
70,07	$\mathbf{C_4H_8N^+}$	**Lym**
72,08	$C_4H_{10}N^+$	HSA, Lym
84,04	$\mathbf{C_4H_6NO^+}$	**Lym**
84,09	$\mathbf{C_5H_{10}N^+}$	**Lym**
86,10	$C_5H_{12}N^+$	Lym
110,07	$\mathbf{C_5H_8N_3^+}$	**Lym**
120,08	$\mathbf{C_8H_{10}N^+}$	**Lym**

B.3 PCA on HSA and Avi on pure gold

The same procedure was applied to gold samples coated with HSA and with Avi to determine their fingerprints. Two characteristic peaks for avidin can be determined : CH_4N^+ at $30.04\,\mathrm{g\,mol^{-1}}$, and $C_2H_6N^+$ at $44.05\,\mathrm{g\,mol^{-1}}$. A list of 21 fingerprints for HSA and Avi is selected and listed in Table B.2. Peaks shown in bold characters are the most characteristic.

Table B.2. HSA and Avi positive fingerprints

m/z	Fragments	Proteins
28,02	CH_2N^+	
30,04	$\mathbf{CH_4N^+}$	**Avi**
42,03	$C_2H_4N^+$	
43,02	$C_2H_3O^+$	HSA
43,03	$\mathbf{CH_3N_2^+}$	**HSA**
44,04	$CH_4N_2^+$	Avi
44,05	$\mathbf{C_2H_6N^+}$	**Avi**
54,03	$C_3H_4N^+$	
56,05	$C_3H_6N^+$	
58,07	$\mathbf{C_3H_8N^+}$	**HSA**
59,05	$CH_5N_3^+$	
70,03	$C_3H_4NO^+$	
70,07	$C_4H_8N^+$	HSA, Avi
72,08	$C_4H_{10}N^+$	
73,06	$\mathbf{C_2H_7N_3^+}$	**HSA**
74,06	$C_3H_8NO^+$	
77,04	$C_6H_5^+$	Avi
84,04	$C_4H_6NO^+$	
84,09	$\mathbf{C_5H_{10}N^+}$	**Avi**
86,10	$C_5H_{12}N^+$	Avi
110,07	$\mathbf{C_5H_8N_3^+}$	**HSA**

B.4 PCA on HSA and Fb on pure gold

Table B.3 contains the fingerprints of HSA and Fb adsorbed on pure gold. The peaks shown in bold characters are those showing the largest differences in relative intensities between both proteins when analyzing each loading separately.

Table B.3. HSA and Fb positive fingerprints.

m/z	Fragments	Proteins
28,019	CH_2N^+	Fb
30,0352	CH_4N^+	Fb
42,0336	$C_2H_4N^+$	Fb, HSA
43,0166	$C_2H_3O^+$	HSA, Fb
43,0277	$CH_3N_2^+$	HSA
44,0514	$\mathbf{C_2H_6N^+}$	**Fb**
54,033	$\mathbf{C_3H_4N^+}$	**Fb**
56,0492	$\mathbf{C_3H_6N^+}$	**Fb**
58,0658	$\mathbf{C_3H_8N^+}$	**HSA**
59,0484	$CH_5N_3^+$	Fb, HSA
61,0091	$\mathbf{C_2H_5S^+}$	**HSA**
69,0339	$C_4H_5O^+$	Fb, HSA
70,0707	$\mathbf{C_4H_8N^+}$	**Fb**
72,0832	$C_4H_{10}N^+$	
84,0438	$\mathbf{C_4H_6NO^+}$	**Fb**
84,09	$\mathbf{C_5H_{10}N^+}$	**Fb**
86,101	$C_5H_{12}N^+$	Fb
110,0736	$\mathbf{C_5H_8N_3^+}$	**Fb**
120,0824	$\mathbf{C_8H_{10}N^+}$	**Fb**

B.5 Spectra of loadings for PCA on pairs of proteins

HSA/Lym

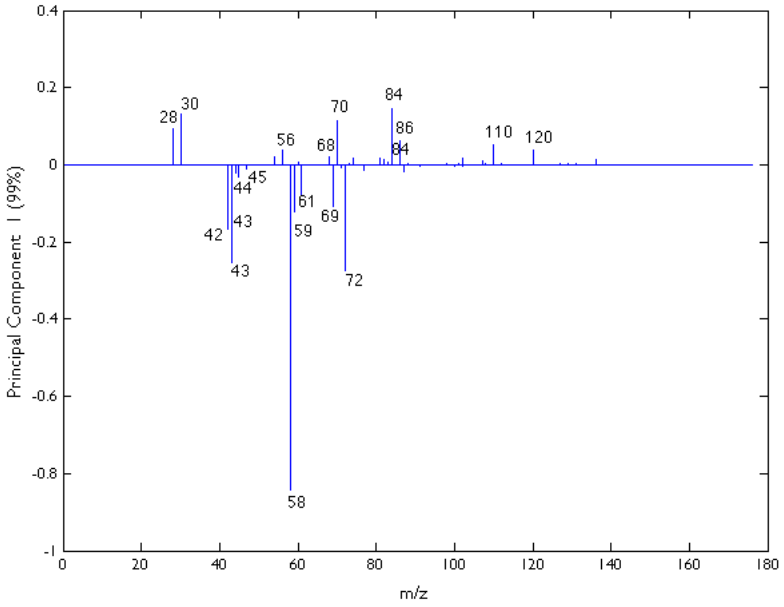

(a) PC1

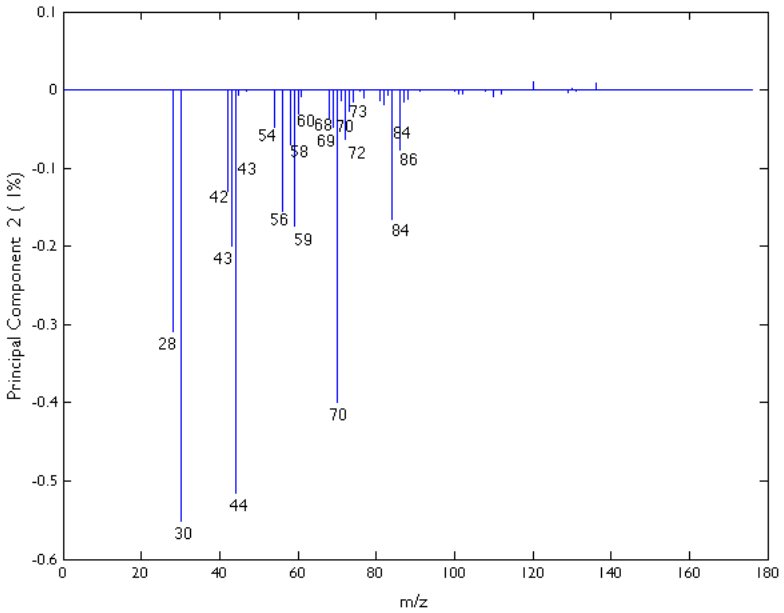

(b) PC2

Fig. 80. Loadings for HSA on PDMAEMA/PEO 70/30, and Lym on pure gold (a) on PC1, and (b) on PC2.

HSA/Avi

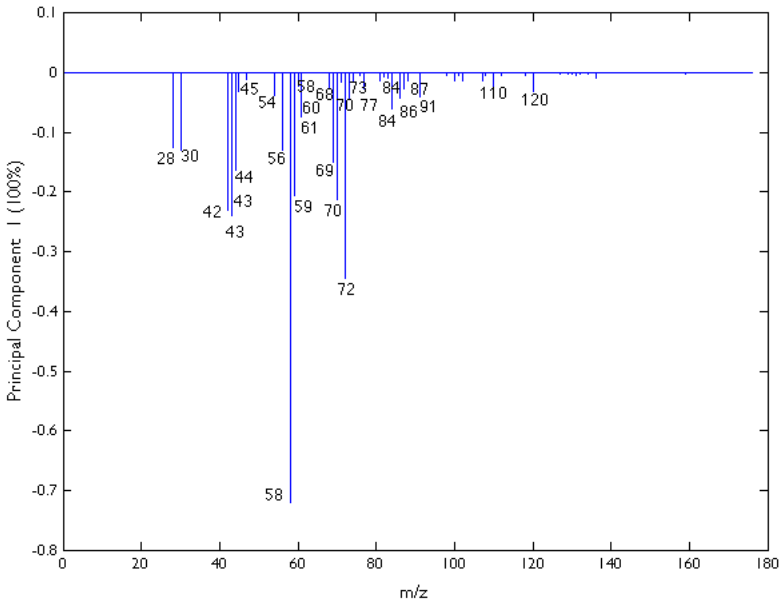

(a) PC1

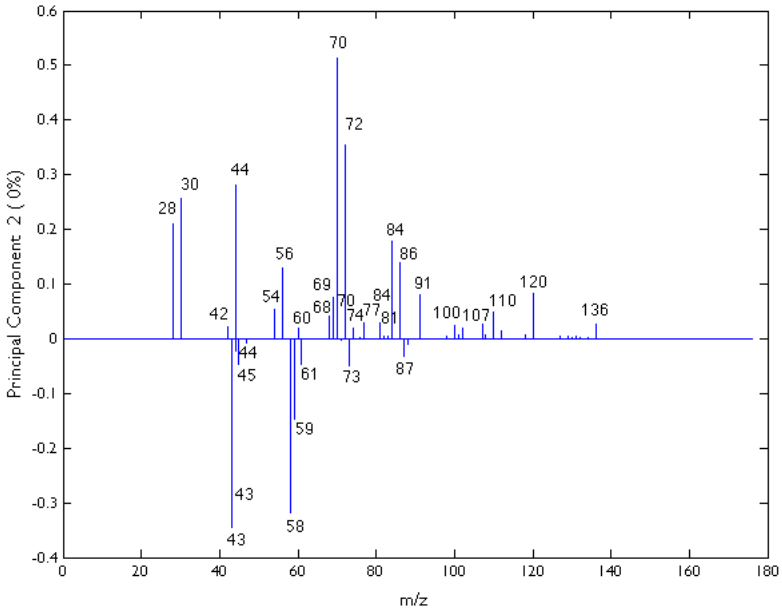

(b) PC2

Fig. 81. Loadings for HSA on PDMAEMA/PEO 70/30, and Avi on pure gold (a) on PC1, and (b) on PC2.

HSA/Fb

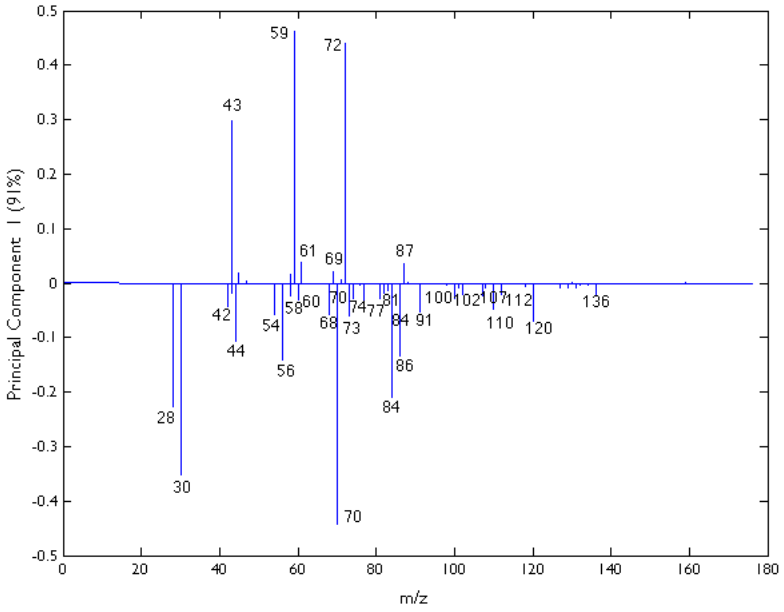

(a) PC1

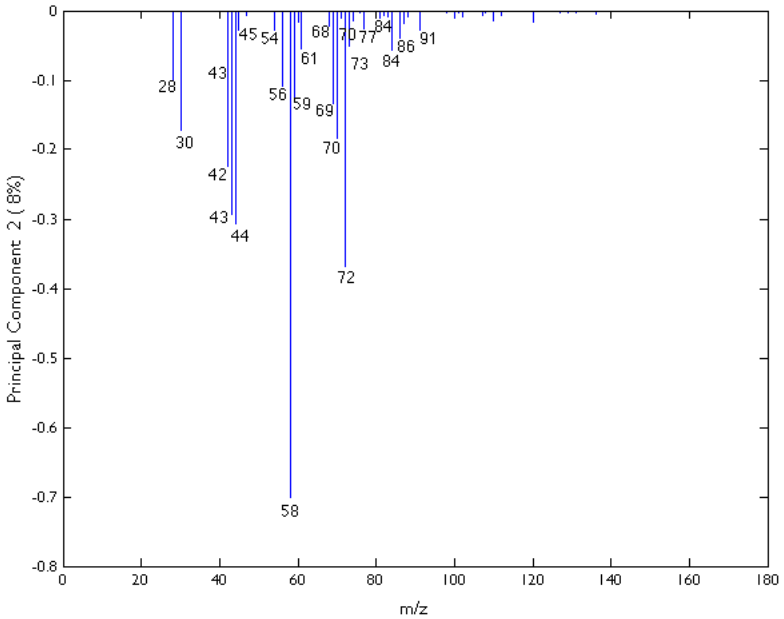

(b) PC2

Fig. 82. Loadings for HSA and Fb on PDMAEMA/PEO 70/30, (a) on PC1, and (b) on PC2.

B.6 Relative intensities of loadings on PC1 for HSA and Avi

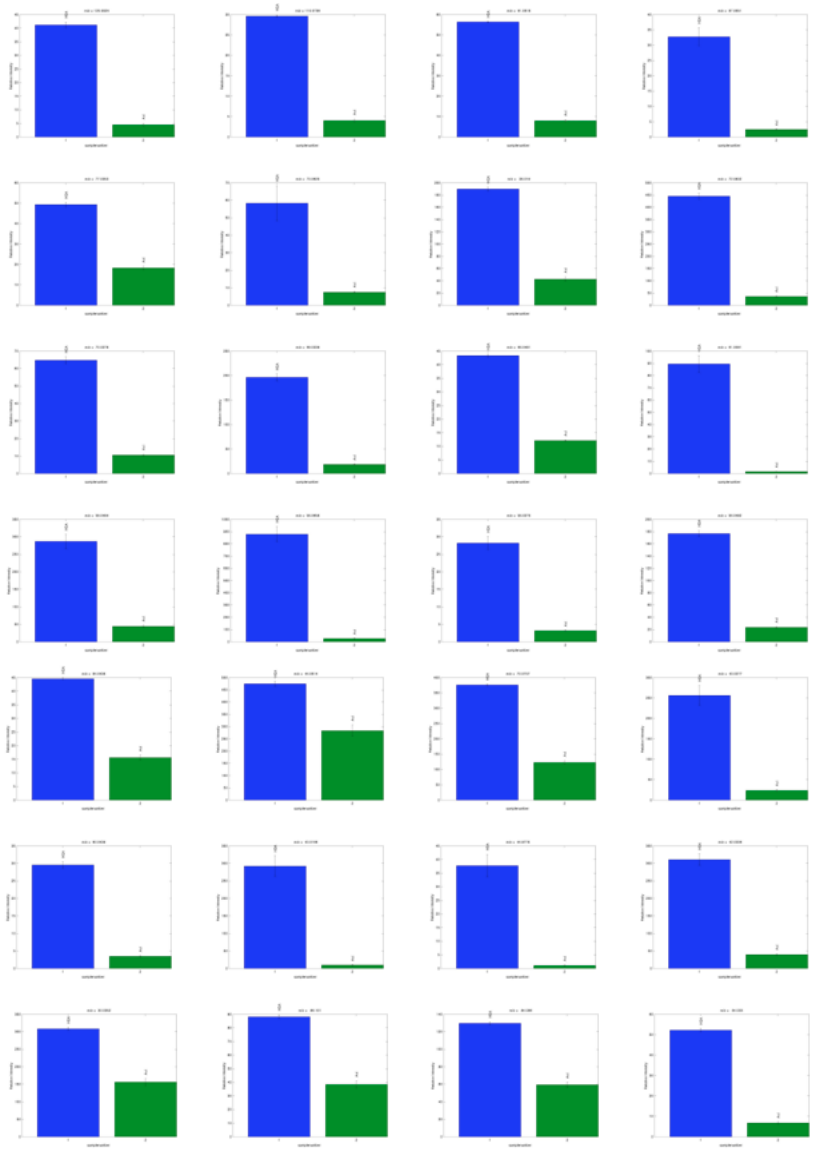

Fig. 83. Relative intensities of loadings on PC1 for HSA (blue) and Avi (green).

Rue Archimède, 1 bte L6.11.01, 1348 Louvain-la-Neuve **www.uclouvain.be/epl**